

**THE PHOTOPHYSICAL PROPERTIES OF LOW  
SYMMETRY PHTHALOCYANINES IN CONJUNCTION  
WITH QUANTUM DOTS**

**A thesis submitted in fulfilment of the requirements for the degree of**

**MASTER OF SCIENCE**

**Of**

**RHODES UNIVERSITY**

**By**

**SARAH D' SOUZA**

**February 2011**

"As a blind man has no idea of colours, so we have no idea of the manner by which the all-wise God perceives and understands all things."

*- Isaac Newton*

## ACKNOWLEDGEMENTS

I would like to convey my sincere gratitude and heartfelt thanks to my supervisor, Professor T. Nyokong for her guidance, patience and assistance throughout the course of my studies, the preparation of this thesis and also for providing me with financial assistance and access to laboratory equipment. It has been a pleasure working under her supervision.

A special thanks to Dr Edith Antunes for her advice, assistance, guidance and especially her support. I am forever grateful for the time she has sacrificed. I would also like to acknowledge Dr Christian Litwinski for his invaluable contribution to this work. Thanks also to Ms Sharon Moeno and Dr Wadzanai Chidawanyika for their guidance and sharing their experience as well as their theoretical and practical knowledge.

A special thanks to the S22 research group. They were constantly supportive and a source of much fun and laughter at the best and worst of times. It has been a privilege working with everyone - and learning from them. My heartfelt thanks to all my friends, particularly Ms Megan Coates and Ms Henusha Jhundoo, for their unwavering support and encouragement. They have enriched my life. A very special thanks to Ms Gail Cobus for all her assistance with the administrative work.

I would like to extend my love and gratitude to my sister Ms Nicole D' Souza. I am forever grateful and blessed to have her in my life. To my parents. Thank you for your

love, faith, prayers, support, encouragement and financial assistance throughout my academic career and my entire life. I am eternally grateful for the beliefs you instilled in me, as well as the sacrifices and decisions you made in order to support my education.

Last but not least, I am very grateful to the Department of Science and Technology/ MINTEK Nanotechnology Innovation Centre (DST/MINTEK/NIC) and the African Laser Centre (ALC) who funded this research project.

## ABSTRACT

The synthesis, extensive spectroscopic characterization and photophysical studies of low symmetry zinc phthalocyanine have been conducted. Comparisons have been made taking into consideration the influence of the solvent properties as well as substituent type and position.

Photosensitizing properties of the zinc phthalocyanine derivatives in the presence of thiol capped CdTe quantum dots (QDs) were compared. The QDs were used as energy transfer donors and to facilitate with energy transfer through Förster resonance energy transfer (FRET) from the QDs to the MPcs. The linkage of unsymmetrically substituted 4-monoaminophenoxy zinc phthalocyanine (ZnAPPc) to CdTe quantum dots capped with mercaptopropionic acid (MPA), L-cysteine (L-cys) or thioglycolic acid (TGA) has been achieved using the coupling agents ethyl-N(3-dimethylaminopropyl) carbodiimide (EDC) and N-hydroxy succinimide (NHS), which facilitate formation of an amide bond to form the QD-ZnAPPc-linked complex.

The formation of the amide bond was confirmed using UV-Vis, Raman and IR spectroscopies, as well as AFM (atomic force microscopy). Förster resonance energy transfer (FRET) resulted in stimulated emission of ZnAPPc in both the linked (QD-ZnAPPc-linked) and mixed (QD:ZnAPPc-mixed) conjugates for MPA only. The linked L-cys and TGA complexes (QD-ZnAPPc-linked) gave the largest FRET efficiencies hence showing the advantages of covalent linking. Fluorescence quantum yields of QDs

were decreased in QD:ZnAPPc-mixed and QD:ZnAPPc-linked. High triplet state quantum yields were obtained for the linked QD-phthalocyanine derivatives (ZnAPPc) and monoaminozinc phthalocyanine (ZnAPc) compared to when ZnAPPc and ZnAPc were mixed with MPA QDs without a chemical bond.

# CONTENTS

Title Page	i
Quote	ii
Acknowledgements	iii
Abstract	v
Contents	vii
List of Abbreviations	xii
List of Symbols	xv
List of Figures	xvii
List of Schemes	xxi
List of Tables	xxii
1. INTRODUCTION	1
1.1 Nanoparticles	2
1.1.1 Absorption and fluorescence spectra of QDs	4
1.1.2 Synthesis of water-soluble CdTe colloidal nanoparticles	7

1.1.3 Characterization of nanoparticles	8
1.2 Phthalocyanine (Pc) chemistry	10
1.2.1 The history and structure of phthalocyanines	10
1.2.2 Synthesis of low-symmetry A <sub>3</sub> B type phthalocyanines	13
1.2.3 Ground state electronic absorption spectra of phthalocyanines	16
1.2.4 Phthalocyanine aggregation	17
1.2.5 The interaction of mixed and linked MPc - QD conjugates	19
1.3 Photophysical properties	23
1.3.1 Fluorescence quantum yields and lifetimes	26
1.3.2 Förster resonance energy transfer (FRET)	32
1.3.3 Triplet quantum yields and lifetimes	38
1.4 Summary of Aims of Thesis	42
2. EXPERIMENTAL	43
2.1 Materials	44
2.1.1 Solvents	44

2.1.2 Synthesis and photophysical reagents	44
2.2 Instrumentation	45
2.3 Methods	49
2.3.1 UV-vis absorption studies	49
2.3.2 Fluorescence spectra and quantum yields	49
2.3.3 Fluorescence lifetimes	50
2.3.4 Triplet quantum yields and lifetimes	50
2.4 Synthesis	51
2.4.1 Synthesis of Quantum Dots (QDs)	51
2.4.2 Synthesis of low symmetry zinc phthalocyanines (ZnPcs)	53
2.4.2.1. Synthesis of 4-monoaminophenoxy zinc phthalocyanine (Scheme 3.1)	53
2.4.2.2. Synthesis of zinc monoamino phthalocyanine (Scheme 3.2)	54
2.4.3 Conjugation of CdTe QDs to ZnPcs (Scheme 3.3)	55
RESULTS AND DISCUSSION	57
PUBLICATIONS	57

3. SYNTHESIS AND SPECTROSCOPIC CHARACTERIZATION	58
3.1 Synthesis and characterization of thiol capped CdTe quantum dots (QDs)	59
3.2 Low-symmetry zinc phthalocyanines	64
3.2.1. 4-Monoaminophenoxy zinc phthalocyanine (Scheme 3.1)	64
3.2.2. Zinc monoaminophthalocyanine (Scheme 3.2)	67
3.3 Interaction of low-symmetry zinc phthalocyanines with QDs (Scheme 3.3)	70
4. PHOTOPHYSICAL PROPERTIES	75
4.1 Fluorescence quantum yields	76
4.2 Fluorescence lifetimes	79
4.3 Förster resonance energy transfer (FRET)	84
4.4 Triplet state quantum yields and lifetimes	89
5. GENERAL CONCLUSIONS	93



## List of Abbreviations

<b>A</b>	=	Absorption
<b>AE</b>	=	Acceptor emission
<b>AFM</b>	=	Atomic force microscopy
<b>ASE</b>	=	Acceptor sensitized emission
<b>DA</b>	=	Donor absorption
<b>DBU</b>	=	1,8-Diazabicyclo[5.4.0]undec-7-ene
<b>DCM</b>	=	Dichloromethane
<b>DE</b>	=	Donor emission
<b>DMF</b>	=	<i>N,N</i> -dimethylformamide
<b>DMSO</b>	=	Dimethylsulfoxide
<b>EDC</b>	=	1-Ethyl-3-(3-dimethylaminopropyl) carbodiimide
<i>Eff<sub>tr</sub></i>	=	Efficiency of energy transfer
<b>ET</b>	=	Energy transfer
<b>F</b>	=	Fluorescence
<b>FRET</b>	=	Förster resonance energy transfer
<b>FWHM</b>	=	Full width at half maximum
<b>FT-IR</b>	=	Fourier transform-infrared
<b>H<sub>2</sub>Pc</b>	=	Metal free phthalocyanine
<b>HOMO</b>	=	Highest occupied molecular orbital
<b>HPLC</b>	=	High performance liquid chromatography

<b>IC</b>	=	Internal conversion
<b>IR</b>	=	Infrared
<b>ISC</b>	=	Intersystem crossing
<b>L-cys</b>	=	L-cysteine
<b>LUMO</b>	=	Lowest unoccupied molecular orbital
<b>MPA</b>	=	Mercaptopropionic acid
<b>MPc</b>	=	Metallophthalocyanine
<b>NHS</b>	=	N-hydroxysuccinimide
<b>NIR</b>	=	Near infrared
<b>NMR</b>	=	Nuclear magnetic resonance
<b>NR</b>	=	Non-radiative
<b>NRDR</b>	=	Non-radiative donor relaxation
<b>P</b>	=	Phosphorescence
<b>Pc</b>	=	Phthalocyanine
<b>PDT</b>	=	Photodynamic therapy
<b>PMT</b>	=	Photomultiplier tube
<b>QD</b>	=	Quantum dot
<b>TCSPC</b>	=	Time correlated single photon counting
<b>TFA</b>	=	Trifluoric acid
<b>TGA</b>	=	Thioglycolic acid
<b>THF</b>	=	Tetrahydrofuran
<b>T-T</b>	=	Triplet-triplet

**UV** = Ultraviolet  
**UV-Vis** = Ultraviolet-Visible  
**VR** = Vibrational relaxation  
**XRD** = X-ray diffraction

## List of Symbols

$\alpha$	=	Fraction of light absorbed
$\epsilon$	=	Molar extinction coefficient
$h\nu$	=	Light
$I$	=	Intensity of light
$J$	=	Degree of spectral overlap of donor emission and acceptor absorbance spectra
$\kappa^2$	=	Dipole orientation factor
$\lambda_{\text{exc}}$	=	Excitation wavelength of phthalocyanines
$\lambda_{\text{max}}$	=	Wavelength maximum
$n$	=	Refractive index
${}^1\text{O}_2$	=	Singlet molecular oxygen
$\Phi_{\text{F}}$	=	Fluorescence quantum yield
$\Phi_{\text{T}}$	=	Triplet quantum yield
$r$	=	Centre to centre separation distance between donor and acceptor
$R_0$	=	Critical distance at which efficiency of energy transfer is 50 %
$\tau_{\text{D}}$	=	Singlet oxygen lifetime
$\tau_{\text{F}}$	=	Fluorescence lifetime
$\tau_{\text{T}}$	=	Triplet state lifetime
$S_0$	=	Ground singlet state
$S_1$	=	Excited singlet state

$T_1$  = First excited triplet state

$T_2$  = Second excited triplet state

## List of Figures

1.1	Quantum confinement structural features	2
1.2	A comparison of quantum dots with atoms and bulk solid state material	3
1.3	Overlapping fluorescence emission and absorption spectra of CdTe quantum dot with (i) absorption and (ii) emission	5
1.4	Size-dependent fluorescence emission of quantum dots with increasing wavelength	6
1.5	TEM images of CdSe/ZnS QDs in CHCl <sub>3</sub>	9
1.6	XRD spectrum of CdTe QDs	9
1.7	AFM image of CdTe QDs coated with TGA	10
1.8	(a) Numbering system of H <sub>2</sub> Pc and (b) $\alpha$ and $\beta$ positions on the H <sub>2</sub> Pc	12
1.9	Metallated phthalocyanine showing the covalent and partial bonds between the central metal and the nitrogen atoms	13
1.10	Structural representations of the ZnPcs studied in this work	15
1.11	Absorption spectrum of the metallated phthalocyanine with the corresponding electronic transitions showing the Q, B (Soret) and charge transfer (CT) bands	16
1.12	A modified model showing exciton splitting of the Q-band between two MPc molecules in (a) cofacial (H aggregation) and (b) edge-to-	

	edge (J aggregation)	18
1.13	Simplified Jablonski diagram showing the origin of the transitions	25
1.14	A typical fluorescence lifetime trace for a ZnPc derivative	30
1.15	Jablonski diagram showing the origins of Forster resonance energy transfer (FRET) between a donor (QD) and acceptor (Pc)	33
1.16	Spectra showing the typical decrease in QD emission intensity on the addition of Pc and the subsequent increase in the Pc emission intensity, which is expected when FRET occur	34
1.17	The triplet decay trace for silicon phthalocyanine	39
2.1	Schematic diagram of the laser-flash photolysis set-up	46
2.2	Schematic diagram of the TCSPC	47
2.3	Representation of the molecular structure of the capping agents for QDs: L-cysteine (L-cys), mercaptopropionic acid (MPA) and thioglycolic acid (TGA)	51
2.4	Setup for the synthesis of water-soluble CdTe quantum dots	52
3.1	Absorbance (a) and fluorescence (b) spectra of MPA coated CdTe in DMSO:water (9:1)	59
3.2	Vials of MPA-QDs of increasing size (a) with and (b) without UV light	59
3.3	XRD plot for CdTe-MPA capped QDs	61
3.4	Comparison of emission spectra of QDs in (i) 0.1 M	

	NaOH, (ii) DMF:water (9:1), (iii) DMSO:water (9:1) solvent mixtures and (iv) water	62
3.5	AFM images of CdTe-MPA QDs deposited on a glass surface from (A) 0.1M DMSO: water (9:1), (B) NaOH and their corresponding histograms (C and D)	63
3.6	IR spectrum of the ZnAPPc	65
3.7	Absorption spectra of ZnAPPc in DMSO at different concentrations. Inset a plot of absorbance versus concentration ( $3.4 \times 10^{-5}$ to $5 \times 10^{-5}$ M)	66
3.8	Absorbance (i), excitation (ii) and emission (iii) spectra of ZnAPPc in DMSO: water (9:1) solvent mixture (excitation wavelength = 597 nm). Concentration = $5.0 \times 10^{-5}$ M for absorption spectrum and $2.5 \times 10^{-7}$ M for fluorescence studies	67
3.9	IR spectrum of the ZnAPc	68
3.10	Absorption spectra of ZnAPc in DMSO at different concentrations. Inset a plot of absorbance versus concentration ( $1.63 \times 10^{-5}$ to $2.53 \times 10^{-5}$ M)	69
3.11	Absorbance (i), excitation (ii) and emission (iii) spectra of complex ZnAPc in DMSO (excitation wavelength = 603 nm)	70
3.12	AFM image of CdTe-MPA QDs deposited on a glass surface from QDs and ZnAPPc in DMSO:water with the corresponding histogram	72
3.13	Raman spectra of (a) ZnAPPc-CdTe-MPA QD linked,	

	(b) ZnAPPc-CdTe-MPA QD mixed, (c) ZnAPPc alone and	
	(d) CdTe-MPA QDs alone	73
3.14	(A) Ground state electronic absorption spectra and Q band position of	
	(a) CdTe-MPA QDs alone, (b) ZnAPPc alone (673 nm),	
	(c) QD:ZnAPPc-mixed (674 nm) and (d) QD-ZnAPPc-linked (678 nm)	
	in 9:1 <i>v/v</i> DMSO:water solution	
	(B) Ground state electronic absorption spectra (a) ZnAPc alone (676 nm),	
	(b) ZnAPc:QD mixed (674 nm) and (c) ZnAPc-QD linked (674 nm) and	
	(d) CdTe-MPA QDs alone in 9:1 <i>v/v</i> DMSO:water solution	74
4.1	Photoluminescence decay curves of (a) CdTe QDs and (b) CdTe QDs in	
	the presence of ZnAPc in DMSO:water (9:1) solvent mixture	80
4.2	Electronic spectrum showing the overlap between the absorption	
	spectra of the ZnAPPc and the photoemission spectra of the	
	respective QDs	84
4.3	Emission of QDs alone, ZnAPPc, QDs in the mixture with the	
	ZnAPPc or ZnAPPc linked to QD	85
4.4	Transient differential spectrum of ZnAPc in DMSO	89
4.5	Triplet decay curve of ZnAPc in DMSO at 490 nm	90

## List of Schemes

1.1	Statistical condensation of two different phthalonitriles resulting in six possible phthalocyanine products. A = dicyanobenzene and B = substituted ring	14
3.1	Synthesis of ZnAPPc derivative	64
3.2	Synthesis of ZnAPc derivative	67
3.3	Linking of a thiol capped QD to the amino group on the Pc using the coupling agent EDC/NHS	71

## List of Tables

1.1	Mixed and linked Pc derivatives	20
1.2	Fluorescence quantum yields of phthalocyanine derivatives mixed with and linked to thiol capped CdTe QDs	28
1.3	Fluorescence lifetimes and corresponding amplitude data for CdTe-thiol capped QDs using the TCSPC set-up	31
1.4	Förster resonance energy transfer (FRET) parameters for modified Pc mixed with and linked to thiol QDs	36
1.5	Triplet quantum yields of phthalocyanine derivatives mixed with thiol capped CdTe QDs	40
3.1	Emission spectral data and size determination of CdTe QDs using different methods	60
4.1	Fluorescence quantum yield parameters for ZnPc derivatives: CdTe-MPA (size = 3.85 nm) QD interaction in DMSO:water (9:1) or DMF:water (9:1) mixture for both the linked (complexes ZnAPPc and ZnAPc only) and mixed (complexes ZnAPPc, ZnAPc, ZnPc and ZnTSPc) complexes	78

4.2	Fluorescence quantum yield parameters for ZnAPPc: CdTe QD interaction in DMSO:water (9:1) mixture for both the linked and mixed complexes. ( $\lambda_{Exc} = 500$ nm)	79
4.3	Fluorescence lifetimes of QDs in the presence of ZnAPPc and ZnAPc in DMSO:water (9:1). $\lambda_{Exc} = 500$ nm unless otherwise stated	81
4.4	Fluorescence lifetimes of QDs in the presence of ZnPc derivatives in DMF:water (9:1). $\lambda_{Exc} = 500$ nm unless otherwise stated	82
4.5	Energy transfer parameters for ZnAPPc-CdTe: thiol QD interactions (in DMSO:H <sub>2</sub> O (9:1) for linked and mixed complexes)	87
4.6	Photophysical parameters of ZnPc complexes in the presence of QDs in DMSO:water or DMF:water (9:1) ( $\Phi_T$ ZnPc in DMSO = 0.65, $\Phi_T$ ZnPc in DMF = 0.56)	91

## 1. INTRODUCTION

This chapter gives an overview of the basic properties and associated characteristics of nanoparticles and metallophthalocyanines.

## 1.1 Nanoparticles

Nanoparticles are materials which have dimensions in the 1 – 100 nm range [1]. At such small sizes, the physical and chemical properties of these nanoparticles differ from their bulk counterparts [2,3], making them ideal for novel applications [4-11]. Nanomaterials can be tailored to have properties that make them ideal for various applications. For semiconducting materials, at such tiny dimensions, electrons become confined such that the quantization of electron energies becomes significant. If the confinement takes place in one dimension the structures are referred to as quantum wells; if confinement is in two dimensions, the structures are called quantum wires and if there is confinement of the electron in all three dimensions then the structures are known as quantum dots, Figure 1.1 [12]. This work will be focusing on the study of quantum dots.

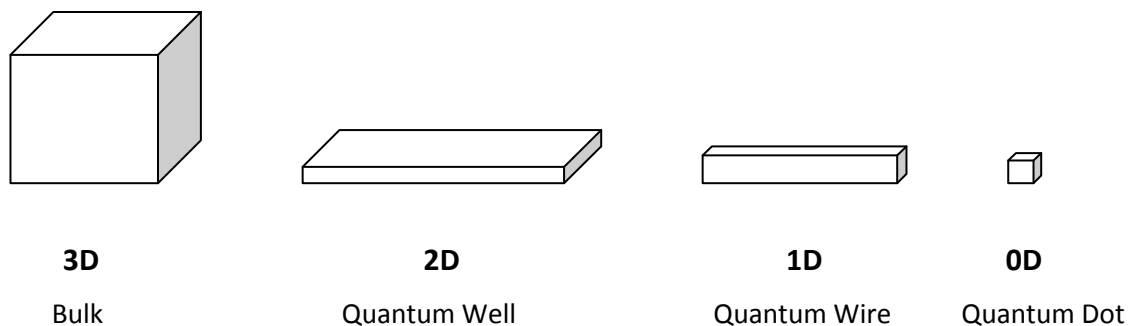


**Figure 1.1: Quantum confinement structural features [12].**

Quantum dots (QDs) are semiconducting nanoparticles approximately 2-10 nm in diameter, and composed of group II-VI (2-6), III-V (3-5) or IV-VI (4-6) elements [6,13,14].

Properties of these semiconducting nanoparticles fall between the bulk material and atoms.

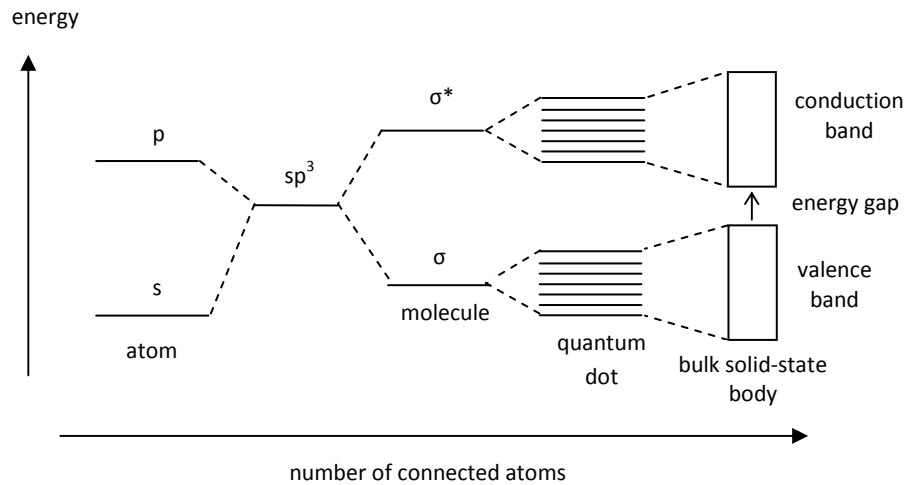


**Figure 1.2: A comparison of quantum dots with atoms and bulk solid state material [8].**

QDs have distinct energy levels unlike bulk semiconducting materials which have conduction and valence bands, Figure 1.2 [8]. The energy levels are separated by a band gap and when sufficient energy is supplied electrons are excited across this gap. The space left behind is referred to as a hole and the electron-hole pair is called an exciton pair, with the distance between the hole and the electron is known as the exciton Bohr radius. This is important because at such small sizes, the diameter of the quantum dots is of the same magnitude as the exciton Bohr radius, which means that the size of

the quantum dot directly affects the band gap and its associated energies, and hence its colour, thereby giving quantum dots their characteristic properties.

QDs are known to have high photostability, broad absorption spectra and narrow emission ranges, such that light of the correct wavelength causes simultaneous excitation (fluorescence) of various sizes of QDs [15]. These unique properties make QDs highly versatile and attractive in many disciplines such as physics, chemistry, biology and medicine [16]. This work will be focusing on cadmium telluride (CdTe) QDs which have extended optical properties that overlap well with the phthalocyanines also used in this work.

### **1.1.1 Absorption and fluorescence spectra of QDs**

As mentioned previously, the size of the QDs directly affects the band gap and therefore the absorption spectra. The smaller QDs have a larger band gap and hence exhibit a blue shifted absorption spectrum. The opposite occurs for the larger sized QDs. The absorption spectrum is dependent on a number of factors such as crystalline defects, concentration and size distribution of the QDs, as well as environmental factors such as the solvent and pH. The absorption spectrum of QDs is typically broad while the emission spectrum is narrow as shown in Figure 1.3 [17].

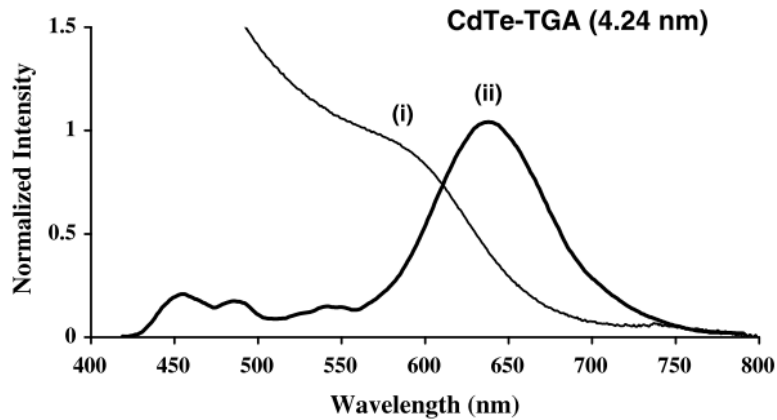


**Figure 1.3: Overlapping fluorescence emission and absorption spectra of CdTe quantum dot with (i) absorption and (ii) emission [17].**

The position of the fluorescence peak is directly related to the average size of the QDs in the sample [18,19], while the full width at half maximum of the fluorescence spectrum provides information on the size distribution. The absorbance and fluorescence emission of QDs can be tuned to span the wavelength range of 400 - 2000 nm by simply altering the size of QDs, Figure 1.4.

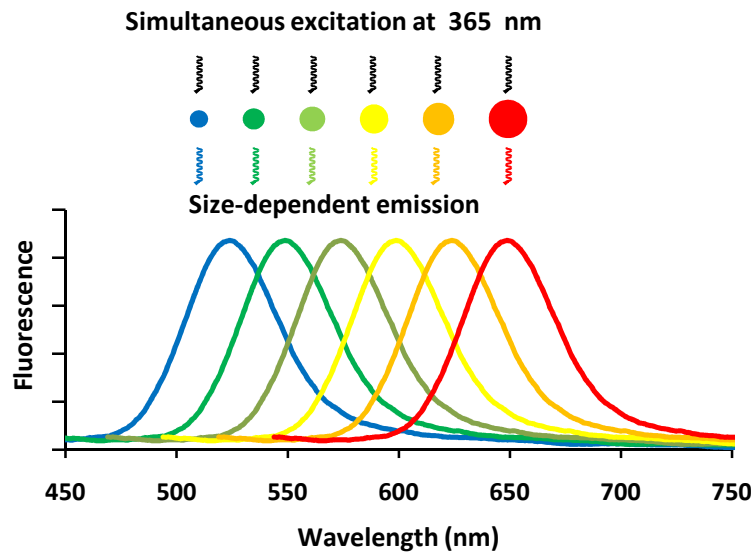


**Figure 1.4: Size-dependent fluorescence emission of quantum dots with increasing wavelength.**

Fluorescence emission of colloidal QDs have been known to exhibit a dramatic on/off behaviour known as 'blinking' [5,6]. This behaviour is believed to occur when two electron-hole pairs are present simultaneously inside the QD. The release of energy from the annihilation of one electron-hole pair is transferred to the other pair, and the resultant excess energy may cause the ejection of one of the charge carriers into the environment of the QD, leaving it charged. If another exciton is produced in this time, the energy from its recombination is transferred non-radiatively to the third carrier so that there is no emission. The QD's radiative emission is restored when the ejected carrier returns inside the QD, or if the QD is neutralized [8]. This process of blinking is referred to as the Auger process [3]. The organic capping of the QDs aid in electronic

passivation by terminating the dangling bonds on the surface of the QDs. These dangling bonds can trap electrons at the surface before they have a chance to emit a photon.

CdTe QDs capped with thiols are known to aggregate in acidic conditions due to detachment of surface ligands [20,21]. Aggregation of QDs results in red shifting in the emission spectra accompanied by broadening. Some aggregation of nanocrystals in organic media have also been reported [22], hence there is an importance in studying the aggregation behaviour of QDs in different solvents employed in this work.

### **1.1.2 Synthesis of water-soluble CdTe colloidal nanoparticles**

In order to be able to use colloidal QDs for biological purposes, QDs need to be water soluble for biocompatibility, non-toxic, easily disposed of by the body, and easily localized to the target cells. The surface of the QDs can be relatively easily modified to alter the functionality of the nanoparticles for various purposes. The large surface area to volume ratio of the QDs further enhances the effect of the functional groups. Examples of aqueous capping agents include the thiol groups 2-mercaptoethanol, 1-thioglycerol, 2,3-dimercapto-1-propanol, thioglycolic acid (TGA), 2-mercaptoethylamine (MA), mercaptopropionic acid (MPA), L-cysteine (L-cys) and 2-(dimethylamino)ethanethiol [23]. More sophisticated cappings have also been used, such as oligomeric phosphines or dendrons [4]. The use of thiol groups is the most

common in the laboratory synthesis of CdTe QDs since the sulphur groups are known to bind effectively to the cadmium atoms.

Parameters such as temperature, atmosphere, pH of the solution, duration of synthesis, and the relative proportions of substrates added as well as appropriate cappings, affect the quantity, quality and size distribution of the nanoparticles synthesized [23-25]. In short, a thiol capping agent is added to a solution of cadmium chloride dissolved in water and the pH of the solution is adjusted by the addition of basic sodium hydroxide. Under inert conditions, sodium hydrogen telluride is added to the basic media resulting in nucleation of the QDs. This is then left to reflux until the desired size of the CdTe QDs is obtained. After cooling, the QDs are precipitated out of solution using excess ethanol and then centrifuged to harvest the QDs.

### **1.1.3 Characterization of nanoparticles**

From literature, there are several methods of analyzing and characterizing nanoparticles. These include UV-vis spectra as discussed before (Section 1.1.1). This method is the most commonly and extensively used analytical technique, and has been well documented. Transmission electron microscopy (TEM) and high resolution TEM (HRTEM) have also been used in order to determine size, shape and atomic structure of the nanoparticles as seen in Figure 1.5 [26-29]. The disadvantage of this technique is the method of sample preparation which can lead to QD aggregation - resulting in inaccurate results.

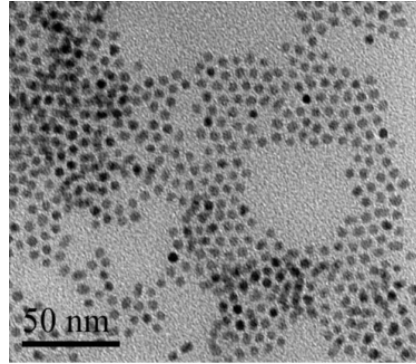


**Figure 1.5:** TEM images of CdSe/ZnS QDs in CHCl<sub>3</sub> [26].

X-Ray Diffraction (XRD) is used to deduce the size of QDs. The particle diameter,  $d$ , is determined using the Scherrer Equation (1.1):

$$d(\text{\AA}) = \frac{k\lambda}{\beta \cos\theta} \quad (1.1)$$

where  $k$  is an empirical constant equal to 0.9,  $\lambda$  is the wavelength of the X-ray source (1.5405 Å),  $\beta$  is the full width at half maximum of the diffraction peak, and  $\theta$  is the angular position of the peak. The typical XRD spectrum for QDs is shown in Figure 1.6 [27,29,30].

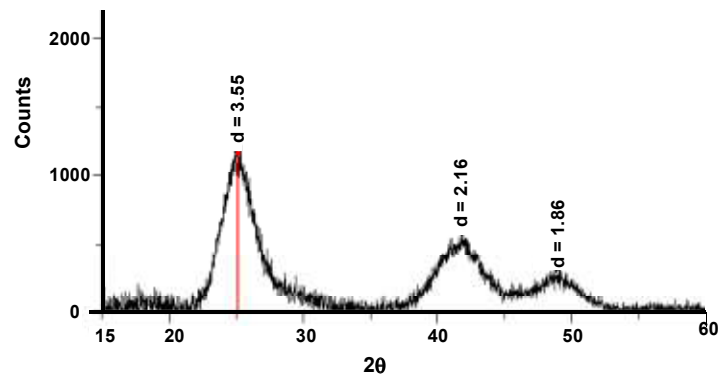


**Figure 1.6:** XRD spectrum of CdTe QDs [30].

Atomic force microscopy (AFM) gives the distribution of nanoparticles and relative sizes as seen in Figure 1.7 [15].

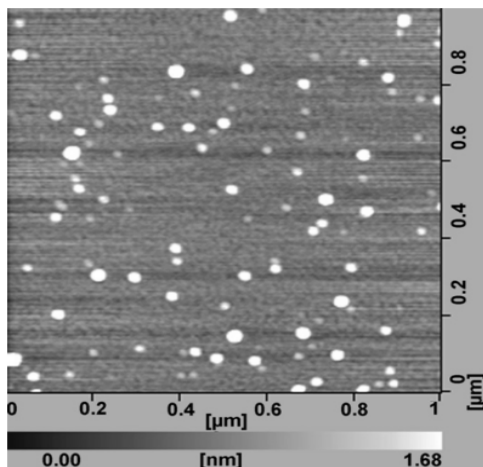


**Figure 1.7:** AFM image of CdTe QDs coated with TGA [15].

The above methods are used in this thesis to characterize QDs. Other methods which have been employed in literature include X-ray photoelectron spectroscopy (XPS) [31-33], infra-red spectroscopy (IR) [28,34,35].

## 1.2 Phthalocyanine (Pc) chemistry

### 1.2.1 The history and structure of phthalocyanines

Phthalocyanines (Pc) were discovered accidentally in 1907 during the synthesis of o-cyanobenzamide by Braun and Tscherniak [36]; but it was not until the industrial discovery in 1928 that further experiments were carried out. After this it was soon

realised that these products could be used as colorants [37]. The molecular structure of phthalocyanines was proposed by Linstead and co-workers, who went on to develop improved synthetic methods for several metal phthalocyanines (MPcs) from 1929 to 1939 [38]. The structure was later confirmed by x-ray structure determination by Robertson. During the 1930's and 1950's the chemical and physical properties of phthalocyanines were thoroughly investigated [37,39-41]. As a result of their insolubility (allowing for fixation to materials) and durability against light, heat and chemicals which can cause fading [42], CuPcs became popular for use as pigments in printing inks, paints and for colouring plastics. Pcs are also very useful in the dyeing of textiles, paper, leather, textile printing or the manufacture of high-quality inks (used in ballpoint pens and ink jets) [37].

Phthalocyanines also have potential for application in many other areas such as in electrophotography, chemical sensors, liquid crystals, nonlinear optics, optical data storage and as carrier generation materials in near-IR devices [43-46]. Water soluble phthalocyanines have also been used as photosensitisers and for use in photodynamic therapy (PDT) [47-49], due to their strong absorption in the red (Q-band) which overlaps with the region of maximum light penetration in tissues [50]. PDT is a method of cancer treatment which requires a sensitizing agent, light energy and oxygen, the combination of which results in the production of singlet oxygen and eventually cell death [47].

The basic unmetallated structure of the Pc consists of four isoindole subunits as seen in Figure 1.8 (a) and is generally known as H<sub>2</sub>Pc. The protons on the peripheral benzene rings can be substituted with various groups on either the peripheral ( $\alpha$ ) or non-peripheral ( $\beta$ ) positions, Figure 1.8 (b). The addition of appropriate functional groups allows for the fine tuning of the physical, chemical and electronic properties of the Pc [42].

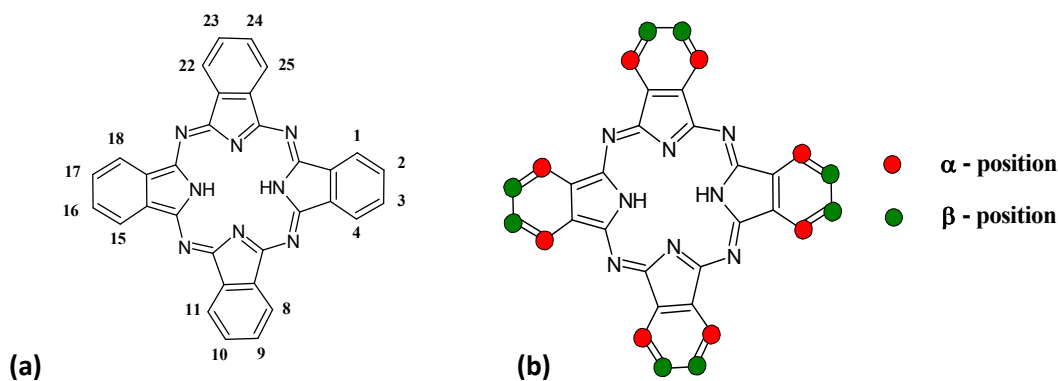


**Figure 1.8: (a) Numbering system of H<sub>2</sub>Pc and (b)  $\alpha$  and  $\beta$  positions on the H<sub>2</sub>Pc.**

A variety of metals can be introduced into the centre of the Pc ring forming two partial bonds with opposing nitrogen atoms. If the Pc is substituted on all the  $\alpha$  or  $\beta$  positions, the Pc is referred to as octa-substituted and if the Pc is substituted on only one position, at either the alpha or the beta positions, then the Pc is known as tetra-substituted. MPcs possess high thermal stability due to both the interlinking nitrogen atoms [51] and an extended  $\pi$  conjugated system [52], Figure 1.9.

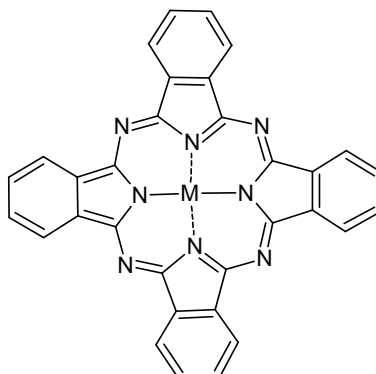
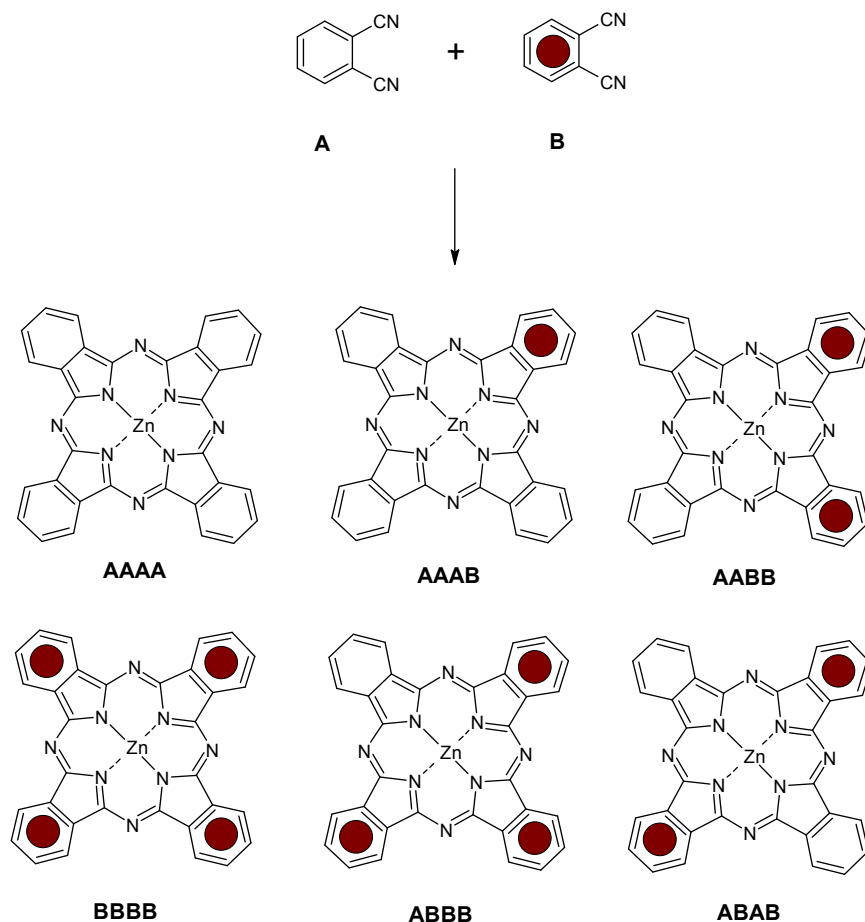


**Figure 1.9: Metallated phthalocyanine showing the covalent and partial bonds between the central metal and the nitrogen atoms.**

### 1.2.2 Synthesis of low-symmetry A<sub>3</sub>B type phthalocyanines

In recent years there has been increasing interest in low symmetry MPc derivatives, which can provide the unique sets of properties required for use in specific practical applications. The presence of different functional groups in the same molecule provides coexistent features which enable better control over the molecule. The design of these low symmetry complexes has become the focus of intense interest amongst many phthalocyanine researchers [30,42,53-56].

Unsymmetrical Pcs can be synthesised using the method of statistical condensation whereby two differently substituted isoindoles or phthalonitriles are used, and their reaction is shown in Scheme 1.1. In principle this reaction produces a mixture of six compounds which requires lengthy chromatographic techniques for their isolation [42].



**Scheme 1.1: Statistical condensation of two different phthalonitriles resulting in six possible phthalocyanine products. A = dicyanobenzene and B = substituted ring [42].**

The reason for a 3 : 1 molar ratio is due to statistical considerations which predict, for two different phthalonitrile derivatives of similar reactivity, a mixture of products in the following percentages:  $A_4$  (33%),  $A_3B$  (44%) and the remaining cross-condensation products (23%), thus producing the unsymmetrical phthalocyanine as the major product. In cases where the reactivity of A and B differ, the molar ratios of A:B can be modified. For example in a case where B is much more reactive than A, a molar ratio of

9:1 (A:B) or higher may be used; although an increase in the amount of A<sub>4</sub> occurs, reducing the number of products with more than one B subunit.

Chromatographic separation of the resultant phthalocyanines can be difficult due to the enormous tendencies of these molecules towards aggregation. Substitution at the  $\beta$  position in Figure 1.8b and the use of bulky or rigid groups as substituents on phthalocyanines have resulted in easier chromatographic separation [42]. For the purposes of this work, focus is given to the A<sub>3</sub>B type phthalocyanines with the synthesis of novel zinc monoaminophenoxy phthalocyanine (ZnAPPc) and zinc monoamino (ZnAPc) phthalocyanines, Figure 1.10. The carboxy or amino groups of the monofunctionalized phthalocyanines are capable of covalently binding to biological targeting agents, such as monoclonal antibodies or lipoproteins, which direct the sensitizer to the tumour, without affecting the normal tissue. This provides an additional level of selectivity allowing for defined coordination.

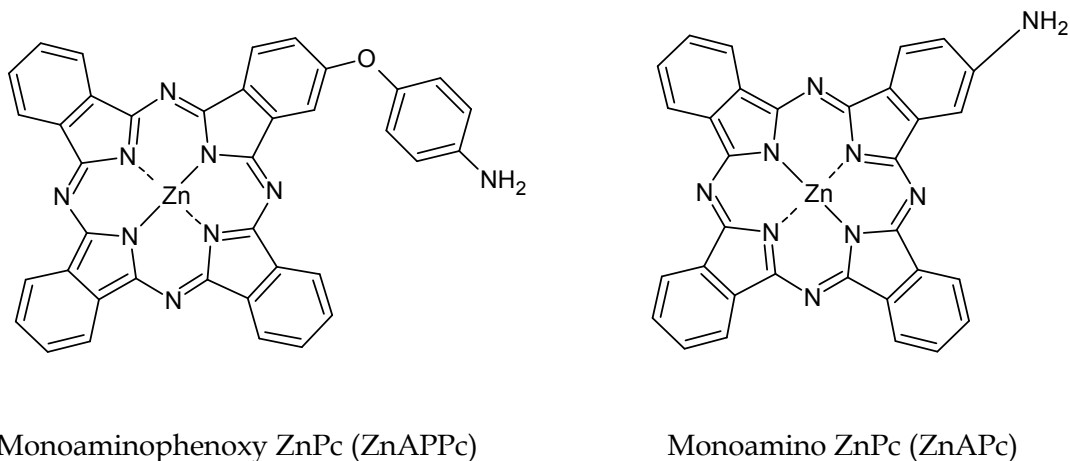


**Figure 1.10: Structural representations of the ZnPcs studied in this work.**

### 1.2.3 Ground state electronic absorption spectra of phthalocyanines

The absorption bands associated with phthalocyanines are derived from the electronic transitions between occupied bonding ( $\pi$ -states) and empty anti-bonding ( $\pi^*$ -states), resulting in two main types of absorption, the Q and B bands (Figure 1.11) [44]. Figure 1.11 shows the typical absorption spectrum of the metallated phthalocyanine in blue, and the absorption of the unmetallated phthalocyanine in red. The unmetallated Pc exhibits a split Q band as a result of a degenerate LUMO ( $e_g$ ) due to the unsymmetrical nitrogen atoms in the centre of the ring.

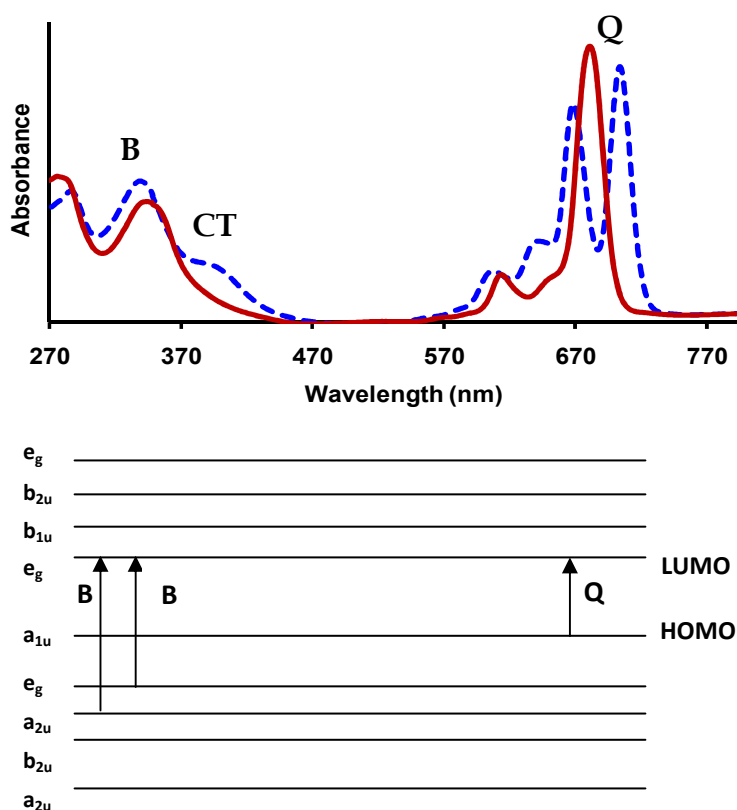


Figure 1.11: Absorption spectrum of the metallated phthalocyanine with the corresponding electronic transitions showing the Q, B (Soret) and charge transfer (CT) bands [44].

### 1.2.4 Phthalocyanine aggregation

Phthalocyanine aggregation is a result of co-planar association of the Pc rings driven by non-bonded attractive interactions, starting with the monomer and progressing to the dimer and higher order complexes [57]. Pcs commonly exhibit H-aggregation, and in rare cases J-aggregation, Figure 1.12. H-aggregation results in a blue shifted band with respect to the Q-band absorption spectra and is a result of linear stacking of the coplanar monomers (cofacial). J-aggregation ('J' presumably for Jelly, one of the first workers to investigate this red shifted band [57]) is caused by the end to end, non-cofacial coupling of Pcs resulting in a red shifted band with respect to the Q-band of the monomer.

Kasha's exciton coupling theory explains that the appearance of four degenerate states occurs when adjacent MPc complexes interact due to the splitting of the excited states; this is illustrated in Figure 1.12 [58]. This results in two symmetry allowed transitions (solid arrows) and two symmetry forbidden transitions (dashed arrows). These forbidden transitions only occur to a small extent. Aggregation is strongly affected by the solvent used and polar solvents are known to enhance the aggregation effect [59,60]. The use of less polar solvents or surfactants, such as Cremophore EL is known to improve the disaggregation of phthalocyanines.

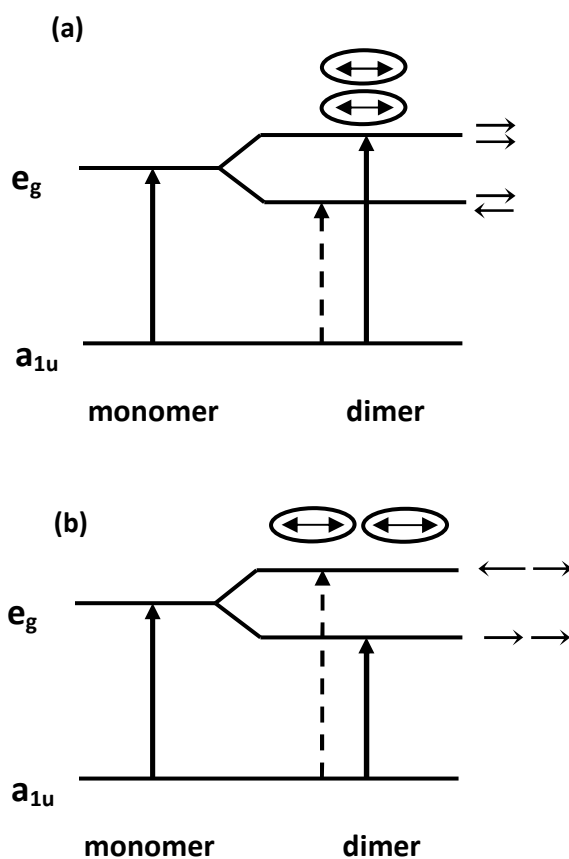


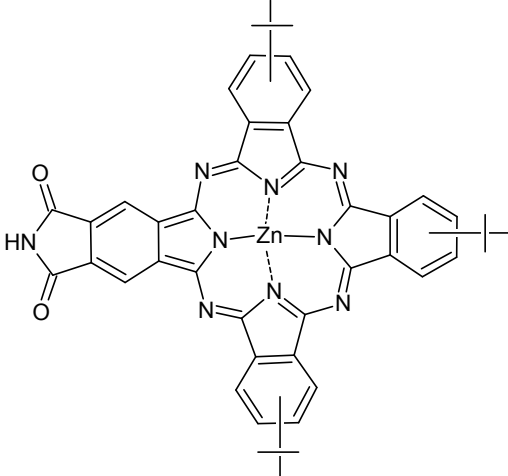
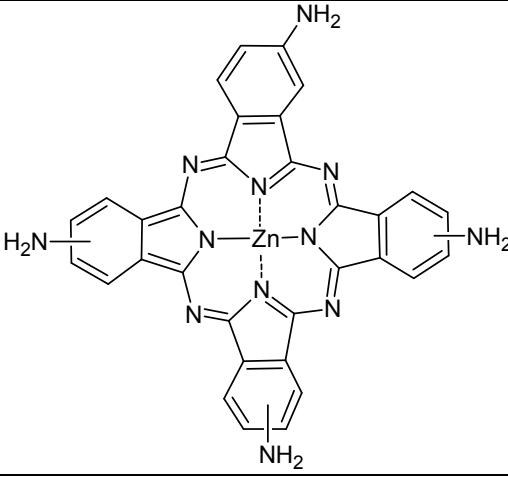
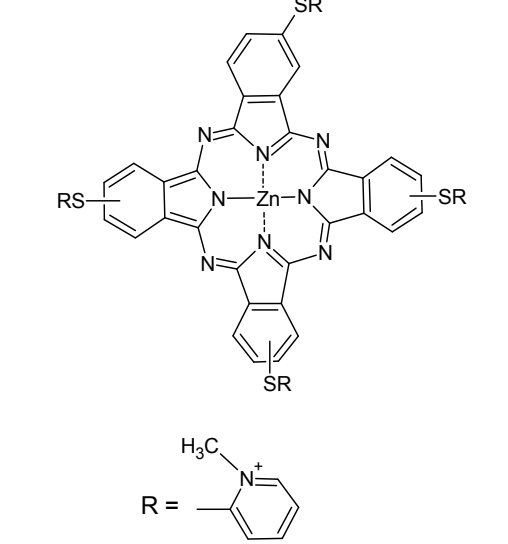
Figure 1.12: A modified model showing exciton splitting of the Q-band between two MPc molecules in (a) cofacial (H aggregation) and (b) edge-to-edge (J aggregation). The solid vertical arrows represent allowed transitions, the dashed vertical arrows represent the forbidden transitions and the horizontal arrows represent the phase transitions. The monomer and dimer ground states are placed at the same energy level for simplicity [60].

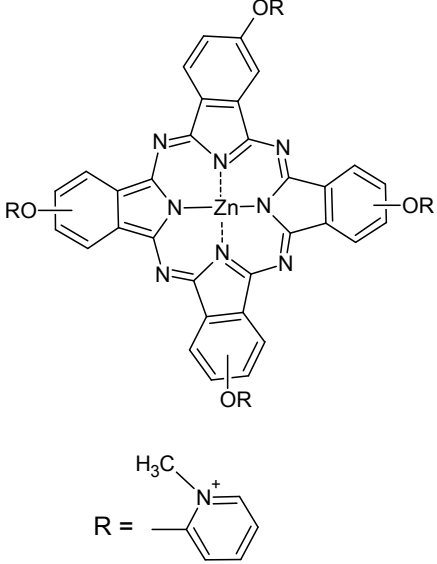
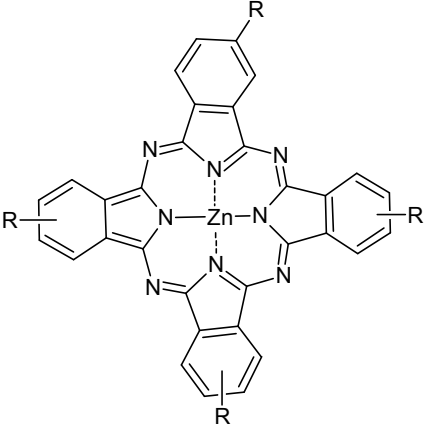
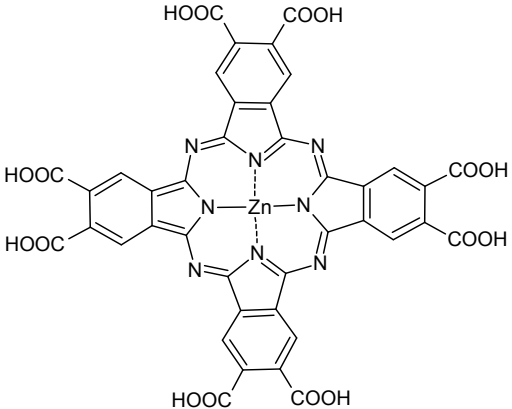
### 1.2.5 The interaction of mixed and linked MPc - QD conjugates

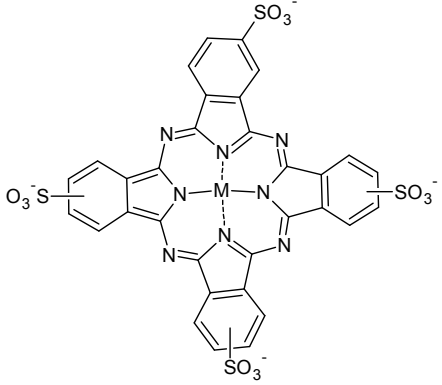
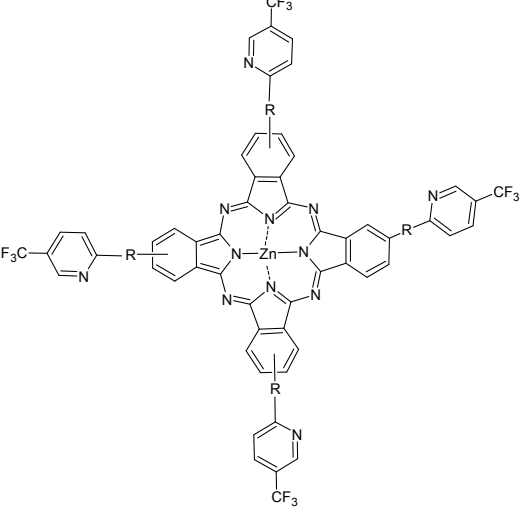
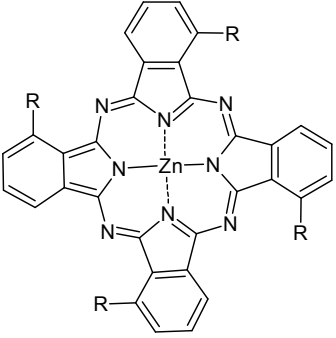
QDs have unique photophysical and chemical properties which can be relatively easily manipulated, allowing for a wide range of applications. Their high fluorescence intensity, important for bioimaging [4,7], and large surface area which is important for targeting specific markers in the body, make QDs ideal candidates for PDT purposes. As such, QDs have been mixed with Pcs in the hope of improving their properties for PDT purposes [5,9,61]. The disadvantage of mixing, however, is the lack of guarantee that both the QDs and Pcs are in the cancerous cells at the same time. In order to overcome this problem QDs are linked to the Pcs in this thesis.

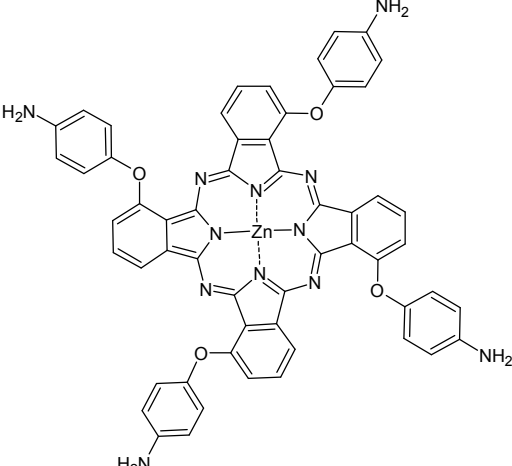
Table 1.1 shows the QDs and Pcs which have been mixed and linked together [30,62-68]. One has to note that since these Pcs are tetra-substituted, the position and number of QDs which attach are not well defined. As a result, this thesis focuses on mono-substituted Pcs. In this work the behaviour of unsymmetrical ZnPcs is compared with that of ZnSPc and ZnPc derivatives which are well known.

Table 1.1: Mixed and linked Pc derivatives

Pc Structure	Pc Name	QD-capping	Ref.
	Tris[9(10),16(17),23(24)- <i>tert</i> -butyl]imidophthalocyaninato zinc (II) (ZnttbIPc)	CdTe-MPA Mixed and linked	[30]
	Zinc tetraamino phthalocyanine (ZnTAPc)	CdTe-MPA Mixed and linked	[62]
	[Tetramethyl-2,(3)-[[tetra-(2-mercaptopyridine phthalocyaninato)]zinc(II)] <sup>4+</sup> (TmTMPyZnPc)	CdTe-TGA CdTe-MPA Mixed	[63]

Pc Structure	Pc Name	QD-capping	Ref.
	<p>[Tetramethyl-2,3]-[tetra-(2-pyridyloxy phthalocyaninato)] zinc(II)]<sup>4+</sup> (TmTPyZnPc)</p>	<p>CdTe-TGA CdTe-MPA Mixed</p>	<p>[63]</p>
 <p>(a) R = SO<sub>3</sub>Na (b) R = COOH</p>	<p>(a) Zinc tetrasulfo phthalocyanine (ZnTSPc) (b) Zinc tetracarboxy phthalocyanine (ZnTCPC)</p>	<p>CdTe-TGA CdTe-2-ME Mixed</p>	<p>[64]</p>
	<p>Zinc octacarboxyphthalocyanine (ZnOCPc)</p>	<p>CdTe-TGA CdTe-2-ME Mixed</p>	<p>[64]</p>

Pc Structure	Pc Name	QD-capping	Ref.
 <p style="text-align: center;">M = Zn, Al(OH), Si(OH)<sub>2</sub>, Ge(OH)<sub>2</sub></p>	Zinc tetrasulfophthalocyanine (ZnTSPc) Aluminium tetrasulfophthalocyanine ((OH)AlTSPc) Silicon tetrasulfophthalocyanine ((OH) <sub>2</sub> SiTSPc) Germanium tetrasulfophthalocyanine ((OH) <sub>2</sub> GeTSPc)	CdTe-MPA CdTe-TGA Mixed	[65]
 <p style="text-align: center;">(a) R = S      (b) R = O</p>	(a) 4-(Tetrakis-5-(trifluoromethyl)-2-mercaptopyridinephthalocyaninato]-phthalonitrile (TfmMPyZnPc) (b) 4-(Tetrakis-5(trifluoromethyl)-2-pyridyloxyphthalocyaninato) zinc(II) (TfmPyZnPc)	CdTe-MPA Mixed	[66]
 <p style="text-align: center;">R = NH<sub>2</sub></p>	(a) tetra(α-amino) zinc phthalocyanine (ZnPc <sup>α</sup> (NH <sub>2</sub> ) <sub>4</sub> ) (b) tetra(β-amino) zinc phthalocyanine (ZnPc <sup>β</sup> (NH <sub>2</sub> ) <sub>4</sub> )	-	[67]

Pc Structure	Pc Name	QD-capping	Ref.
	(Tetra- <i>p</i> -aminophenoxyphthalocyaninato) zinc(II) $ZnPc^{\alpha}(PhNH_2)_4$ (Ph=phenyl)	-	[68]

### 1.3 Photophysical properties

The photophysical behaviour of phthalocyanines will be studied when linked or mixed with QDs and the parameters to be studied are the triplet quantum yields, the triplet lifetimes, fluorescence quantum yields and fluorescence lifetimes. The Jabłoński diagram, Figure 1.13, shows the absorption of energy and subsequent processes which occur. Following absorption and population of the  $S_1$  state, several routes that can be followed by the electron are: it can relax back to the ground state by releasing a photon resulting in fluorescence (F), it can undergo radiationless, vibrational relaxation (VR) back to the ground state, or inter-system crossing (ISC) to the first triplet state,  $T_1$ . This may be followed by internal conversion (IC) and phosphorescence (P) back to the  $S_1$  state. White light may be used to further excite the electron from  $T_1$  to vibrational levels in the  $T_2$  state. In this work T-T absorption will be studied in order to determine the

triplet quantum yields and lifetimes. It is the  $T_1$  state which is involved in photosensitization.

Normally the transition from the singlet ( $S_1$ ) to the triplet state ( $T_1$ ) is spin-forbidden due to the change in spin of the outermost electrons in a complex, as shown in Figure 1.13; from the anti-parallel pair of electrons in the singlet state to the parallel pair of electrons in the triplet state. The spin-forbidden transitions are overcome by coupling the spin with the orbital angular momenta, known as spin-orbit coupling, which relaxes the spin selection rule [69-71]. In general, spin-forbidden transitions are weaker than spin-allowed transitions; however the intensity of the spin-forbidden transitions increases with an increase in the atomic number of the atom in the complex, a phenomenon known as the 'heavy-atom' effect [69,71], which enhances spin-orbit coupling. As a result of this, heavy atoms such as zinc increase ISC, improving triplet quantum yields.

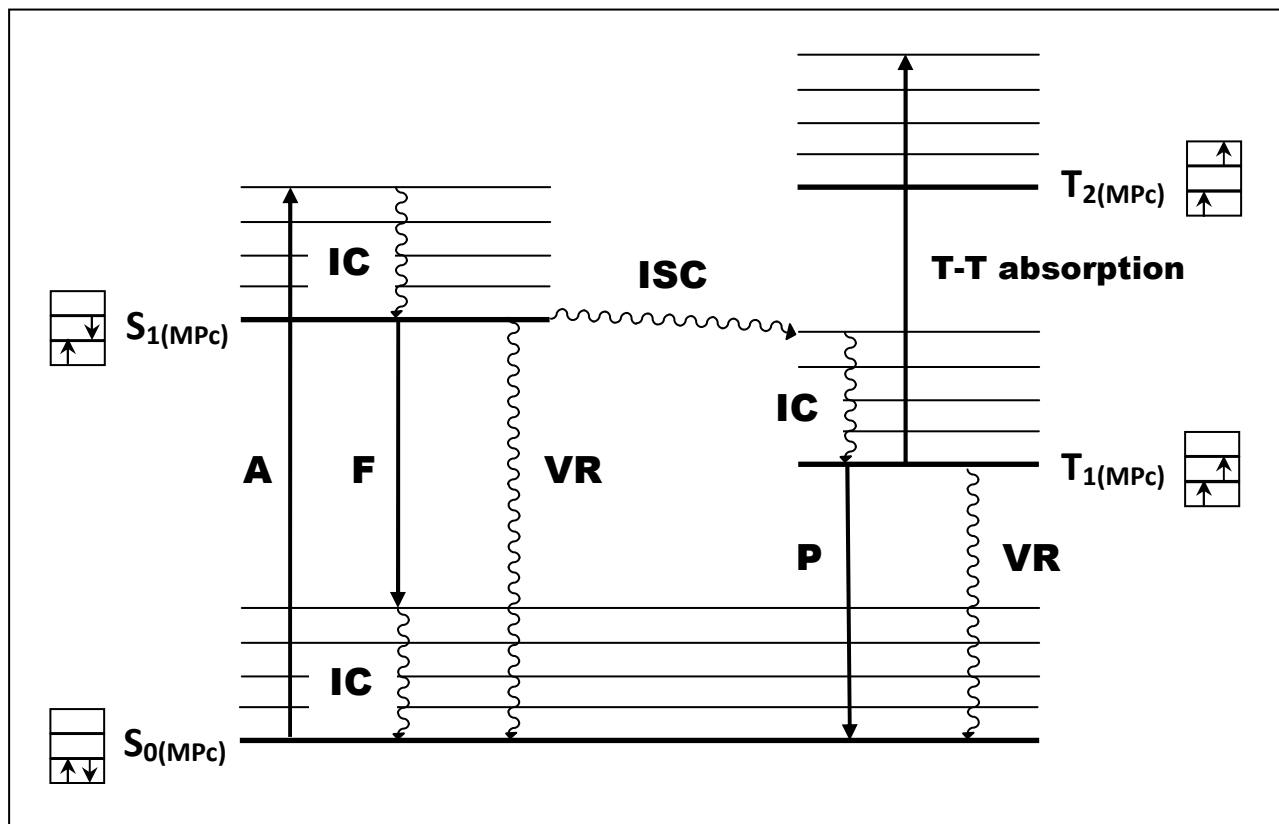


Figure 1.13: Simplified Jablonski diagram showing the origin of the transitions. A = absorption, IC = internal conversion, F = fluorescence, VR = vibrational relaxation, ISC = inter-system crossing, P = phosphorescence, T-T absorption = triplet to triplet absorption.  $S_0$  = singlet ground state,  $S_1$  = first singlet excited state,  $T_1$  = first triplet excited state,  $T_2$  = second triplet excited state.

### 1.3.1 Fluorescence quantum yields and lifetimes

The fluorescence quantum yield ( $\Phi_F$ ) is defined as the number of photons emitted relative to the number of photons absorbed, as shown in Equation (1.2)

$$\Phi_F = \frac{\text{number of photons emitted}}{\text{number of photons absorbed}} \quad (1.2)$$

Fluorescence quantum yields and lifetimes depend on a number of factors such as the central metal, the nature of the substituents and the refractive indices of the solvents, as well as the pH and temperature.

Fluorescence quantum yields ( $\Phi_F$ ) of Pcs and QDs may be determined by the comparative method [72] Equation (1.3),

$$\Phi_F = \Phi_{F(\text{Std})} \frac{F \cdot A_{\text{Std}} \cdot n^2}{F_{\text{Std}} \cdot A \cdot n_{\text{Std}}^2} \quad (1.3)$$

where  $F$  and  $F_{\text{Std}}$  are the areas under the fluorescence curves of the QDs or Pc and the reference respectively.  $A$  and  $A_{\text{Std}}$  are the absorbances of the sample and reference at the excitation wavelength respectively, and  $n$  and  $n_{\text{Std}}$  are the refractive indices of solvents used for the sample and reference, respectively. For ZnPc derivatives, unsubstituted ZnPc in dimethyl sulfoxide,  $\Phi_F = 0.2$  [73] and in dimethylformamide,  $\Phi_F = 0.3$  [73] was employed as a standard in this thesis, while rhodamine 6G in ethanol with  $\Phi_F = 0.94$  was employed as the standard for the quantum dots [74,75]. The determined fluorescence quantum yield values of the QDs are then used in determining their

fluorescence quantum yields in the mixture with the ZnPc derivative ( $\Phi_{F(QD)}^{Mix}$ ) or in the linked sample,  $\Phi_{F(QD)}^{linked}$ , using Equations (1.4a) and (1.4b)

$$\Phi_{F(QD)}^{Mix} = \Phi_{F(QD)} \frac{F_{QD}^{Mix}}{F_{QD}} \quad (1.4a)$$

$$\Phi_{F(QD)}^{linked} = \Phi_{F(QD)} \frac{F_{QD}^{linked}}{F_{QD}} \quad (1.4b)$$

where  $\Phi_{F(QD)}$  is the fluorescence quantum yield of the QDs alone and may be used as standard,  $\Phi_{F(QD)}^{Mix}$  (or  $\Phi_{F(QD)}^{linked}$ ) is the fluorescence intensity of QDs, in the mixture (or linked) with the ZnPc derivative when excited at the excitation wavelength of the QDs, and  $F_{QD}$  is the fluorescence intensity of the QD alone at the same excitation wavelength.

Fluorescence is affected by the surface structures of the QDs as well as the occurrence of charge carrier traps [76] and is thus dependent on the QD size and quality, as shown in Table 1.2. There is a decrease of the QD fluorescence quantum yields ( $\Phi_{F(QD)}$ ) on addition of the phthalocyanine ( $\Phi_{F(QD)}^{Mix}$ ), and a further decrease in fluorescence quantum yield when the Pcs are linked to the QDs ( $\Phi_{F(QD)}^{linked}$ ). In this work monoamino ZnPc is employed; the effects of the QD capping agents on the fluorescence quantum yield values in the presence of Pcs is determined and compared with similar Pcs in Table 1.2 [30,62-66,77].

**Table 1.2: Fluorescence quantum yields of phthalocyanine derivatives mixed with and linked to thiol capped CdTe QDs. See Table 1.1 for complex abbreviations.**

<b>Pc derivatives + QD-capping</b>	<b>QD size (nm)</b>	$\Phi_{F(QD)}$	$\Phi_{F(QD)}^{Mix}$	$\Phi_{F(QD)}^{linked}$	<b>Ref.</b>
ZnttbIPc + CdTe-MPA	3.5	0.09	0.04	0.02	[30]
TmTMPyZnPc/ TmTPyZnPc + CdTe-MPA	4.19	0.21	< 0.21	-	[62]
TmTMPyZnPc/ TmTPyZnPc + CdTe-TGA	4.09	0.12	< 0.12	-	[63]
ZnTSPc + CdTe-TGA	4.2	0.11	0.014	-	[64]
ZnTSPc + CdTe-2-ME	3.3	0.037	0.011	-	[64]
ZnTCPc + CdTe-TGA	4.2	0.11	0.06	-	[64]
ZnTCPc + CdTe-2-ME	3.3	0.037	0.017	-	[64]
ZnOCPc + CdTe-TGA	4.2	0.11	0.018	-	[64]
ZnOCPc + CdTe-2-ME	3.3	0.037	0.012	-	[64]
ZnTSPc + CdTe-MPA1	2.3	0.19	0.17	-	[65]
ZnTSPc + CdTe-MPA2	3.6	0.59	0.33	-	[65]
ZnTSPc + CdTe-TGA1	3.2	0.30	0.12	-	[65]
ZnTSPc + CdTe-TGA2	3.7	0.62	0.45	-	[65]
(OH)AITSPc + CdTe-MPA1	2.3	0.19	0.17	-	[65]
(OH)AITSPc + CdTe-MPA2	3.6	0.59	0.45	-	[65]
(OH)AITSPc + CdTe-TGA1	3.2	0.30	0.27	-	[65]
(OH)AITSPc + CdTe-TGA2	3.7	0.62	0.49	-	[65]
(OH) <sub>2</sub> SiTSPc + CdTe-MPA1	2.3	0.19	0.18	-	[65]
(OH) <sub>2</sub> SiTSPc + CdTe-MPA2	3.6	0.59	0.25	-	[65]
(OH) <sub>2</sub> SiTSPc + CdTe-TGA1	3.2	0.30	0.09	-	[65]
(OH) <sub>2</sub> SiTSPc + CdTe-TGA2	3.7	0.62	0.32	-	[65]

Pc derivatives + QD-capping	QD size (nm)	$\Phi_{F(QD)}$	$\Phi_{F(QD)}^{Mix}$	$\Phi_{F(QD)}^{linked}$	Ref.
(OH) <sub>2</sub> GeTSPc + CdTe-MPA1	2.3	0.19	0.17	-	[65]
(OH) <sub>2</sub> GeTSPc + CdTe-MPA2	3.6	0.59	0.32	-	[65]
(OH) <sub>2</sub> GeTSPc + CdTe-TGA1	3.2	0.30	0.07	-	[65]
(OH) <sub>2</sub> GeTSPc + CdTe-TGA2	3.7	0.62	0.37	-	[65]
TtfmMPyZnPc + CdTe-MPA	4.54	0.22	0.15	-	[66]
TtfmPyZnPc + CdTe-MPA	4.54	0.22	0.12	-	[66]
ZnPc <sup>α</sup> (NH <sub>2</sub> ) <sub>4</sub>	-	0.0011 <sup>a</sup>	-	-	[67]
ZnPc <sup>β</sup> (NH <sub>2</sub> ) <sub>4</sub>	-	0.0043 <sup>a</sup>	-	-	[67]
ZnPc <sup>α</sup> (PhNH <sub>2</sub> ) <sub>4</sub>	-	0.0020 <sup>a</sup>	-	-	[68]
ZnTAPc + CdTe-MPA	3.0	0.16	0.042	0.011	[77]
ZnTAPc + CdTe-MPA	3.3	0.047	0.040	0.017	[77]
ZnTAPc + CdTe-MPA	3.2	0.070	0.023	0.021	[77]

<sup>a</sup> fluorescence quantum yield of the phthalocyanine alone ( $\Phi_{F(Pc)}$ )

Fluorescence lifetimes ( $\tau_F$ ) were obtained by deconvolution of the decay curves, obtained by time correlated single photon counting (TCSPC). A typical fluorescence lifetime trace is shown in Figure 1.14 [30]. The trace can either have biexponential decay with two lifetimes, suggesting the sample in this case is comprised of two components, or multiexponential decay, with more than two lifetimes. Each lifetime has an amplitude value attributed to it, showing the percentage abundance of each component/lifetime within the sample. Accompanying the fitted decay curve is the line of best fit, indicating the residuals lie close to zero and thus implying the data is well fitted to the model.

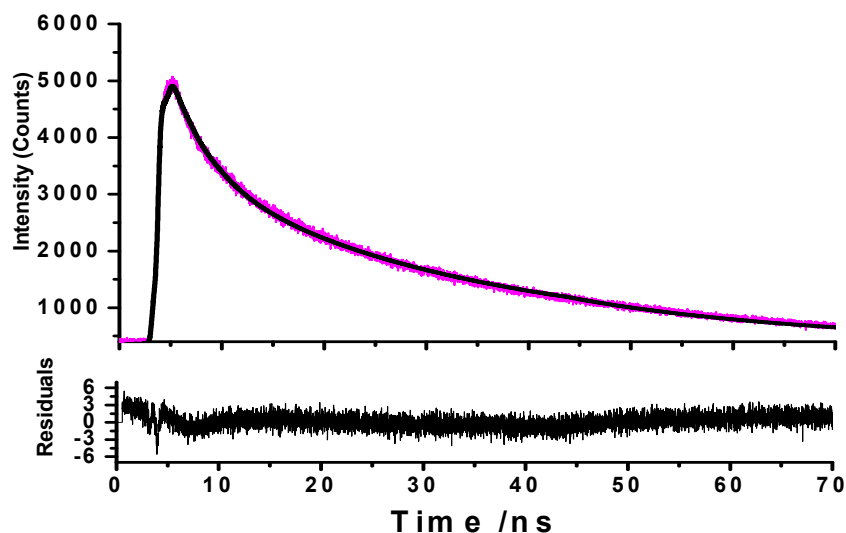


**Figure 1.14:** A typical fluorescence lifetime trace for a ZnPc derivative [30].

The fluorescence lifetimes ( $\tau_F$ ) for MPcs are generally of the order of picoseconds to nanoseconds. Typical values for CdTe QDs are shown in Table 1.3 [66,76,78]. This data shows that the QDs have either two or three components which range in time from picoseconds to nanoseconds. It can be seen that the addition of Pcs (mixed conjugates) reduces the fluorescence lifetime in some cases such as with ZnttbIPc [30], and linking of the Pcs to the QDs further decreases the lifetime values. However, an increase is seen for other cases such as with TtfmMPyZnPc [66]. One possible reason for this could be the solvent systems used in the experiments. Considering QDs alone, the first and second lifetimes were reported to increase with size, Table 1.3 [78].

**Table 1.3: Fluorescence lifetimes and corresponding amplitude data for CdTe-thiol capped QDs using the TCSPC set-up. See Table 1.1 for complex abbreviations.**

Sample	Solvent	$\lambda$ (nm)	$\tau_1$ (ps)	$a_1$ (%)	$\tau_2$ (ps)	$a_2$ (%)	$\tau_3$ (ns)	$a_3$ (%)	Ref.
CdTe-MPA	DMSO (1% H <sub>2</sub> O)	~640	-	-	3700	25	34.0	75	[66]
TtfmMPyZnPc- CdTe-MPA mixed		-	-	-	3800	35	34.1	65	
TtfmPyZnPc- CdTE-MPA mixed		-	-	-	4000	40	33.3	60	
CdTe-MPA	DMF: H <sub>2</sub> O (4:1 v/v)	640	-	-	3400	43	26.4	57	[76]
ZnttbIPc-CdTe- MPA mixed		-	-	-	3200	43	28.6	57	
ZnttbIPc-CdTe- MPA linked		-	-	-	1700	79	9.6	21	
CdTe -TGA (3.6 nm)	H <sub>2</sub> O	540	50	64	725	17	15.2	19	[78]
		580	44	37	650	20	16.8	43	
		600	47	39	830	19	17.3	42	
		630	48	45	710	14	17.5	41	
CdTe-TGA (3.1 nm)	H <sub>2</sub> O	500	40	70	575	15	17.9	15	
		540	41	38	485	14	21.2	48	
		580	37	49	550	13	21.1	38	
		620	40	44	545	15	22.0	41	

Another method of determining fluorescence lifetimes is via the use of the program PhotochemCAD [79]. This is a software package that utilizes the Strickler-Berg equation to calculate the fluorescence lifetimes using the acceptor absorption and donor emission spectra. The equation however is only valid for molecules that which do not interact with the solvent and those that do not undergo geometric changes when excited.

### 1.3.2 Förster resonance energy transfer (FRET)

Förster resonance energy transfer (FRET) is the transfer of energy from an excited fluorophore which acts as the donor (such as the QDs) to the acceptor molecule such as the phthalocyanines (Figure 1.15 [25,80,81]). In order for FRET to occur, an overlap between the absorbance spectrum of the donor and fluorescence spectrum of the acceptor is required as well as a minimal centre-to-centre separation distance ( $r$ ). Successful energy transfer results in the reduced fluorescence intensity of the donor with a corresponding increase in the absorption intensity of the acceptor, as seen in Figure 1.16 [25]. Thus the mixing or linking of QDs (donor) and Pcs (acceptor) may result in this energy transfer.

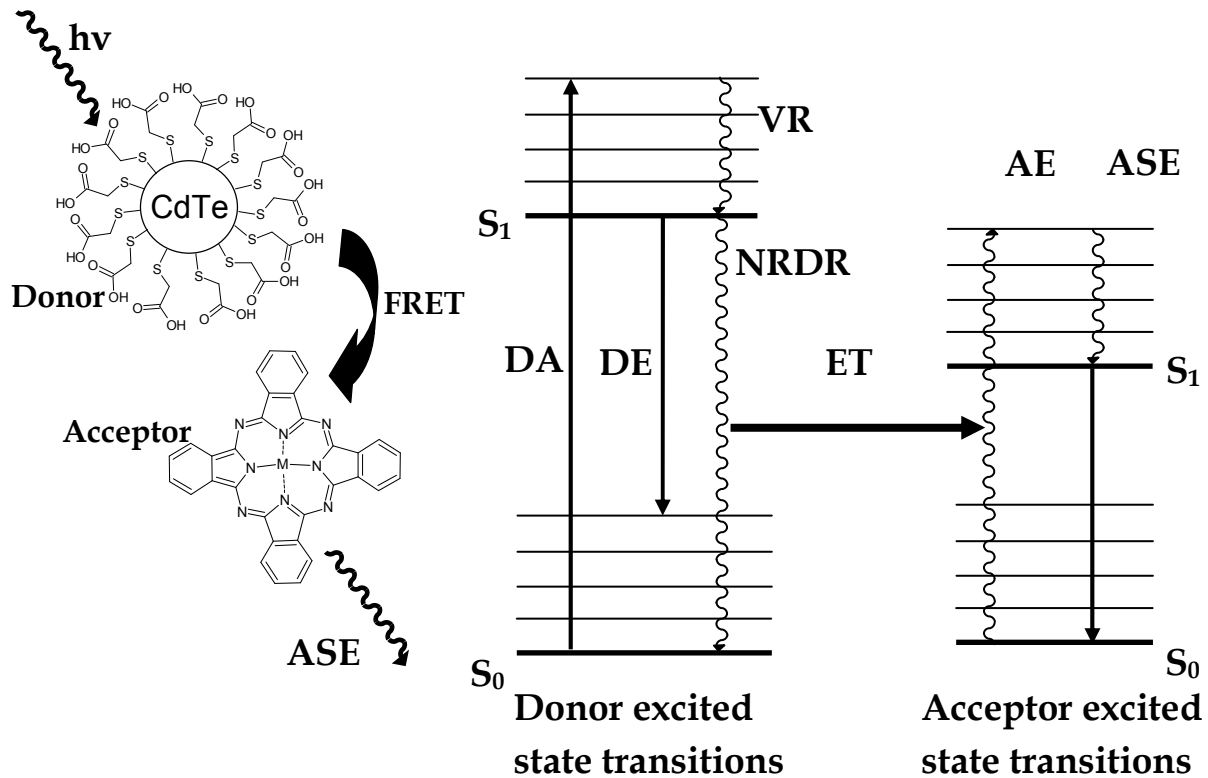


Figure 1.15: Jablonski diagram showing the origins of Förster resonance energy transfer (FRET) between a donor (QD) and acceptor (Pc). DA = donor absorption, DE = donor emission, VR = vibrational relaxation, NRDR = non-radiative donor relaxation, ET = energy transfer (FRET), AE = acceptor non-radiative excitation, ASE = acceptor sensitized emission.  $S_0$  = singlet ground state and  $S_1$  = singlet excited state [25,81].

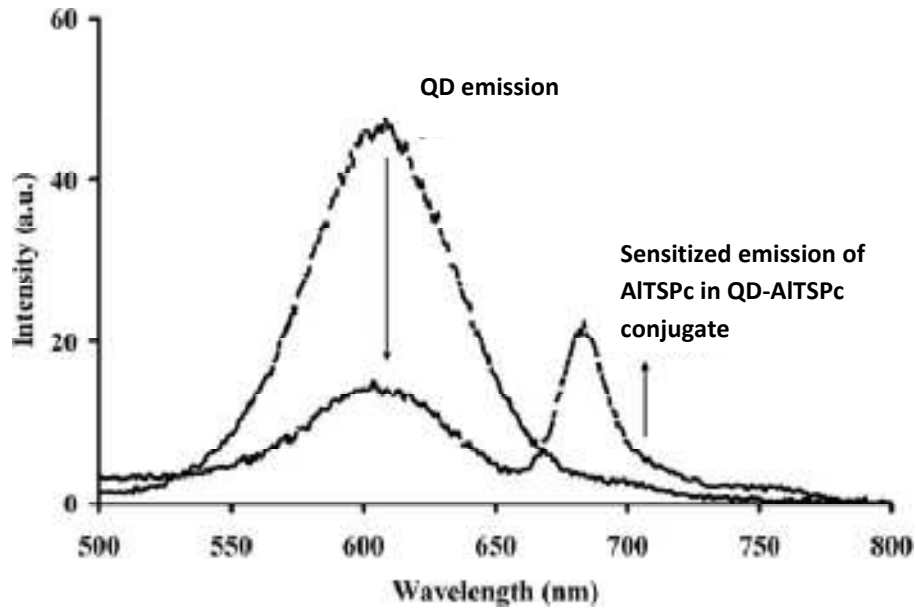


Figure 1.16: Spectra showing the typical decrease in QD emission intensity on the addition of Pc and the subsequent increase in the Pc emission intensity, which is expected when FRET occurs [25].

FRET efficiency ( $Eff$ ) is determined experimentally from the fluorescence quantum yields of the donor in the absence ( $\Phi_{F(QD)}$ ) and presence ( $\Phi_{F(QD)}^{Mix}$ ) of the acceptor using Equation (1.5) [75,82,83]:

$$Eff = 1 - \frac{(\Phi_{F(QD)}^{Mix})}{(\Phi_{F(QD)})} \quad (1.5)$$

$Eff$  is related to  $r$  ( $\text{\AA}$ ), the centre-to-centre separation distance between donor and acceptor, by Equation (6) [83,84]:

$$\text{Eff} = \frac{(R_0^6)}{(R_0^6 + r^6)} \quad (1.6)$$

where  $R_0$  (the Förster distance, Å) is the critical distance between the donor and the acceptor molecules at which the efficiency of energy transfer is 50%. This depends on the quantum yield of the donor, Equation (1.7) [75,85]:

$$R_0^6 = 8.8 \times 10^{23} \kappa^2 n^{-4} \Phi_{\text{F(QD)}} J \quad (1.7)$$

where  $\kappa^2$  is the dipole orientation factor,  $n$  the refractive index of the medium,  $\Phi_{\text{F}}$  the fluorescence quantum yield of the donor in the absence of the acceptor, and  $J$  is the Förster overlap integral, which is defined by Equation (1.8):

$$J = \int f_{\text{QD}}(\lambda) \varepsilon_{\text{ZnPc}}(\lambda) \lambda^4 d\lambda \quad (1.8)$$

where  $f_{\text{QD}}$  is the normalized QD emission spectrum and  $\varepsilon_{\text{ZnPc}}$  is the molar extinction coefficient of each ZnPc derivative, and  $\lambda$  is the wavelength of the acceptor (at the Q-band). In this case, it is assumed that  $\kappa^2$  is 2/3 for QDs mixed with ZnPc derivatives; such an assumption is often made for donor-acceptor pairs in a liquid medium, since their dipole moments are considered to be isotropically oriented during the excited state lifetimes. Although electrostatic interactions are anticipated between QDs and the sterically demanding phthalocyanine derivatives in mixed samples, the exact orientation of the ZnPc derivative with regard to the QD is not known with certainty. Various conformations can be attained by the phthalocyanine complex on the surface of QDs when the two are mixed. For the perpendicular orientation of the ZnPc derivative

on the QD, some degree of movement of the donor/acceptor species is expected. As a result the isotropic dynamical average ( $\kappa^2 = 2/3$ ) is more appropriate than the static isotropic average ( $\kappa^2 = 0.476$ ), because the donor-acceptor pair is not in a rigid medium. The former  $\kappa^2$  value was also employed for the linked QDs-ZnPc derivatives. FRET parameters may be computed using the program PhotochemCAD [79]. Literature values for FRET parameters are shown in Table 1.4 [30,64,66,77].

**Table 1.4: Förster resonance energy transfer (FRET) parameters for modified Pcs mixed with and linked to thiol QDs. See Table 1.1 for complex abbreviations.**

ZnPc derivatives	QD capping	J ( $10^{-14}\text{cm}^6\text{K}$ )	$R_0$ ( $10^{-10}\text{m}$ )	r ( $10^{-10}\text{m}$ )	Eff (%)	Ref.
ZnTSPc (mixed)	TGA	1.80	57.0	67.0	30	[64]
ZnTCPc (mixed)	TGA	0.72	49.0	63.0	20	[64]
ZnttbIPc (mixed)	MPA	64	44.68	44.08	52	[30]
ZnttbIPc (linked)	MPA	64	44.68	34.70	82	[30]
TtfmMPyZnPc (mixed)	MPA	107	51.59	58.95	31	[66]
TtfmPyZnPc (mixed)	MPA	117	52.15	53.56	45	[66]
ZnTAPc (mixed)	MPA (3.0nm)	3.43	30.8	25.9	74	[77]
ZnTAPc (linked)	MPA (3.0nm)	3.43	30.8	20.0	93	[77]
ZnTAPc (mixed)	TGA (3.0nm)	2.18	24.8	22.0	68	[77]
ZnTAPc (linked)	TGA (3.0nm)	2.18	24.8	21.6	70	[77]
ZnTAPc (mixed)	MPA (3.5nm)	8.90	29.3	39.2	16	[77]
ZnTAPc (linked)	MPA (3.5nm)	8.90	29.3	26.6	65	[77]

$J$  values are generally of the order  $10^{-14} \text{ cm}^6$  for porphyrin based molecules; values larger than this indicate good spectral overlap between the emission spectrum of the donor and the absorption spectrum of the acceptor, increasing the probability for FRET. When the centre-to-centre distance ( $r$ ) is smaller than the Förster distance ( $R_0$ ), which is the critical distance between the donor and the acceptor molecules at which the efficiency of energy transfer is 50%, the FRET efficiency is greater than 50%. The efficiency values in Table 1.3 show that the linked conjugates are higher than the mixed species due to the rigid bond of the linked conjugates which may increase the probability of FRET. The effect of monosubstituted phthalocyanines on these values will be determined in this work.

The efficiency of energy transfer based on the fluorescence lifetimes ( $Eff_{tr}$ ) was also calculated in this thesis from the lifetime measurements of the donor (QDs), in the absence ( $\tau_D$ ) and presence ( $\tau_{DA}$ ) of the acceptor (Pc) using Equation (1.9) [74,79]:

$$Eff_{tr} = 1 - \frac{(\tau_{DA})}{(\tau_D)} \quad (1.9)$$

This equation, however, makes the assumption that the decay of the donor is a single exponential in the absence ( $\tau_D$ ) and presence ( $\tau_{DA}$ ) of acceptor and is therefore only valid for a homogeneous system (i.e. identical donor-acceptor complexes) [75]. These single-exponential decays are rare in biomolecules; so for donor-acceptor systems decaying with multiexponential lifetimes the energy transfer efficiency must be determined from the amplitude weighted lifetimes, Equation (1.10):

---

$$\tau = \sum_i \alpha_i \tau_i \quad (1.10)$$

where  $\alpha_i$  is the relative amplitude contribution to the lifetime  $\tau$ . As such we used the amplitude weighted time constants for  $\tau_D$  and  $\tau_{DA}$  to determine the transfer efficiency for the mixed and linked species, using Equation (1.9).

### 1.3.3 Triplet quantum yields and lifetimes

The triplet quantum yield is the number of molecules that undergo ISC from the first excited state ( $S_1$ ) to the triplet state ( $T_1$ ). The technique used to measure the excited state of the molecule is the laser flash photolysis which monitors the absorption from the excited  $T_1$  to higher energy states  $T_n$  of the excited molecule. A triplet decay curve of change in absorbance ( $\Delta A$ ) versus time in seconds is obtained from the experiment and from this the triplet lifetime ( $\tau_T$ ) can be determined. Most Pcs exhibit triplet-triplet absorption around the 500 nm region which can be observed in a transient differential curve, which shows  $\Delta A$  versus wavelength, as seen in Figure 1.17 [86]. The data collected from the laser flash photolysis technique is used to calculate the triplet quantum yield of the sample.

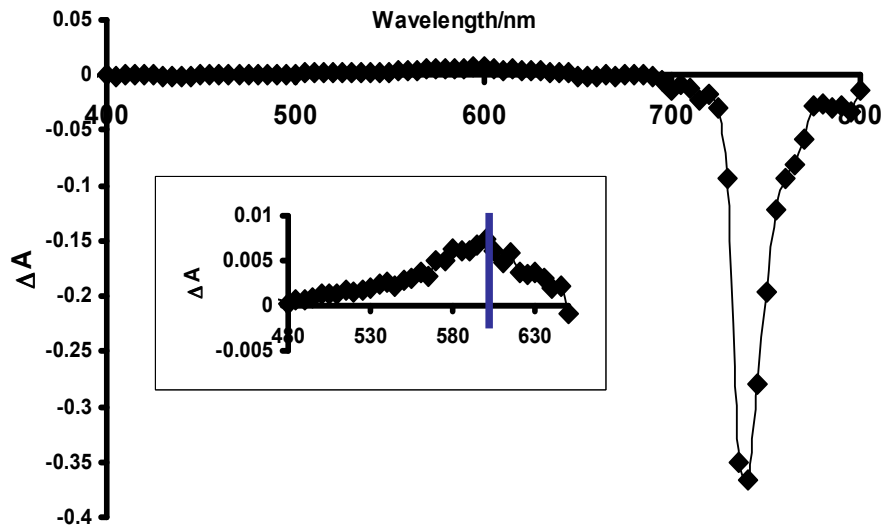


**Figure 1.17: The triplet decay trace for silicon phthalocyanine [86].**

Triplet quantum yields may be determined using a comparative method based on triplet decay [87] using ZnPc as the standard, Equation (1.11):

$$\Phi_{\text{T}}^{\text{Sample}} = \frac{\Phi_{\text{T}}^{\text{Std}} (\Delta A_{\text{T}}^{\text{Sample}} \varepsilon_{\text{T}}^{\text{Std}})}{(\Delta A_{\text{T}}^{\text{Std}} \varepsilon_{\text{T}}^{\text{Sample}})} \quad (1.11)$$

where  $\Delta A_{\text{T}}^{\text{Sample}}$  and  $\Delta A_{\text{T}}^{\text{Std}}$  are the changes in the triplet state absorbance of the ZnPc derivatives and the standard, respectively.  $\varepsilon_{\text{T}}^{\text{Sample}}$  and  $\varepsilon_{\text{T}}^{\text{Std}}$  are the triplet state extinction coefficients for the ZnPc derivative and standard, respectively.  $\Phi_{\text{T}}^{\text{Std}}$  is the triplet state quantum yield for zinc phthalocyanine (ZnPc) used as a standard in DMSO,  $\Phi_{\text{T}}^{\text{Std}} = 0.65$  [87], and  $\Phi_{\text{T}}^{\text{Std}} = 0.58$  in DMF [84].  $\Phi_{\text{T}}$  are also determined for ZnPc derivatives in the presence of QDs in this thesis. Literature values are shown in Table 1.5 [30,63-66].

As stated above, triplet quantum yield values are affected by the central metal of the Pc. This is known as the heavy atom effect which generally encourages intersystem crossing to the triplet state resulting in an increased triplet quantum yield. Longer triplet lifetimes increase the chances of collision between the Pc derivatives and ground state molecular oxygen molecules, ensuring a greater production of cytotoxic singlet oxygen which is necessary in photosensitized reactions.

**Table 1.5: Triplet quantum yields of phthalocyanine derivatives mixed with thiol capped CdTe QDs.**

Phthalocyanine derivatives	QD capping	QD size (nm)	$\Phi_T^{Pc}$	$\Phi_T^{Mix}$	$\tau_T$ ( $\mu$ s)	Ref.
ZnttbIPc (mixed)	MPA	3.5	0.77	0.81	15.0	[30]
ZnttbIPc (linked)	MPA	3.5	0.77	0.73	0.48	[30]
TmTPyZnPc (mixed)	MPA	4.19	0.78	0.80	360	[63]
ZnTSPc (mixed)	TGA	4.2	0.56	0.25	230	[64]
ZnTSPc (mixed)	2-ME	3.3	0.56	0.44	160	[64]
ZnTCPc (mixed)	TGA	4.2	0.50	0.53	1300	[64]
ZnTCPc (mixed)	2-ME	3.3	0.50	0.34	730	[64]
ZnOCPc (mixed)	TGA	4.2	0.75	0.63	190	[64]
ZnOCPc (mixed)	2-ME	3.3	0.75	0.72	130	[64]
TtfmMPyZnPc (mixed)	MPA	4.54	0.86	0.88	263	[66]
TtfmPyZnPc (mixed)	MPA	4.54	0.74	0.88	262	[66]
(OH)AlPcS <sub>4</sub> (mixed)	MPA1	2.3	0.36	0.46	600	[64]
	MPA2	3.6		0.43	610	
	TGA1	3.2		0.41	610	
	TGA2	3.7		0.46	560	

Phthalocyanine derivatives	QD capping	QD size (nm)	$\Phi_T^{Pc}$	$\Phi_T^{Mix}$	$\tau_T$ ( $\mu$ s)	Ref.
ZnPcS <sub>4</sub> (mixed)	MPA1	2.3	0.56	0.51	240	[64]
	MPA2	3.6		0.42	220	
	TGA1	3.2		0.49	250	
	TGA2	3.7		0.45	290	
(OH) <sub>2</sub> SiPcS <sub>4</sub> (mixed)	MPA1	2.3	0.56	0.45	140	[64]
	MPA2	3.6		0.55	310	
	TGA1	3.2		0.53	340	
	TGA2	3.7		0.54	340	
(OH) <sub>2</sub> GePcS <sub>4</sub> (mixed)	MPA1	2.3	0.81	0.85	240	[65]
	MPA2	3.6		0.87	280	
	TGA1	3.2		0.81	350	
	TGA2	3.7		0.85	360	

## 1.4 Summary of Aims of Thesis

The aims of this work are as follows:

1. Synthesis and spectroscopic characterization of monoamino (ZnAPc) and monoaminophenoxy (ZnAPPc) zinc phthalocyanine complexes.
2. Synthesis and characterization of CdTe quantum dots capped with mercaptopropionic acid (MPA), thioglycolic acid (TGA) and L-cysteine (L-cys).
3. Characterization of the mixed and chemically linked thiol capped CdTe QD-Pc conjugates.
4. Investigation of the photophysical properties of the ZnAPc and ZnAPPc in the presence (both mixed and chemically linked) of CdTe QDs.

## 2. EXPERIMENTAL

**This chapter incorporates all synthetic procedures and methods of characterization for all molecules used in this work.**

## 2.1 Materials

### 2.1.1 Solvents

Dimethylsulfoxide (DMSO), dichloromethane (DCM), tetrahydrofuran (THF), ethanol (EtOH), sulfuric acid (98 %) and dimethylformamide (DMF) were obtained from SAARCHEM. Ultra pure water was obtained from a Milli-Q Water System (Millipore Corp, Bedford, MA, USA). DMSO- $d_6$  and D<sub>2</sub>O were obtained from Sigma-Aldrich. The rest of the solvents were obtained from commercial suppliers and used as received.

### 2.1.2 Synthesis and photophysics reagents

Tellurium powder (200 mesh), sodium hydroxide, cadmium chloride, sodium borohydride, sodium hydroxide and 3-mercaptopropionic acid (MPA) were obtained from SAARCHEM. 1,8-Diazabicyclo[5.4.0]undec-7-ene (DBU), N-ethyl-N(3-dimethylaminopropyl) carbodiimide (EDC), N-hydroxy succinimide (NHS) and 4-nitrophthalonitrile were purchased from Fluka. Zinc acetate dihydrate was obtained from British Drug House (BDH) Chemicals. Pd/C, thioglycolic acid (TGA), L-cysteine (L-cys), *p*-aminophenol and zinc phthalocyanine (ZnPc) were obtained from Sigma-Aldrich and zinc tetrasulfophthalocyanine (ZnTSPc) was synthesized according to literature [88]. C<sub>18</sub> Phenomenex reverse phase column and Sephadex G25 column was employed for chromatographic separations. The rest of the reagents were obtained from commercial suppliers and used as received.

## 2.2 Instrumentation

1. Ultraviolet-visible (UV-vis) spectra were recorded on a Cary 500 UV/Vis/NIR spectrophotometer or a Shimadzu 2001 UV Pc spectrophotometer and fluorescence emission and excitation spectra on Varian Eclipse spectrofluorimeter.
2. Mass spectra data were collected with a Bruker AutoFLEX III Smartbeam TOF/TOF Mass spectrometer. The instrument was operated in positive ion mode using an  $m/z$  range of 400 – 3000. The voltage of the ion sources were set at 19 and 16.7 kV for ion sources 1 and 2 respectively, while the lens was set at 8.50 kV. The reflector 1 and 2 voltages were set at 21 and 9.7 kV respectively. The spectra were acquired using dithranol as the MALDI matrix, using a 355 nm Nd:YAG laser.
3.  $^1\text{H}$  NMR spectra were obtained using a Bruker AMX 400 MHz or a Bruker Advance II+ 600 MHz NMR spectrometer.
4. Elemental analysis was carried out using a VARIO ELEMENTAR EL III CHNS instrument.
5. FT-IR spectra were recorded on a Perkin-Elmer Universal ATR Sampling accessory spectrum 100 FT-IR spectrometer.
6. Laser flash photolysis experiments were performed to determine the triplet decay kinetics. Light pulses were produced by a Quanta-Ray Nd:YAG laser providing 100 mJ, 9 ns pulses of laser light at 10 Hz, pumping a Lambda Physic FL 3002 dye (Pyridin 1 dye in methanol). Single pulse energy ranged from 1 to 3

mJ. The analysing beam source was from a Thermo Oriel 66902 xenon arc lamp, and a photomultiplier tube was used as a detector, Figure 2.1. Signals were recorded with a two-channel 300 MHz digital real-time oscilloscope (Tektronix TDS 3032C); the kinetic curves were averaged over 256 laser pulses. OriginPro 7.5 was used to fit the kinetic curves in order to determine the triplet lifetimes.

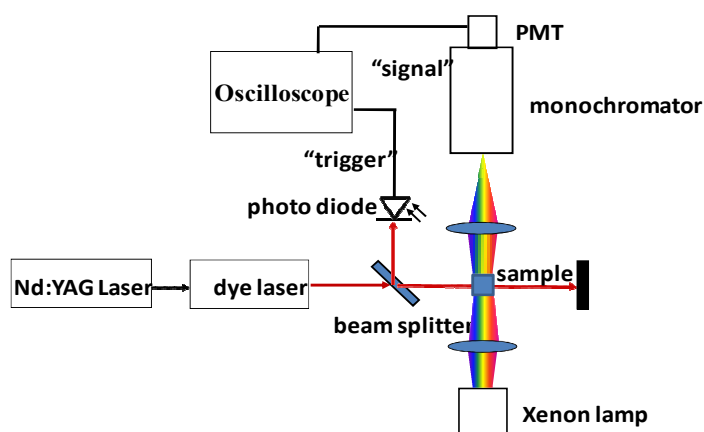


**Figure 2.1: Schematic diagram of the laser-flash photolysis set-up.**

7. Fluorescence lifetimes were measured using a time correlated single photon counting (TCSPC) setup (FluoTime 200, Picoquant GmbH), Figure 2.2. For study of the fluorescence lifetimes of the ZnPc derivatives, a diode laser (LDH-P-670 driven by PDL 800-B, 670 nm, 20MHz repetition rate, Picoquant GmbH) was employed. For the mixed and linked QD samples, a diode laser (LDH-P-C-485 driven by PDL 800-B, 480 nm, 10MHz repetition rate, Picoquant GmbH) was employed. Fluorescence was detected under the magic angle with a Peltier cooled photomultiplier tube (PMT) (PMA-C 192-N-M, Picoquant GmbH) and

integrated electronics (PicoHarp 300E, Picoquant GmbH). A monochromator with a spectral width of about 4 nm was used to select the required emission wavelength band. The response function of the system, which was measured with a scattering Ludox solution (DuPont), had a full width at half maximum (FWHM) of about 300 ps. The ratio of stop to start pulses was kept low (below 0.05) to ensure good statistics. All luminescence decay curves were measured at the maximum of the emission peak. The data were analysed with the program FluoFit (Picoquant GmbH). The support plane approach was used to estimate the errors of the decay times.

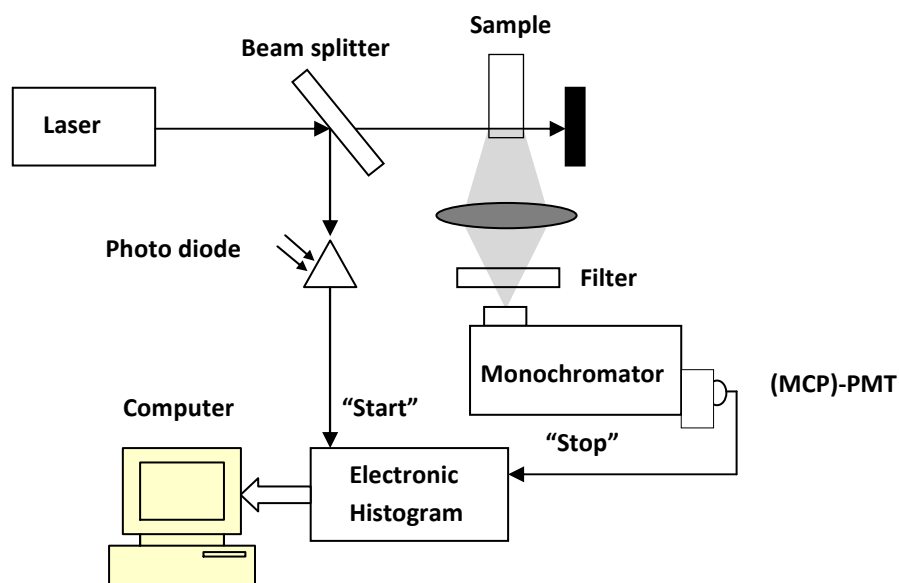


Figure 2.2: Schematic diagram of the TCSPC

8. X-ray powder diffraction (XRD) patterns were recorded on a Bruker D8, Discover equipped with a proportional counter, using Cu-K $\alpha$  radiation ( $\lambda = 1.5405 \text{ \AA}$ , nickel filter). Data were collected in the range from  $2\theta = 5^\circ$  to  $60^\circ$ , scanning at  $1^\circ \text{ min}^{-1}$  with a filter time-constant of 2.5 s per step and a slit width of 6.0 mm. Samples were placed on a silicon wafer slide. The X-ray diffraction data were treated using the freely-available Eva (evaluation curve fitting) software. Baseline correction was performed on each diffraction pattern by subtracting a spline fitted to the curved background and the full-width at half-maximum values used in this study were obtained from the fitted curves.
9. Raman spectral data were collected with a Bruker RAM II spectrometer (equipped with a 1064 nm Nd:YAG laser and a liquid nitrogen cooled germanium detector). Liquid samples with DMSO: H<sub>2</sub>O as the solvent were employed.
10. Atomic force microscopy (AFM) images were recorded in the non-contact mode in air with a CP-11 Scanning Probe Microscope from Veeco Instruments (Carl Zeiss, South Africa) at a scan rate of 1 Hz. Samples for AFM were prepared by spin coating onto glass slides.

## 2.3 Methods

### 2.3.1 UV-vis absorption studies

The interaction of the QDs with the modified ZnPc complexes was studied spectroscopically. The spectra for the QDs alone were compared for the different thiol cappings and in different solvents. The studies of ZnPc complexes, mixed or linked to QDs were carried out in a DMSO:water (9:1 *v/v*) mixture or in a DMF:water (9:1 *v/v*) mixture. The solvent mixture enables the solubilization of the quantum dots and the phthalocyanine whilst ensuring the monomeric nature of the phthalocyanine. All spectral measurements were performed in a 1 cm quartz cell at room temperature.

### 2.3.2 Fluorescence spectra and quantum yields

Fluorescence spectra for the ZnPcs and QDs, as well as the required standards were prepared such that the absorbance of each at their respective excitation wavelength was approximately 0.05. For the mixed and linked QD-ZnPc conjugates, absorption corrections (with respect to the ZnPcs) were made to ensure that excitation occurs for ZnPc only. The area under the curves was measured and fluorescence quantum yields ( $\Phi_F$ ) calculated using equations 1.3 and 1.4, with ZnPc in DMSO ( $\Phi_F = 0.2$ ) and DMF ( $\Phi_F = 0.3$ ) [73], and Rhodamine 6G in ethanol ( $\Phi_F = 0.94$ ) [74,75] as standards. For comparative purposes the settings on the instrument remained unchanged for the duration of the experiment.

### 2.3.3 Fluorescence lifetimes

Fluorescence lifetimes ( $\tau_F$ ) for the mixed and linked QD-ZnPc conjugates, or ZnPc derivatives alone were determined from TCSPC measurements using the setup shown in Figure 2.2. The luminescence decay curves were measured at the maximum of the emission peak whilst the lifetimes were obtained by deconvolution of the decay curves using the FluorFit Software program (PicoQuant GmbH, Germany).

### 2.3.4 Triplet quantum yields and lifetimes

Triplet quantum yields ( $\Phi_T$ ) and lifetimes ( $\tau_T$ ) were determined by recording the triplet absorption and decay kinetics using the laser flash photolysis set-up (Figure 2.1). Solutions of the ZnPc derivatives alone, or ZnPc mixed or linked with QDs (absorbance  $\sim 1.5$ ) were de-aerated with argon gas for  $\sim 15$  min in a 1 cm pathlength spectrophotometric cell. The samples were then irradiated at the Q band using the above described set-up. The triplet quantum yields ( $\Phi_T$ ) of the samples were determined using Equation (1.11) with ZnPc in DMSO  $\Phi_T = 0.65$  [87]. The triplet lifetimes were determined using OriginPro 7.5 software to fit the kinetic curves.

## 2.4 Synthesis

### 2.4.1 Synthesis of Quantum Dots (QDs)

The preparation of the thiol derivative capped QD was via a modified method adopted from literature [23,25]. Briefly, 2.35 mmol of  $\text{CdCl}_2 \cdot \text{H}_2\text{O}$  was dissolved in 125 ml of water and 5.7 mmol of the respective thiol derivative L-cysteine (L-cys), 3-mercaptopropionic acid (MPA) and thioglycolic acid (TGA), Figure 2.3, was added with stirring. The solution was adjusted to a pH between 11 and 12 on addition of 1M NaOH. Nitrogen gas was bubbled through the solution for about 1 h.

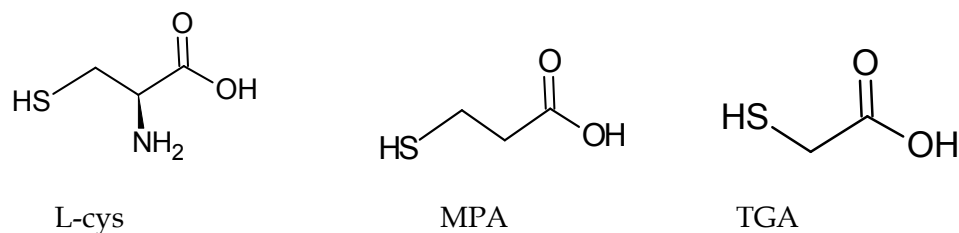


**Figure 2.3: Representation of the molecular structure of the capping agents for QDs: L-cysteine (L-cys), mercaptopropionic acid (MPA) and thioglycolic acid (TGA).**

The aqueous solution was reacted with  $\text{H}_2\text{Te}$  gas, which was generated by the reaction of  $\text{NaBH}_4$  with Te powder in the presence of 0.5 M  $\text{H}_2\text{SO}_4$  under a flow of nitrogen gas. A change of colour of the solution containing  $\text{CdCl}_2$  and the thiol was observed on addition of  $\text{H}_2\text{Te}$  gas. The solution was then refluxed under air at 100 °C for different times in order to obtain different sizes of the CdTe QDs, Figure 2.4.

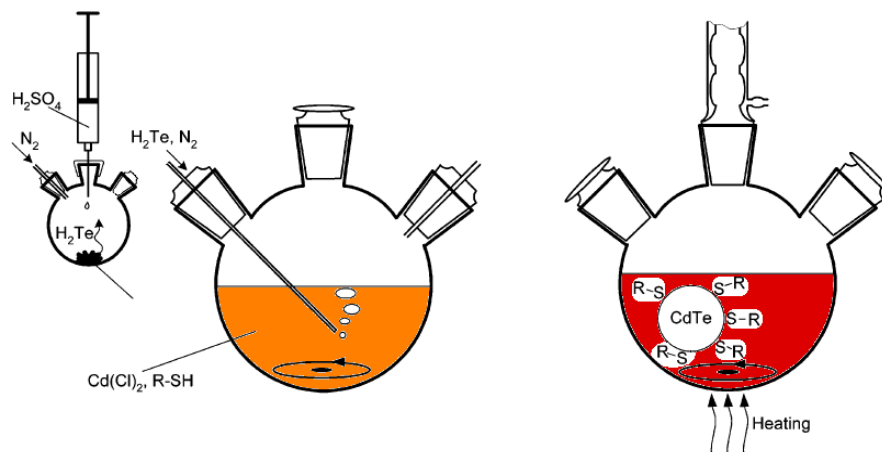


**Figure 2.4: Setup for the synthesis of water-soluble CdTe quantum dots**

On cooling, the QDs were precipitated out from solution using excess ethanol. The solutions were then centrifuged to harvest the QDs. Sizes ( $D$ ) of the synthesized QDs were estimated using the polynomial fitting function [89] Equation (2.1),

$$D = (9.8127 \times 10^{-7})\lambda^3 - (1.7147 \times 10^{-3})\lambda^2 + (1.0064)\lambda - (194.84) \quad (2.1)$$

where  $\lambda$  is the absorption maxima of the QDs. The fitting function is not valid for sizes of quantum dots outside the size range 1-9 nm [89]. The size was also determined using XRD, Equation (1.1).

**MPA:** IR [(KBr)  $\nu_{\max}$ /  $\text{cm}^{-1}$ ]: 3347  $\text{cm}^{-1}$  (O-H), 1552  $\text{cm}^{-1}$  (C=O).

**TGA:** IR [(KBr)  $\nu_{\max}$ /  $\text{cm}^{-1}$ ]: 3347  $\text{cm}^{-1}$  (O-H), 1567  $\text{cm}^{-1}$  (C=O).

**L-Cys:** IR [(KBr)  $\nu_{\max}$ /  $\text{cm}^{-1}$ ]: 3320  $\text{cm}^{-1}$  (O-H), 1565  $\text{cm}^{-1}$  (C=O).

## 2.4.2 Synthesis of low symmetry zinc phthalocyanines (ZnPcs)

### 2.4.2.1. Synthesis of 4-monoaminophenoxy zinc phthalocyanine (Scheme 3.1)

#### *4-Aminophenoxy phthalonitrile (3)*

To a suspension of 0.76 g (6.94 mmol) of 4-aminophenol (**1**) and 1 g (5.78 mmol) of 4-nitrophthalonitrile (**2**) in 25 mL of dry DMSO was added 1.64 g of anhydrous  $K_2CO_3$  (11.56 mmol). The mixture was left to reflux under argon overnight with stirring. A further 0.8 g of  $K_2CO_3$  (5.48 mmol) was added after 24 h to the suspension. After 48 h, the resulting product was poured into 1 M HCl (260 mL), forming a precipitate that was recrystallized from methanol/water (1:1) to yield a dark brown product (**3**). Yield: 0.613g (45.1%). IR [(KBr)  $\nu_{max}/cm^{-1}$ ]: 3088, 3077 ( $NH_2$ ), 2924 (CH), 2234 (CN), 1592 (NH bend), 1485 (C=C), 1248 (C-O-C).  $^1H$  NMR (DMSO- $d_6$ ):  $\delta$ , ppm 8.25-8.31 (1H, m, Ar-H), 7.68-7.73 (1H, m, Ar-H), 8.00-8.70 (1H, m, Ar-H), 7.13-7.48 (4H, m, Ar-H).

#### *4-Monoaminophenoxy zinc phthalocyanine (ZnAPPc)*

To a suspension of 0.11 g (0.84 mmol) of 1,2 dicyanobenzene (**4**), 0.066 g (0.28 mmol), 4-monoaminophenoxy phthalonitrile (**3**) and 0.0671g (0.306 mmol) of zinc acetate in 5 mL of pentanol, 2 mL of DBU was added. The mixture was left to reflux under argon overnight with stirring. The resulting product was cooled before the addition of methanol, precipitating the ZnAPPc complex from the solution. The precipitate was collected using centrifugation and further purified by centrifuging with a 1:1 mixture of chloroform and dichloromethane. This solvent mixture was then removed using a

rotary evaporation. The product was further purified using a Phenomenex C<sub>18</sub> Sep-Pak column with 0.05% trifluoroacetic acid (TFA) in methanol as the solvent. Yield: 0.055g (29%). UV/vis (DMSO),  $\lambda_{\max}$  (nm) (log  $\epsilon$ ): 673 (4.6), 608 (3.8), 346 (4.1). IR [(KBr)  $\nu_{\max}/\text{cm}^{-1}$ ]: 3414 (NH<sub>2</sub>), 2929 (CH), 1647-1596 (NH bend), 1484 (C=C), 1327 (C-O-C), 1114-1060 (CN), 731 (Zn-N). <sup>1</sup>H NMR (DMSO-*d*<sub>6</sub>):  $\delta$ , ppm 9.68-9.71 (2H, br s, Ar-NH<sub>2</sub>), 9.43-9.45 (6H, m, Pc-H), 8.25-8.29 (6H, m, Pc-H), 7.9-7.96 (3H, m, Pc-H), 7.82-7.84 (4H, m, Ph-H). Anal. Calc. for C<sub>38</sub>H<sub>21</sub>N<sub>9</sub>OZn: C, 66.57; H, 3.09; N, 18.41. Found: C, 67.32; H, 3.29; N, 18.10%. MALDI-TOF MS *m/z* calc. 685.04 amu, found 684.14 amu [M]<sup>+</sup>.

#### 2.4.2.2. Synthesis of zinc monoamino phthalocyanine (ZnAPc) (Scheme 3.2)

##### *4-Aminophthalonitrile*

The preparation of 4-aminophthalonitrile was via a modified method adapted from literature [89]. 4-Nitrophthalonitrile 1.0 g (0.058 mol) was placed in a round bottom flask and 250 mL of ethanol added to obtain a suspension. The catalyst Pd/C (150 mg) was added to the flask, the apparatus evacuated and then filled with hydrogen and the mixture vigorously and stirred at room temperature until the absorption of hydrogen had completely stopped. The reaction mixture was subsequently filtered over celite and the solution evaporated in vacuo. Yield: 0.87g (87%). IR [(KBr)  $\nu_{\max}/\text{cm}^{-1}$ ]: 3495, 3391, 3375 (NH<sub>2</sub>), 2214 (CN). <sup>1</sup>H NMR (DMSO-*d*<sub>6</sub>):  $\delta$ , ppm 7.60-7.65 (1H, d, Ar-H), 7.27-7.29 (1H, d, Ar-H), 6.84-6.89 (1H, m, Ar-H).

*Zinc monoaminophthalocyanine (ZnAPc)*

To a suspension of 1,2-dicyanobenzene (**4**, 1 g, 7.8 mmol), 4-aminophthalonitrile (**5**, 0.38 g, 2.6 mmol) and zinc acetate (0.68 g, 3.1 mmol) in 25 mL of pentanol, DBU (10 drops) was added. The mixture was left to reflux under argon for 6 h with stirring. After cooling, the solution was dropped in methanol. The green solid product was precipitated and collected by filtration and washed with methanol. The product was purified by passing through a silica gel column, using 1:1 THF:DCM mixture as the eluting solvent. Yield: 0.166 g (10.3%). UV/vis (DMSO),  $\lambda_{\max}$  (nm) ( $\log \epsilon$ ): 668 (5.2), 605 (4.4), 350 (4.7). IR [(KBr)  $\nu_{\max}/\text{cm}^{-1}$ ]: 3272 (NH<sub>2</sub>), 1602 (NH bend), 1124-1080 (CN), 718 (Zn-N). <sup>1</sup>H NMR (DMSO-*d*<sub>6</sub>):  $\delta$ , ppm 8.29-8.31 (7H, dd, Pc-H), 7.66-7.73 (7H, dd, Pc-H), 7.24-7.27 (1H, m, Pc-H). Anal. Calcd. For C<sub>32</sub>H<sub>17</sub>N<sub>9</sub>Zn: C, 64.82; H, 2.89. Found: C, 63.78; H, 3.94%. MALDI-TOF-MS (*m/z*) Calculated: 592.94. Found [M-2H]<sup>+</sup>: 591.10.

**2.4.3 Conjugation of CdTe QDs to ZnPcs (Scheme 3.3)**

For the formation of the amide-linked QD-ZnPcs (ZnAPPc or ZnAPc), a mixture containing 1 equivalent of 2 mM NHS, 1 equivalent of 5 mM EDC, 1 equivalent of CdTe QDs (0.001 g/mL) and 1 equivalent of complex ZnAPPc or ZnAPc ( $1 \times 10^{-4}$  M) in DMSO was allowed to react for 1 h. NHS and EDC were used for the activation of the carboxylic acid group of the QDs, and the resulting complex is represented as linked QD-ZnPc (ZnAPPc or ZnAPc). Experiments, where the ZnPc derivatives were mixed with QDs without chemical linking, resulting in mixed QD:ZnPc were also performed

using the same ratio of QDs to complex ZnAPPc or ZnAPc as was used for the formation of the linked complex. The linked QDs-ZnPc complex was purified by first washing with water to remove excess NHS, EDC and unlinked QDs (as the linked complexes are not soluble in 100% water). The sample was then run through a Sephadex column to separate any residual impurities such as the unlinked ZnPc from the linked which elutes first whilst the remaining bands are discarded.

## RESULTS AND DISCUSSION

The results obtained in this study are presented in two sections:

### 3. SYNTHESIS AND SPECTROSCOPIC CHARACTERIZATION

### 4. PHOTOPHYSICAL AND PHOTOCHEMICAL PROPERTIES

## PUBLICATIONS

The results discussed in the following chapters have been presented in the articles listed below, that have been published or submitted for publication in peer-reviewed journals.

These articles have not been referenced in this thesis:

1. Synthesis and photophysical studies of CdTe quantum dot-monosubstituted zinc phthalocyanine conjugate, **Sarah D' Souza**, Edith Antunes, Tebello Nyokong, *Inorg. Chim. Acta.* **367** (2011) 173-181.
2. Photophysical effects of zinc monoamino phthalocyanines linked to mercaptopropionic-capped CdTe quantum dots, **Sarah D' Souza**, Edith Antunes, Christian Litwinski, Tebello Nyokong, *J. Photochem. Photobiol. A* (Accepted with corrections).

### **3. SYNTHESIS AND SPECTROSCOPIC CHARACTERIZATION**

**This chapter reports the syntheses and spectroscopic characterization of the nanoparticles and metallophthalocyanines used in this work.**

### 3.1 Synthesis and characterization of thiol capped CdTe quantum dots (QDs)

The CdTe MPA QDs were hydrothermally grown to the size of 3.85 nm. Figure 3.1 shows the broad absorbance and narrow fluorescence emission spectra of the synthesized QDs in DMSO:water (9:1), using CdTe-MPA.

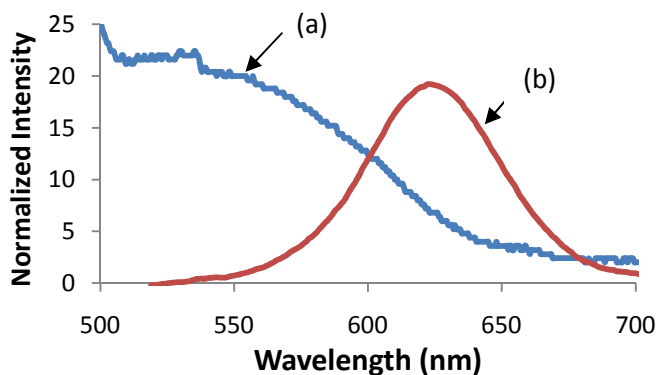


**Figure 3.1:** Absorbance (a) and fluorescence (b) spectra of MPA coated CdTe in DMSO:water (9:1).  $\lambda_{\text{exc}} = 500 \text{ nm}$ .

QDs grow through the Ostwald ripening process during the course of heating. As they grow, both the absorbance and the emission spectra shift to longer wavelengths. Figure 3.2 shows the colours of MPA-QDs with increasing size from left to right with a size range of 0.6-3.3 nm using the polynomial equation 2.1.



**Figure 3.2:** Vials of MPA-QDs of increasing size (a) with and (b) without UV light.

The QDs emission wavelengths chosen for FRET work are shown in Table 3.1. The full width at half maximum, (FWHM, Table 3.1) is an indication of the quality of the QDs and should be  $\sim 70$  nm or less. The synthesized QDs show the FWHM to be in this region. According to the estimate obtained using equation 2.1, the size of the MPA coated CdTe core QDs chosen for this work is 3.45 nm whilst the XRD calculation (Equation 1.1) gives the size to be 3.85 nm (Table 3.1) using Figure 3.3.

**Table 3.1: Emission spectral data and size determination of CdTe QDs using different methods. For the polynomial fitting water was employed as the solvent.**

Thiol Capping	$\lambda$ (emission), nm	Size (nm)		FWHM <sup>a</sup>
		Polynomial (Eq. 2.1)	XRD	
MPA	621	3.45	3.85	60
TGA	614	3.24	3.37	59
L-cysteine	601	3.51	4.08	73

<sup>a</sup>FWHM = full width at half maximum.

The X-ray diffraction pattern of CdTe QDs employed in this work is shown in Figure 3.3. Although the diffraction pattern is rather broad, it corresponds well with the three characteristic peaks for bulk CdTe structure. X-ray powder diffraction can provide important details about the crystal structure and properties of the QDs and so this technique was employed to determine the size of the CdTe QDs.

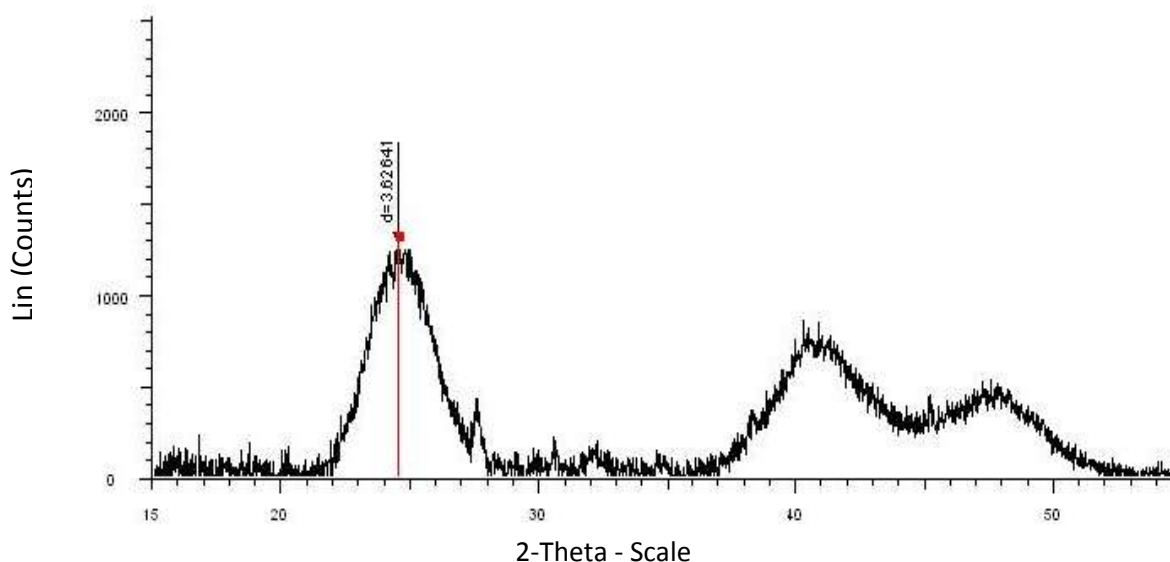


**Figure 3.3: XRD plot for CdTe-MPA capped QDs.**

The values for CdTe-TGA and CdTe-L-cys are also slightly higher when using XRD as opposed to the polynomial. Since the polynomial used is only an estimate, the sizes determined by XRD will be employed in this work.

CdTe QDs capped with thiols are known to aggregate in acidic conditions (a pH lower than 7) due to detachment of surface ligands [22]. Aggregation of QDs result in red shifting in the emission spectra accompanied by broadening [21], hence there is an importance in studying the aggregation behaviour of QDs in different solvents employed in this work [21]. The 3.85 nm CdTe-MPA QDs gave an emission wavelength of about 610 nm in 0.1M NaOH, DMSO:water (9:1) and DMF:water (9:1) (Figure 3.4(i-iii)). The MPA QDs showed a large red shift in unbuffered water alone (and without NaOH) pH = 6.8 (< 7), with an emission wavelength of 621 nm, Figure

3.4(iv). The red shift suggests aggregation in water. This shows that the use of a solvent mixture (or basic media) results in the blue shifting of the respective emission wavelengths. These solvent mixtures (DMF:water and DMSO:water) were employed in order to reduce the aggregated nature of the zinc phthalocyanine derivatives and to enable both ZnPc derivatives and the QDs to dissolve.

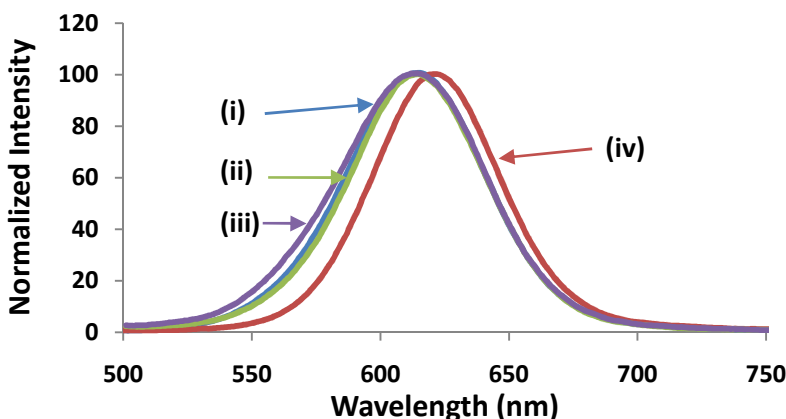


**Figure 3.4:** Comparison of emission spectra of QDs in (i) 0.1 M NaOH, (ii) DMF:water (9:1), (iii) DMSO:water (9:1) solvent mixtures and (iv) water.

Atomic force microscopy data, (Figure 3.5) provided information about surface morphology of CdTe QDs on a cross section of the glass surface coating from a 0.1 M NaOH, DMSO:water solvent mixture and their corresponding histograms. In 0.1 M NaOH solution only, the CdTe QDs show a size distribution from 4 nm to 27 nm however populations with size distributions from 12 nm and below in the section analysed occurred more frequently suggesting that CdTe QDs are not totally

monodispersed even in basic media. In DMSO:water the QDs show a size distribution of up to 48 nm which is a very wide distribution, suggesting that aggregation tendencies are worsened in this solvent system, and also showing the reported solvent dependency [90].

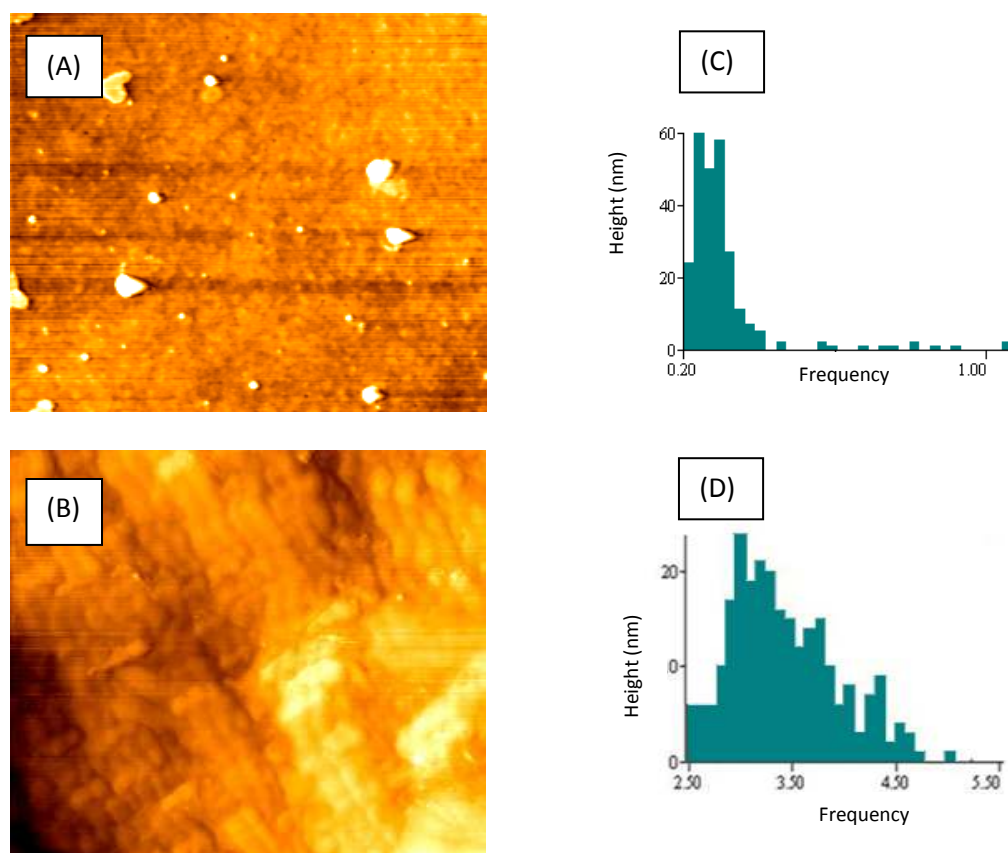


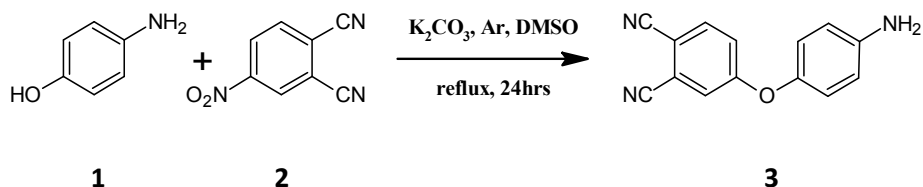
**Figure 3.5: AFM images of CdTe-MPA QDs deposited on a glass surface from (A) 0.1M DMSO: water (9:1), (B) NaOH and their corresponding histograms (C and D).**

### 3.2 Low-symmetry zinc phthalocyanines

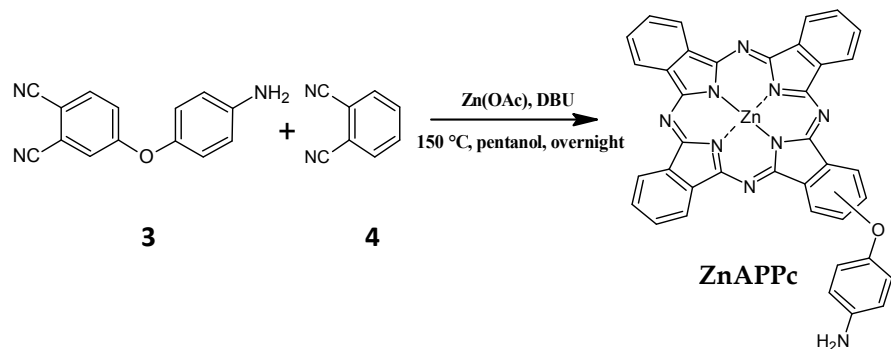
#### 3.2.1. 4-Monoaminophenoxy zinc phthalocyanine (ZnAPPc) (Scheme 3.1)

The synthesis of the dinitrile precursor (4-aminophenoxy phthalonitrile) was adapted from literature [91] for similar compounds with moderate yields. The synthetic procedure outlined in Scheme 3.1 shows the statistical condensation approach used for the synthesis of the ZnAPPc complex. This method is based on the reaction of two differently substituted phthalonitriles in a ratio of 3:1. Following extensive purification, the target compound was obtained in low yields (29 %).

Reacting ratio of 1.2: 1



Reacting ratio of 1: 3



Scheme 3.1: Synthesis of ZnAPPc derivative

$^1\text{H}$  NMR, IR, mass spectra and elemental analysis confirmed the synthesis of the phthalonitrile (**3**) and ZnAPPc. The  $^1\text{H}$  NMR showed the aromatic protons between 9.43 and 7.82 integrating for 19 as expected, with the  $\text{NH}_2$  protons between 9.68 and 9.71 ppm. The ZnAPPc IR spectrum (Figure 3.6) showed the characteristic vibrations of the phthalocyanine skeleton between 1000 and 700  $\text{cm}^{-1}$ . Vibrations due to the amino group ( $\text{NH}_2$ ) were observed at 3414  $\text{cm}^{-1}$  and the NH bend was observed between 1647 and 1596  $\text{cm}^{-1}$ , whilst the ether group (C-O-C) vibration was observed at 1327  $\text{cm}^{-1}$ . The mass spectra confirmed the ionic peak at 684.14 amu, the molecular weight of the molecule and a proton,  $[\text{M}]^+$  as expected. The elemental analysis showed the difference between the calculated and experimental values to be within 1 % of each other.

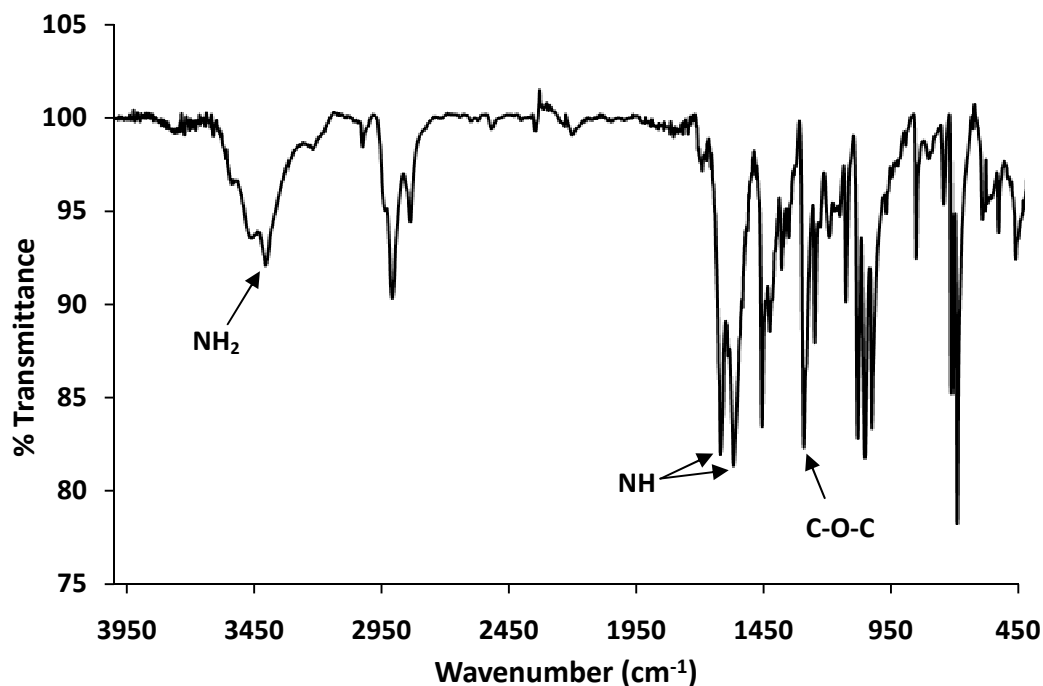
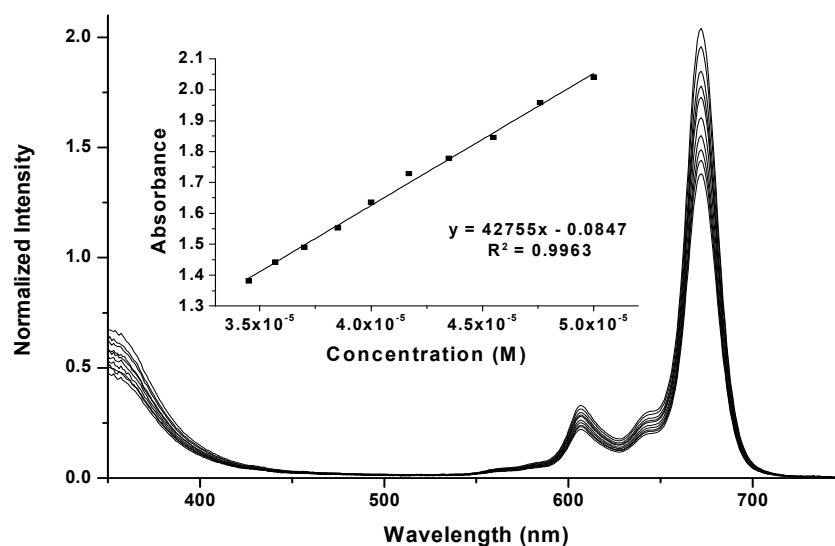


Figure 3.6: IR spectrum of the ZnAPPc.

The Q band of ZnAPPc was observed at 673 nm in DMSO, Figure 3.7 and at 668 nm in DMSO:water Figure 3.8. Beer's law was observed for the ZnAPPc complex for concentrations less than  $5 \times 10^{-5}$  M. The complex is unsymmetrically substituted and it would be expected that there is some Q band splitting due to loss of symmetry, however, this is not clear from the absorption spectra in Figure 3.8.



**Figure 3.7: Absorption spectra of ZnAPPc in DMSO at different concentrations. Inset a plot of absorbance versus concentration ( $3.4 \times 10^{-5}$  to  $5 \times 10^{-5}$  M)**

Figure 3.8 shows broadening on the excitation spectrum when compared to the absorption spectrum, suggesting loss of symmetry on excitation. The loss of symmetry, due to the unsymmetrical nature of the molecule, is even more evident in the fluorescence spectrum (Figure 3.8(iii)). A Stokes shift of 16 nm is typical of MPC complexes [73].

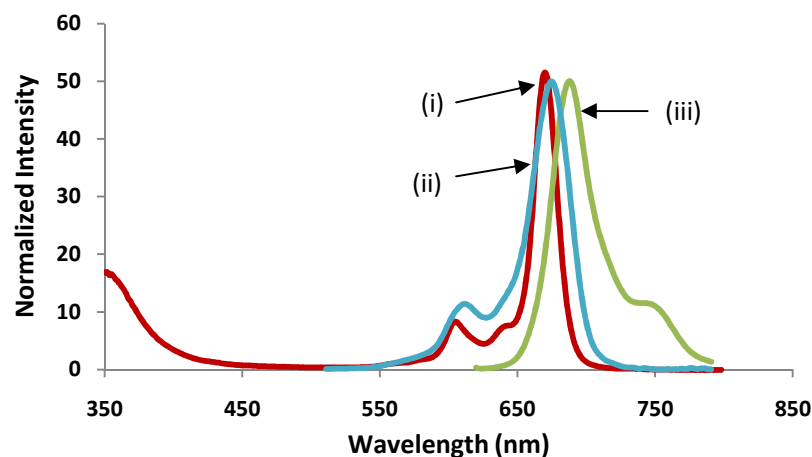
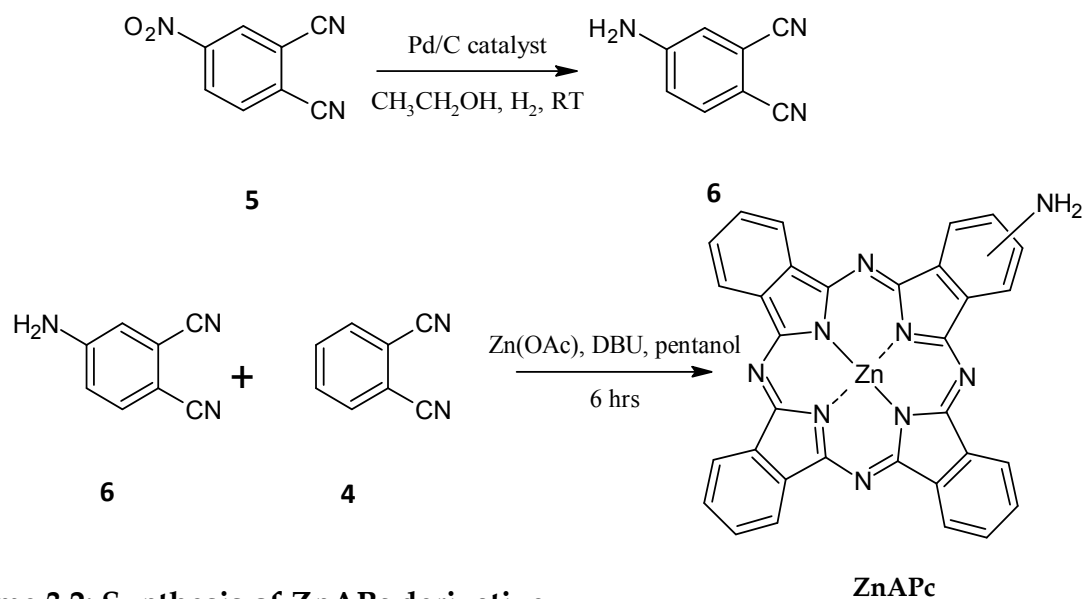


Figure 3.8: Absorbance (i), excitation (ii) and emission (iii) spectra of ZnAPPc in DMSO: water (9:1) solvent mixture (excitation wavelength = 597 nm). Concentration =  $5.0 \times 10^{-5}$  M for absorption spectrum and  $2.5 \times 10^{-7}$  M for fluorescence studies.

### 3.2.2. Zinc monoaminophthalocyanine (Scheme 3.2)



Scheme 3.2: Synthesis of ZnAPc derivative

The ZnAPc was also synthesized and characterized by various spectroscopic methods; IR, UV-vis,  $^1\text{H}$  NMR and elemental analysis as described previously. After extensive purification a yield of 10.3% was obtained.

The IR spectra, Figure 3.9, showed characteristic peaks due to the phthalocyanine skeletal vibrations between 1000 and 700  $\text{cm}^{-1}$ . The complex showed vibrations due to the amino group ( $\text{NH}_2$ ) at 3272  $\text{cm}^{-1}$ , and 1602  $\text{cm}^{-1}$ . The  $^1\text{H}$  NMR spectra for the ZnAPc was complex as was the case for ZnAPPc. The presence of isomers for mono-substituted complex and the high possibility of phthalocyanine aggregation at the concentrations used for the NMR measurements may lead to broadening of the aromatic signals; however such the observed spectra of the complexes were relatively well resolved. The ZnAPc showed two sets of double doublets at 8.29-8.31, 7.66-7.73 ppm for the phthalocyanine ring protons, each integrating for seven protons each, and a multiplet at 7.24-7.27 ppm for a single phthalocyanine ring proton. Mass spectra gave a molecular ion peak at 591.10  $[\text{M}-2\text{H}]^+$ .

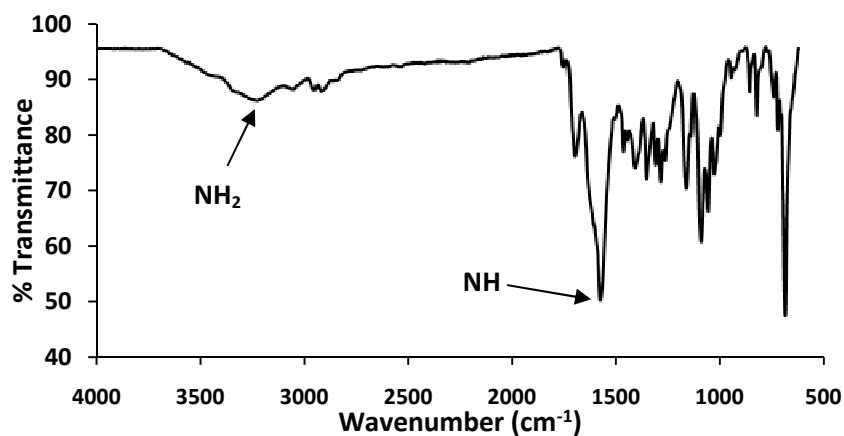
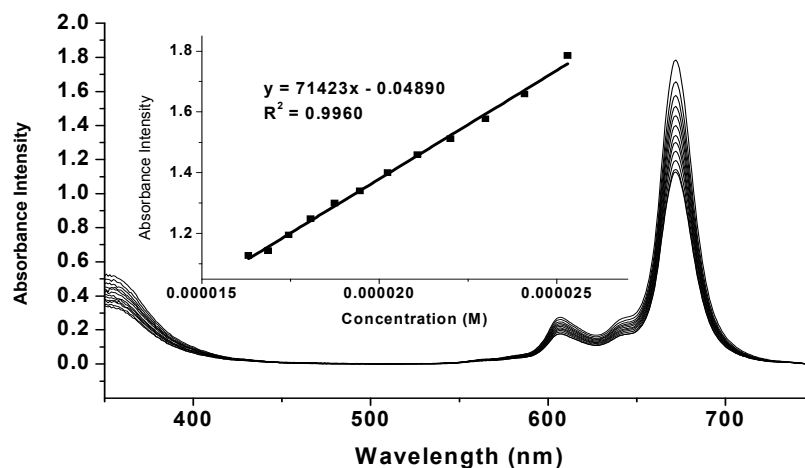


Figure 3.9: IR spectrum of the ZnAPc.

The Beer-Lambert law was obeyed for ZnAPc for concentrations less than  $2.53 \times 10^{-5}$  M, Figure 3.10. Again, there is no splitting of the Q band which is expected for unsymmetrically substituted Pcs.



**Figure 3.10: Absorption spectra of ZnAPc in DMSO at different concentrations. Inset a plot of absorbance versus concentration ( $1.63 \times 10^{-5}$  to  $2.53 \times 10^{-5}$  M)**

Figure 3.11 shows broadening (and splitting) of the excitation spectrum when compared to the absorption spectrum, suggesting loss of symmetry on excitation due to unsymmetric nature of the molecule. The loss of symmetry would result in the splitting of the  $e_g$  orbital (the lowest unoccupied molecular orbital) of the phthalocyanines resulting in two transitions from the highest occupied molecular orbital instead of one as is typical of low symmetry Pcs such metal free complexes [92]. A Stokes shift of 9 nm was observed and is typical of MPc complexes [73].

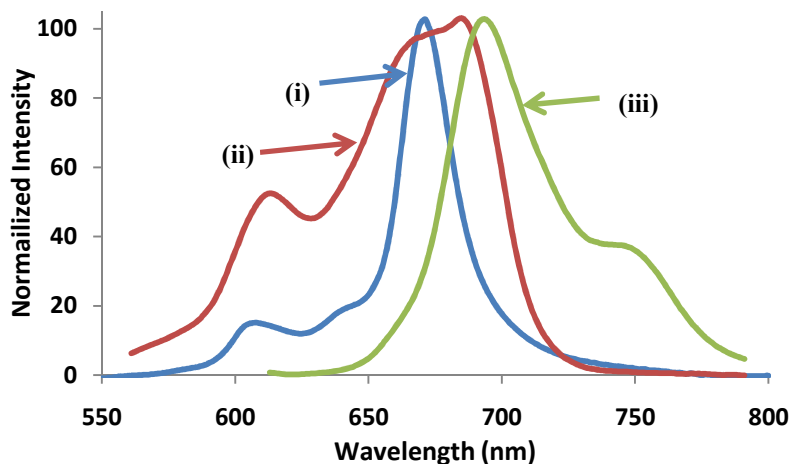
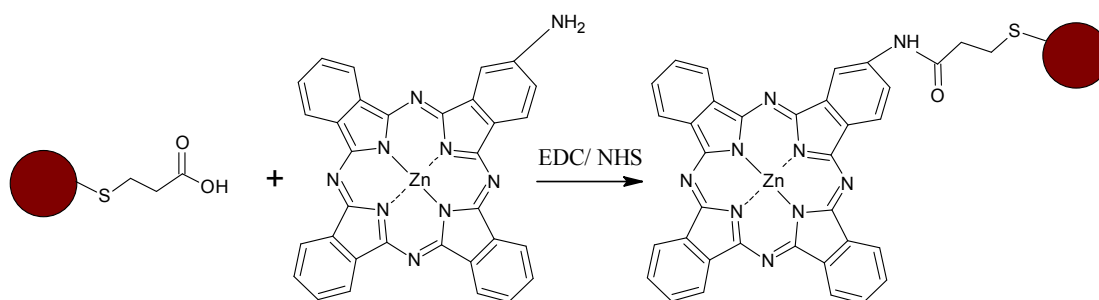
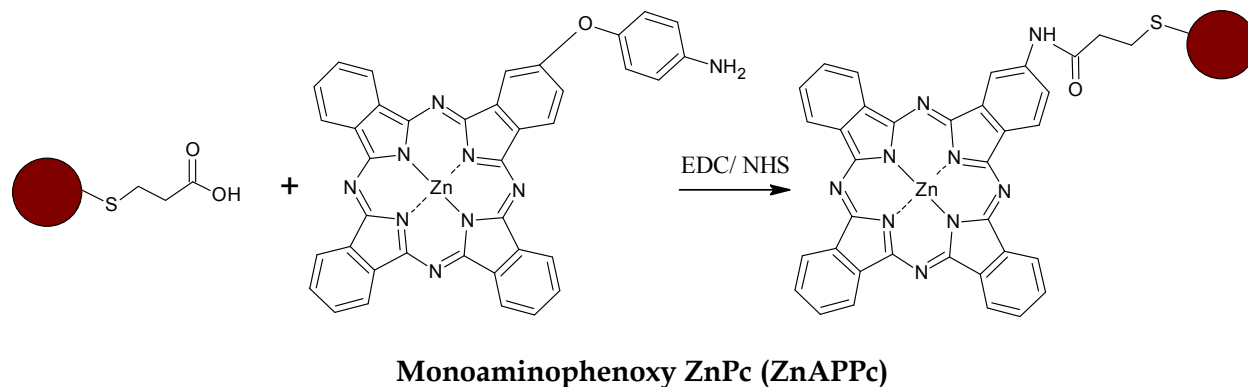


**Figure 3.11:** Absorbance (i), excitation (ii) and emission (iii) spectra of complex ZnAPc in DMSO (excitation wavelength = 603 nm). Concentration =  $2.53 \times 10^{-5}$  M for absorption spectrum and  $3.15 \times 10^{-7}$  M for fluorescence studies.

### 3.3 Interaction of low-symmetry zinc phthalocyanines with QDs (Scheme 3.3)

The Pcs used in this work contain an amino group which is used for attachment to the terminal carboxyl groups of the thiol capping agents, mercaptopropionic acid (MPA), thioglycolic acid (TGA) and L-cysteine. Carboxyl activating agents, N-ethyl-N(3-dimethylaminopropyl) carbodiimide (EDC) and N-hydroxy succinimide (NHS) are used as linking agents to form an amide bond between the Pc and QD, Scheme 3.3.



**Scheme 3.3: Linking of a thiol capped QD to the amino group on the ZnPc using the coupling agent EDC/NHS.**

The AFM images in the presence of the ZnAPPc complex, Figure 3.12, shows more enhanced clusters as opposed to smaller dots observed for QDs alone in DMSO:water, Figure 3.5.

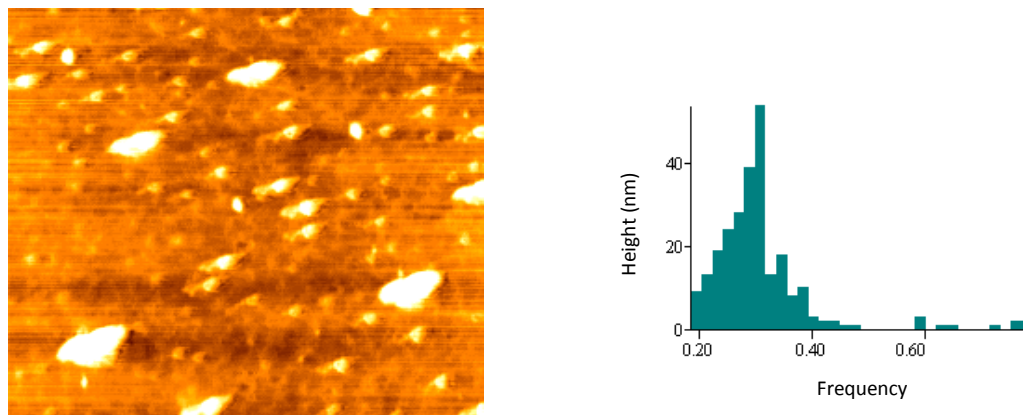


**Figure 3.12: AFM image of CdTe-MPA QDs deposited on a glass surface from QDs and ZnAPPc in DMSO:water with the corresponding histogram.**

Raman spectra were collected in order to characterize the new complex, Figure 3.13. The main difference between the linked (QD-ZnAPPc-linked, Figure 3.13a) and mixed (QD:ZnAPPc-mixed, Figure 3.13b) conjugates was the position of the main peaks attributed to the phthalocyanine structure alone (Figure 3.13c) at 2916 and 3004  $\text{cm}^{-1}$ . A shift of the peak at 3004  $\text{cm}^{-1}$  for the QD-ZnAPPc-linked complex suggests the presence of a change in the molecular structure as a result of bond formation between the QDs and ZnAPPc.

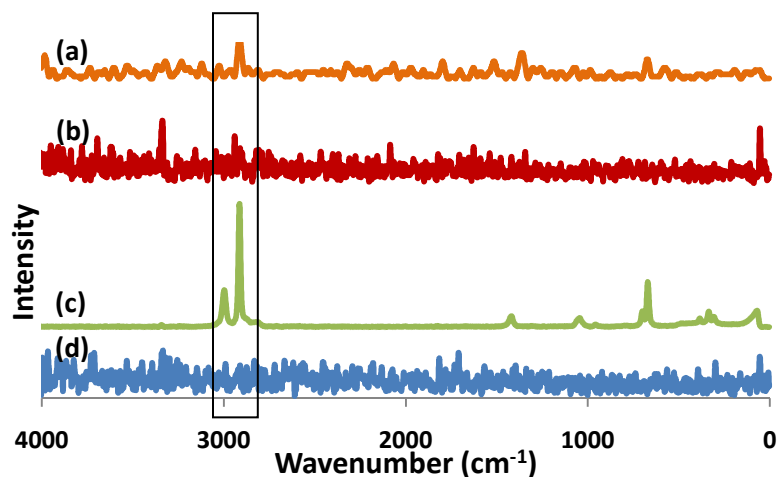


Figure 3.13: Raman spectra of (a) ZnAPPc-CdTe-MPA QD linked, (b) ZnAPPc-CdTe-MPA QD mixed, (c) ZnAPPc alone and (d) CdTe-MPA QDs alone.

Absorption spectra were used for further characterization of the mixed and linked species in the DMSO:water solvent mixture (Figure 3.14). Interestingly there was a shift in the Q band, (Figure 3.14B) from 676 nm (of ZnAPc alone) to 674 nm upon formation of the linked complex between ZnAPc and QDs. However, a shift from 673 nm to 678 nm was observed for the ZnAPPc (Figure 3.14A) alone and linked respectively, showing changes in the environment. This difference in spectra between the linked and mixed is an indirect way of confirming the linkage. Both of the mixed samples exhibited similar Q bands to their respective ZnPc derivatives. There was an increase in absorption in the 500 nm region for QD-ZnAPPc-linked and QD:ZnAPPc-mixed due to the presence of QDs (using MPA capped QDs as an example). The QD-ZnAPPc-linked shows a lower absorption in the 500 nm region than QD:ZnAPPc-mixed, which is also observed for the QD:ZnAPc, due to different amounts of QDs in the two.

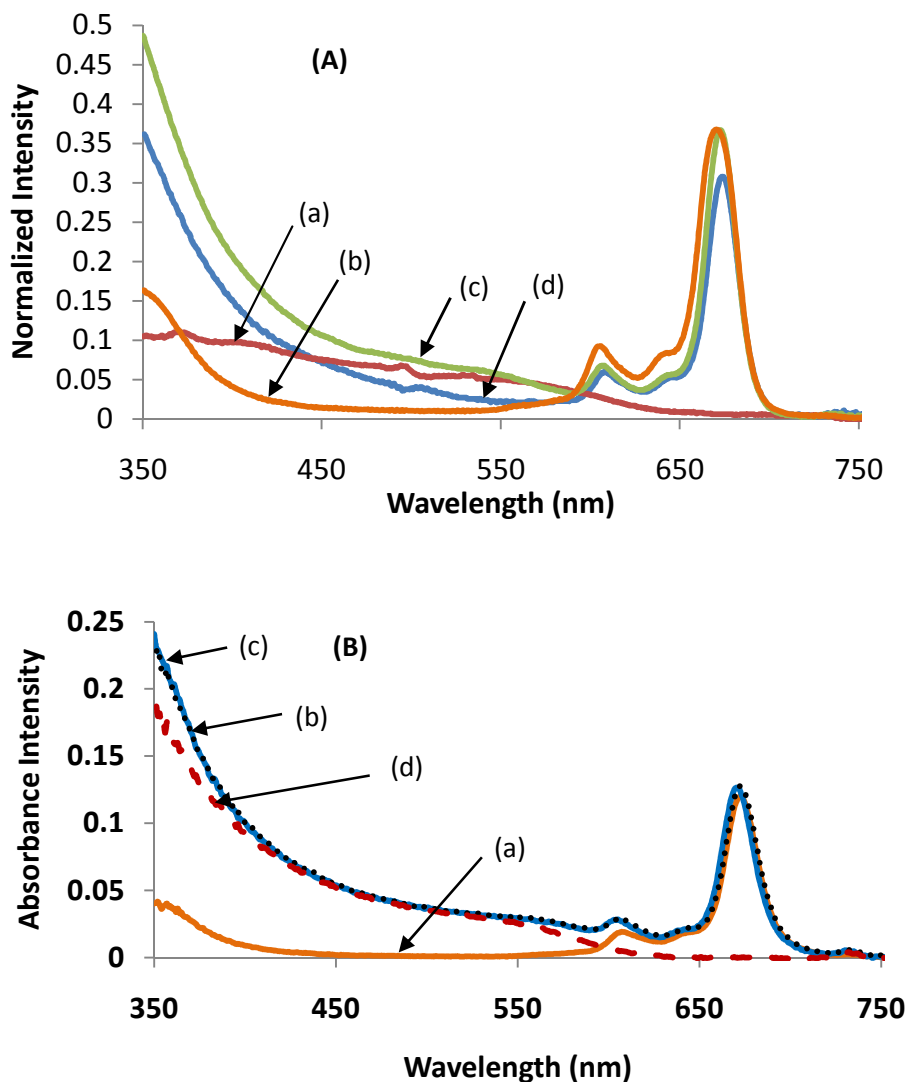


Figure 3.14: (A) Ground state electronic absorption spectra and Q band position of (a) CdTe-MPA QDs alone, (b) ZnAPPc alone (673 nm), (c) QD:ZnAPPc-mixed (674 nm) and (d) QD-ZnAPPc-linked (678 nm) in 9:1 *v/v* DMSO:water solution. (B) Ground state electronic absorption spectra (a) ZnAPc alone (676 nm), (b) ZnAPc:QD mixed (674 nm) and (c) ZnAPc-QD linked (674 nm) and (d) CdTe-MPA QDs alone in 9:1 *v/v* DMSO:water solution.

#### 4. PHOTOPHYSICAL PROPERTIES

The photophysical properties of the synthesized QDs and MPCs are discussed in this chapter.

#### 4.1 Fluorescence quantum yields

The fluorescence quantum yields of the ZnPc ( $\Phi_F = 0.20$ ) and ZnTSPc ( $\Phi_F = 0.14$ ) in DMSO only are known [73]. The fluorescence quantum yields for ZnPc were  $\Phi_F = 0.17$  in DMSO:H<sub>2</sub>O, and  $\Phi_F = 0.15$  in DMF:H<sub>2</sub>O, for ZnTSPc the values were  $\Phi_F = 0.25$  and  $\Phi_F = 0.19$  in DMSO:H<sub>2</sub>O and DMF:H<sub>2</sub>O, respectively. The values for the ZnTSPc are higher than for the rest of the MPc complexes in Table 4.1. The  $\Phi_F$  value for complex ZnAPc was determined to be 0.16 in DMSO:water and 0.14 in DMF:water, and for ZnAPPc these values are 0.16 and 0.13, respectively. These values are typical of MPc complexes containing zinc [73]. Very low  $\Phi_F$  values (0.0011 and 0.0043) were obtained for the ZnPc <sup>$\alpha$</sup> (NH<sub>2</sub>)<sub>4</sub> which is substituted at non-peripheral positions with amino groups and the ZnPc <sup>$\beta$</sup> (NH<sub>2</sub>)<sub>4</sub>, (substituted at the peripheral position) respectively, were obtained in DMF [67], due to the quenching effects of the amino group. The ZnAPc monosubstituted derivative from this work gave a high  $\Phi_F$  value of 0.14 due to the presence of a fewer number of amino groups. The low value of  $\Phi_F = 0.0020$  was also obtained for ZnPc <sup>$\alpha$</sup> (PhNH<sub>2</sub>)<sub>4</sub> (Ph=phenyl) [68], while the corresponding monosubstituted derivative (complex **3**), gave a high value of  $\Phi_F = 0.13$  in DMF:water, Table 1, showing the effects of the number of NH<sub>2</sub> substituents. The presence of water in the solvent mixtures employed in this work is not expected to increase  $\Phi_F$  values.

Fluorescence quantum yields ( $\Phi_{F(QD)}$ ) of CdTe-MPA QDs were calculated using equation (1.3). The ( $\Phi_{F(QD)}$ ) of CdTe-MPA QDs is 0.57 in DMSO:water. On mixing the QDs with complex ZnAPPc in DMSO:water, the ( $\Phi_{F(QD)}$ ) of CdTe-MPA QDs decreases

to 0.21 with the linked species giving a value of 0.04. The ZnAPc complex reported the same  $\Phi_F$  of 0.06 for the mixed and linked species in DMSO:water. A decrease on mixing the MPA QD with Pc was also observed with ZnPc and ZnTSPc for DMSO:water solutions.

The  $\Phi_F$  value of QDs alone in DMF:water is 0.58, Table 4.1 and also showed a decrease on mixing or linking. The decrease in ( $\Phi_{F(QD)}$ ) of CdTe-MPA QDs in the presence of ZnPc derivatives has been observed before [22,25,64] and was attributed to the transfer of energy from the donor QDs to the phthalocyanine acceptor molecules. Non-radiative (NR) decay processes may also be used to account for the decline in  $\Phi_F$  values. There is only one linking point for the QD onto the ZnPc derivatives, but it is possible for more than one Pc molecule to link to a QD. Reports have shown that one or two MPc molecules are associated to one QD depending on the size of the QD [25,63,77], for the mixed MPc:QDs conjugates. This is also possible for the linked QDs-complex conjugates.

**Table 4.1: Fluorescence quantum yield parameters for ZnPc derivatives: CdTe-MPA (size = 3.85 nm) QD interaction in DMSO:water (9:1) or DMF:water (9:1) mixture for both the linked (complexes ZnAPPc and ZnAPc only) and mixed (complexes ZnAPPc, ZnAPc, ZnPc and ZnTSPc) complexes.**

ZnPc derivative	solvent	$\Phi_{F(\text{ZnPc})}$	$\Phi_{F(\text{QD})}^{\text{mix}}$ <sup>a</sup> ( $\lambda_{\text{Exc}} = 500 \text{ nm}$ )	$\Phi_{F(\text{QD})}^{\text{linked}}$ ( $\lambda_{\text{Exc}} = 500 \text{ nm}$ )
ZnAPPc	DMSO: H <sub>2</sub> O	0.16 ( $\lambda_{\text{Exc}} = 611 \text{ nm}$ )	0.21	0.04
ZnAPPc	DMF: H <sub>2</sub> O	0.13 ( $\lambda_{\text{Exc}} = 611 \text{ nm}$ )	0.18	0.09
ZnAPc	DMSO:H <sub>2</sub> O	0.16 ( $\lambda_{\text{Exc}} = 615 \text{ nm}$ )	0.06	0.06
ZnAPc	DMF: H <sub>2</sub> O	0.14 ( $\lambda_{\text{Exc}} = 615 \text{ nm}$ )	0.03	0.01
ZnPc	DMSO: H <sub>2</sub> O	0.17 ( $\lambda_{\text{Exc}} = 613 \text{ nm}$ )	0.13	-
ZnPc	DMF: H <sub>2</sub> O	0.15 ( $\lambda_{\text{Exc}} = 613 \text{ nm}$ )	0.08	-
ZnTSPc	DMSO: H <sub>2</sub> O	0.25 ( $\lambda_{\text{Exc}} = 627 \text{ nm}$ )	0.11	-
ZnTSPc	DMF: H <sub>2</sub> O	0.19 ( $\lambda_{\text{Exc}} = 620 \text{ nm}$ )	0.31	-

<sup>a</sup>  $\Phi_{F(\text{QDs})}$  alone ( $\lambda_{\text{Exc}} = 500 \text{ nm}$ ) in DMF:water = 0.58 and in DMSO:water = 0.57.

Fluorescence quantum yield ( $\Phi_F$ ) values for the CdTe QDs in DMSO:H<sub>2</sub>O (9:1) are listed in Table 4.2. The QDs show slightly lower quantum yields in DMSO:water compared to the values reported in pH 7.4 buffer for similar sized QDs [25]. When QDs were mixed with ZnAPPc, the  $\Phi_{F(\text{QD})}^{\text{Mix}}$  were even lower due to the known quenching effects of MPC complexes on QDs [25], Table 4.2. The L-cys capped QD yielded the lowest  $\Phi_F$  values before or after mixing and linking to the ZnAPPc. The decrease in  $\Phi_F$  for QDs in the presence of phthalocyanine units is a regular occurrence [25] and the quenching has

been attributed to the transfer of energy from donor QDs to phthalocyanine acceptor molecules. This results in a lowering of QD fluorescence intensity, in either a QD:ZnAPPc-mixed or QD-ZnAPPc-linked species, and therefore a reduction in fluorescence quantum yields of the QDs. Non-radiative (NR) decay processes may also be used to account for the decline in  $\Phi_F$  values.

**Table 4.2: Fluorescence quantum yield parameters for ZnAPPc: CdTe QD interaction in DMSO:water (9:1) mixture for both the linked and mixed complexes. ( $\lambda_{Exc} = 500$  nm).**

Thiol Capping <sup>a</sup>	$\Phi_{F(QD)}$	$\Phi_{F(QD)}^{Mix}$	$\Phi_{F(QD)}^{Linked}$	Ref
MPA (3.85)	0.57	0.21	0.04	TW
TGA (3.37)	0.57	0.48	0.03	TW
LCys (4.08)	0.04	0.03	0.004	TW
MPA (3.7)	0.59	-	-	[25] <sup>b</sup>
TGA (3.6)	0.62	-	-	[25] <sup>b</sup>
LCys (3.5)	0.09	-	-	[25] <sup>b</sup>

<sup>a</sup>QD size in brackets. <sup>b</sup>Data in pH 7.4 buffer. TW = This Work

## 4.2 Fluorescence lifetimes

Fluorescence lifetimes ( $\tau_F$ ) were determined in a DMSO:water or DMF:water 9:1 (v/v) mixture, and the data obtained is shown in Tables 4.3 and 4.4 respectively. Photoluminescence decay curves of CdTe-MPA QDs (a) and CdTe QDs in the

presence of ZnAPc (b) in DMSO: water (9:1) solvent mixture on excitation at 480 nm are shown in Figure 4.1, as an example.

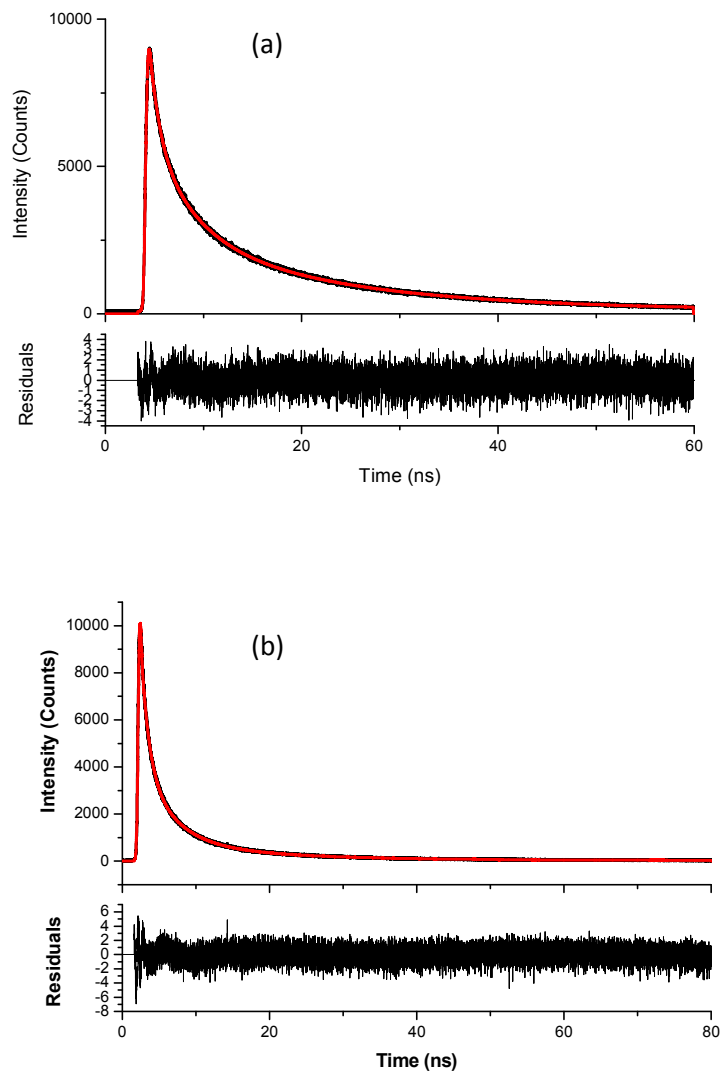


**Figure 4.1: Photoluminescence decay curves of (a) CdTe QDs and (b) CdTe QDs in the presence of ZnAPc in DMSO:water (9:1) solvent mixture.**

Quality of the fit in Figure 4.1 was judged on the basis of the chi-squared statistic values,  $\chi^2$ , which were close to unity. Tables 4.3 and 4.4 show that changing the

solvent has an effect on the fluorescence lifetimes for all samples. Two lifetimes are observed for the ZnPc derivatives, however the second lifetimes are insignificant since their respective amplitudes are less than or close to 0.1. The lifetimes are in the reported range for ZnPc derivatives [55]. The second lifetimes (which are present in insignificant amount) could be due to traces of ZnPc(NH<sub>2</sub>)<sub>4</sub> or ZnPc (PhNH<sub>2</sub>)<sub>4</sub>, which do not fluoresce significantly due to quenching of excited states, as discussed above.

**Table 4.3: Fluorescence lifetimes of QDs in the presence of ZnAPPc and ZnAPc in DMSO:water (9:1).**

Compound	$\tau_{F1}$ (ns) ( $\pm 2.7$ )	Rel. $A_1$	$\tau_{F2}$ (ns) ( $\pm 1.2$ )	Rel. $A_2$	$\tau_{F3}$ (ns) ( $\pm 0.2$ )	Rel. $A_3$	$\chi^2$	$Eff_{tr}$
Complex ZnAPc alone <sup>a</sup>	3.0	0.90	4.1	0.10	-	-	1.06	-
Complex ZnAPPc alone <sup>a</sup>	3.0	0.92	4.3	0.08	-	-	1.11	-
MPA QDs alone <sup>b</sup>	19.0	0.23	4.8	0.33	0.9	0.45	1.04	-
QDs mixed with ZnAPc <sup>b</sup>	16.7	0.21	4.2	0.33	0.8	0.45	1.03	0.17
QDs linked to ZnAPc <sup>b</sup>	9.0	0.15	2.6	0.30	0.5	0.55	1.07	0.62
QDs mixed with ZnAPPc <sup>b</sup>	14.1	0.25	3.8	0.37	0.8	0.38	1.29	0.18
QDs linked to ZnAPPc <sup>b</sup>	8.5	0.16	3.1	0.34	0.6	0.50	1.37	0.57

<sup>a</sup>  $\lambda_{Exc} = 670$  nm, <sup>b</sup>  $\lambda_{Exc} = 480$  nm

**Table 4.4: Fluorescence lifetimes of QDs in the presence of ZnPc derivatives in DMF:water (9:1).**

Compound	$\tau_{F1}$ (ns) ( $\pm 1.5$ )	Rel. $A_1$	$\tau_{F2}$ (ns) ( $\pm 0.6$ )	Rel. $A_2$	$\tau_{F3}$ (ns) ( $\pm 0.2$ )	Rel. $A_3$	$\chi^2$	$Eff_{tr}$
Complex ZnAPc alone <sup>a</sup>	3.0	0.94	1.2	0.06	-	-	1.02	-
Complex ZnAPPc alone <sup>a</sup>	3.0	0.93	1.0	0.07	-	-	1.13	-
MPA QDs alone <sup>b</sup>	18.8	0.20	5.6	0.4	1.4	0.40	1.07	-
QDs mixed with ZnAPc <sup>b</sup>	12.2	0.12	3.4	0.35	0.8	0.53	1.10	0.53
QDs linked to ZnAPc <sup>b</sup>	12.1	0.12	3.4	0.35	0.8	0.53	1.27	0.53
QDs mixed with ZnAPPc <sup>b</sup>	11.1	0.06	3.1	0.27	0.7	0.68	1.32	0.70
QDs linked to ZnAPPc <sup>b</sup>	9.8	0.1	2.8	0.34	0.7	0.56	1.30	0.65

<sup>a</sup>  $\lambda_{Exc} = 670$  nm, <sup>b</sup>  $\lambda_{Exc} = 480$  nm

Although biexponential decay kinetics has been shown to occur for QDs [63], this report presents the presence of triple decay kinetics as observed by other researchers [93]. The origin of the longer lifetime component  $\tau_{F1}$  may be due to the involvement of surface states in the carrier recombination process [93], where the increase in radiative lifetime is a result of trapping of carrier states, by surface states, is a well established feature [93]. This is clearly observed by the large decrease in  $\tau_{F1}$  compared to  $\tau_{F2}$  and  $\tau_{F3}$ , due to attachment or mixing of Pcs which affects the surface, resulting in the shorter fluorescence lifetime in DMSO:water, Table 4.3. The second fluorescence lifetime component, ( $\tau_{F2}$ ), is a result of radiative electron-hole recombination processes due to surface defects [94]. According to some researchers [78,93,95], the shortest component  $\tau_{F3}$  is caused by the band-edge recombination at

the surface; but this is contradicted by others who attribute this short lifetime to intrinsic recombination of initially populated core states [93,96,97]. As expected, the mixed conjugates show longer lifetimes than the linked, though the changes are insignificant in DMF:water for ZnAPPc (for all lifetimes) and ZnAPc (for the third lifetime). The reasons for the differences in the fluorescence lifetime behaviour of QDs linked or mixed with the ZnPc complexes are not clear, but they could be related to the presence of a phenyl linker between the Pc ring and the amino group in ZnAPPc, and the direct coordination of the amino group in ZnAPc. Judging by a larger decrease in the long lifetime ( $\tau_{F1}$ ) in the presence of complex ZnAPPc compared to ZnAPc, the former attaches to the QDs surface more efficiently in both DMF:water and DMSO:water, Tables 4.3 and 4.4. It is however not clear why  $\tau_{F1}$  for ZnAPc mixed with QDs or linked to them remain the same. It can only be postulated that since the  $\text{NH}_2$  group is directly on the ring for ZnAPc, the distances between the QDs and Pc in the linked and mixed complexes are not too different and hence affect the fluorescence lifetimes the same way. However this is solvent dependent since in DMSO:water, there is a difference in  $\tau_{F1}$  for linked and mixed ZnAPc complexes. The covalent bond in the linked conjugates allows a closer proximity between the QD and Pc derivative, further encouraging the possibility of FRET or the radiationless loss of energy through the bonds.

When compared to the values shown in Table 1.3, the QD fluorescence lifetimes compare well with the CdTe-TGA results. However, three lifetimes are obtained for the mixed and linked QD-Pc conjugates as opposed to the two lifetimes shown in

Table 1.3, as mentioned above. The values obtained in this work for the mixed and linked CdTe-MPA conjugates, show lifetimes shorter to those obtained in Table 1.3.

### 4.3 Förster resonance energy transfer (FRET)

In order for FRET to occur, there should be an overlap between the fluorescence spectra of each QD with the absorption spectrum of ZnAPPc (or ZnAPc), and this is observed in Figure 4.2 for ZnAPPc.

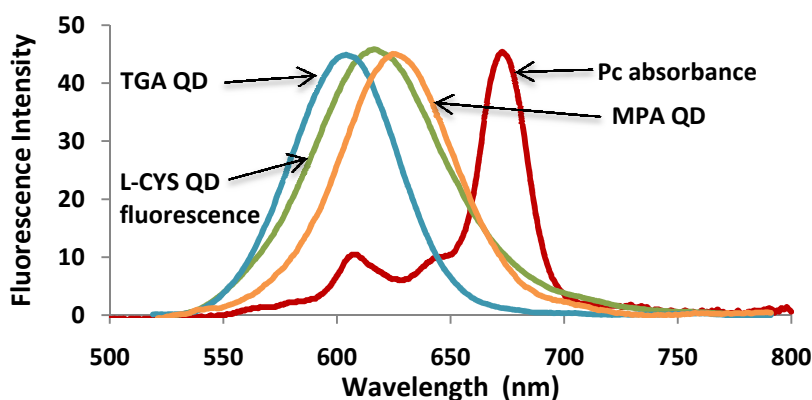


**Figure 4.2:** Electronic spectrum showing the overlap between the absorption spectra of the ZnAPPc and the photoemission spectra of the respective QDs. Solvent: water (QDs) and DMSO (ZnAPPc).

On mixing solutions of ZnAPPc with QDs and monitoring the emission spectra of the QDs, a decrease in the fluorescence emission (on exciting at 500 nm where QDs absorb and ZnAPPc does not) of the latter was observed, Figure 4.3.

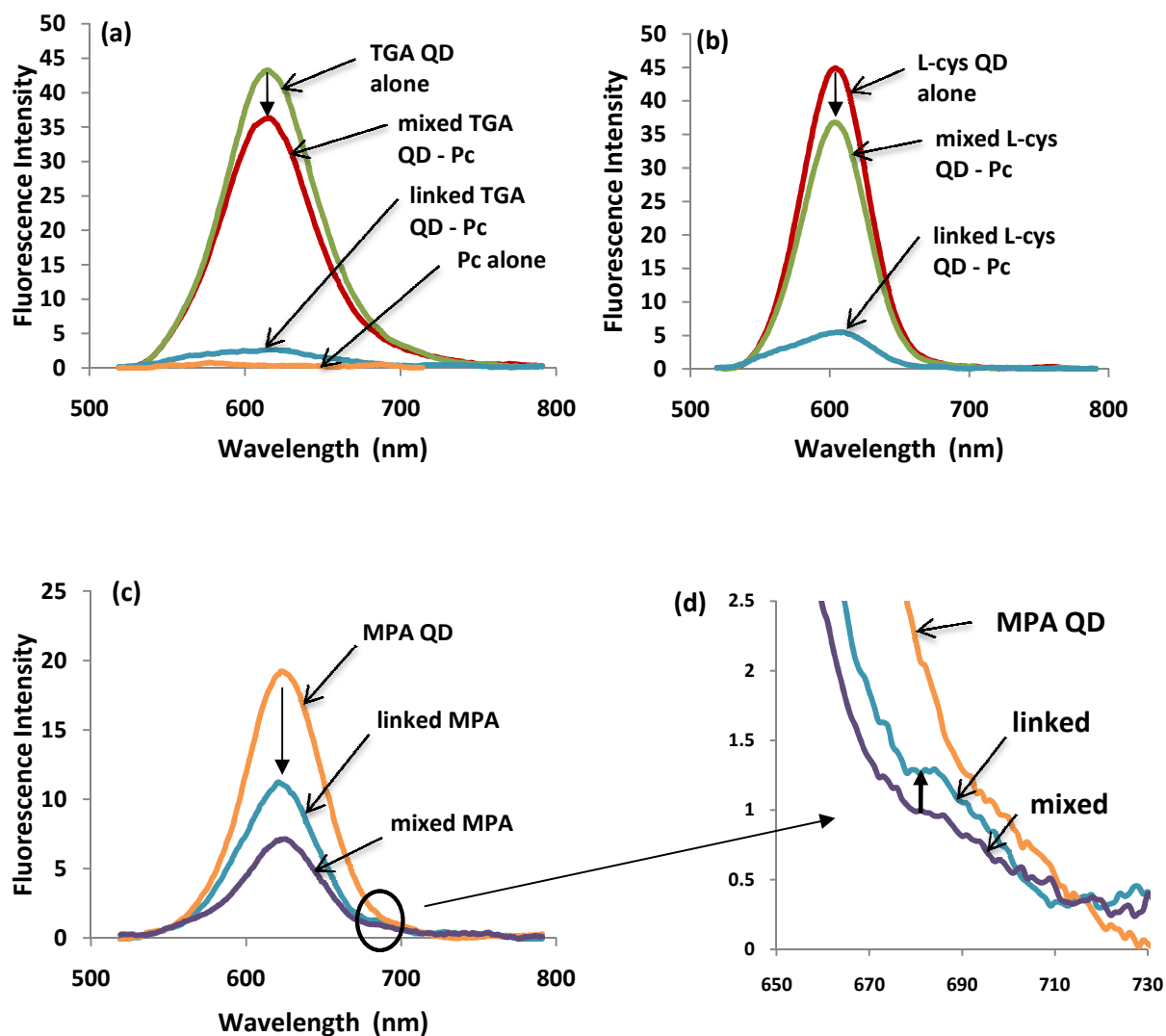


Figure 4.3: Emission of QDs alone, ZnAPPc, QDs in the mixture with the ZnAPPc or ZnAPPc linked to QDs. (a) TGA, (b) L-cys, (c) MPA capped QDs and (d) magnification of (c). ( $\lambda_{\text{excitation}} = 500 \text{ nm}$ , in (9:1) DMSO:water solvent mixture).

These changes are due to energy transfer from the QDs to ZnAPPc. There is no clear emission for ZnAPPc in the presence of TGA and L-cys capped QDs, Figure 4.3a and b.

For MPA capped QDs there is a very weak stimulated emission for both mixed and linked QDs, Figure 4.3c, which is enhanced and shown in Figure 4.3d. The larger FRET efficiency is expected for the linked complexes due to the presence of a bond. It is feasible that the FRET efficiency observed for the linked species also comprises non-radiative processes, due to the strong involvement of surface states that may deactivate the QD fluorophores. Thus the data obtained may not be a true reflection of FRET alone; hence the weak (or no) stimulated emission in Figure 4.3. The lack of clear FRET for TGA and L-cys suggests loss of energy by other means and not FRET. It is important to note that the relative amounts of ZnAPPc and QDs will be different in the mixed and linked QD-ZnAPPc, making comparison between the two difficult.

FRET facilitates the non-radiative transfer of energy from the donor to the acceptor molecule. The efficiency of FRET is known to be dependent on a number of parameters such as the spectral overlap term ( $J$ ) estimated by overlapping QD emission with the absorbance of ZnPc derivatives, shown in Figure 4.2. This extent of overlap has varied units and in this work the units used were in  $\text{cm}^6$  [75]. The PhotochemCAD program gives  $J$  units as  $\text{cm}^6$  following the use of  $\epsilon_{\text{ZnPc}}$  in  $\text{M}^{-1}\text{cm}^{-1}$  and the wavelength  $\lambda$  in nm in Equation (1.8). The Förster distance,  $R_0$  (Å), is the critical distance between the donor and the acceptor molecule fluorophores for which efficiency of energy transfer is 50% [75], and  $r$  (Å) is the centre-to-centre separation distance between donor and acceptor chromophores. The  $J$  and  $R_0$  values in this work were computed using PhotochemCAD [79] while the  $r$  values were calculated using Equation (1.6) and are listed in Table 4.5.

**Table 4.5: Energy transfer parameters for ZnAPPc-CdTe: thiol QD interactions (in DMSO:H<sub>2</sub>O (9:1) for linked and mixed complexes).**

Capping Thiol	$J$ ( $\times 10^{-13} \text{ cm}^6$ )	$R_0$ ( $\times 10^{-10} \text{ m}$ )	$r$ ( $\times 10^{-10} \text{ m}$ )	$Eff$
ZnAPPc-CdTe-MPA QD mixed	1.36	46.52	42.57	0.63
ZnAPPc-CdTe-MPA QD linked	1.09	44.38	29.54	0.92
ZnAPPc- CdTe-TGA QD mixed	1.24	45.71	60.26	0.16
ZnAPPc- CdTe-TGA QD linked	0.84	42.53	26.04	0.95
ZnAPPc CdTe-L-cys QD mixed	0.78	26.46	34.46	0.17
ZnAPPc CdTe-L-cys QD linked	1.30	29.37	20.36	0.90

$J$  values are generally of the order of  $10^{-14} \text{ cm}^6$  for porphyrin based molecules. The values obtained in this work were of the order  $10^{-13} \text{ cm}^6$  for the overlap between the QDs and the ZnAPPc complex, as shown in Table 4.5, thus confirming good spectral overlap, which is desirable since a greater value of  $J$  indicates good spectral overlap between the emission spectrum of the donor and the absorption spectrum of the acceptor giving an estimation of a good donor-acceptor oscillator match and hence a greater probability for FRET. This large  $J$  value would probably enhance the efficiency of energy transfer (FRET). The efficiency of FRET ( $Eff$ ) values calculated using Equation (1.5) from the QD to the ZnAPPc derivative are shown in Table 4.5.

The values of  $r$  were smaller than for  $R_0$  for mixed MPA capped QDs, showing that  $Eff$  will be greater than 50% as observed in Table 4.5 and vice versa for the mixed TGA and L-cys capped QDs. Higher  $Eff$  values were observed for the linked QDs-ZnAPPc when

compared to the mixed QDs-ZnAPPc combinations, showing the advantages of chemical linking as expected. It has been reported before that MPA capped QDs show better  $Eff$  than their TGA counterparts for mixed MPC:QDs conjugates [25] and this is evident in Table 4.5, comparing the mixed complexes. For the linked complexes, MPA and TGA capped QDs show better efficiencies than the L-cys capped QDs. Also as seen in Figure 4.3, stimulated emission for TGA and L-cys capped QDs in the presence of ZnAPPc was unclear, whereas for the MPA capped QDs stimulated emission of ZnAPPc was visible though weak.

In addition to this, Equations (1.5) to (1.8) are only valid for fixed distances [75] between the QDs and the ZnPc derivatives. FRET efficiency were also calculated using Equations (1.9) and (1.10), and shown in Tables 4.3 and 4.4 for DMSO:H<sub>2</sub>O and DMF:H<sub>2</sub>O solvent systems respectively.

The values obtained in Table 4.3 show that the  $Eff_{tr}$  for the mixed QD-Pc are very low (< 20%) in DMSO:water; whereas the linked species show an  $Eff_{tr} > 50\%$ . The  $Eff_{tr}$  for the DMF:H<sub>2</sub>O solvent system were improved for the mixed QD-Pc species. The  $Eff_{tr}$  remained the same for the mixed and linked QD-ZnAPc at 53%. The mixed QD-ZnAPPc species increased to 70% compared to the DMSO:H<sub>2</sub>O solvent system; and the linked species had a slightly lower  $Eff_{tr}$  of 65%. Equations (1.5) and (1.9) are expected to produce the same results [75], however this is not the case for these samples. One reason for such high  $Eff_{tr}$  values (Table 4.5) using Equation (1.5) could be the extremely low fluorescence quantum yields obtained.

#### 4.4 Triplet state quantum yields and lifetimes

The transient absorption spectra were recorded in argon-degassed solutions by exciting the photosensitizer (in DMSO) in the Q band region and recording the spectra point by point from 400 to 800 nm, Figure 4.4, which shows singlet depletion and a very weak triplet-triplet absorption at 500 nm in DMSO.

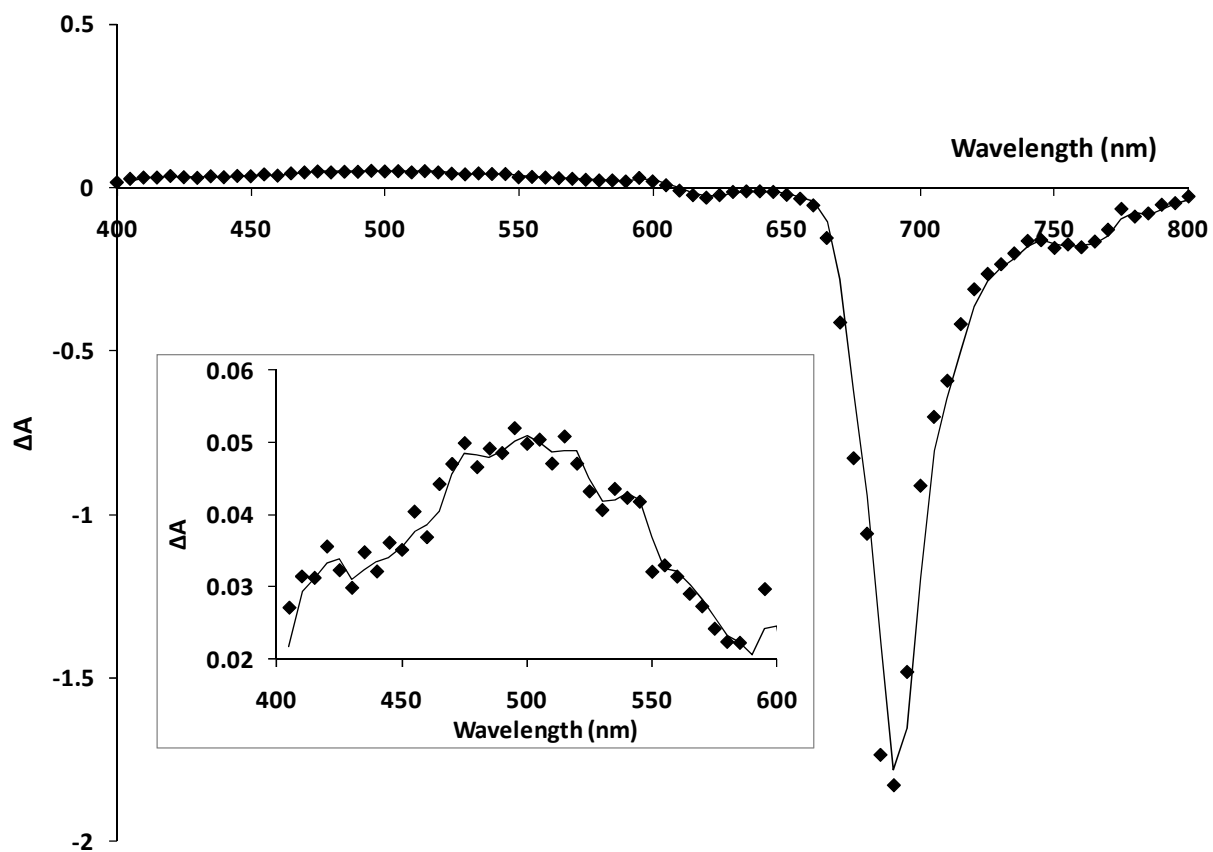
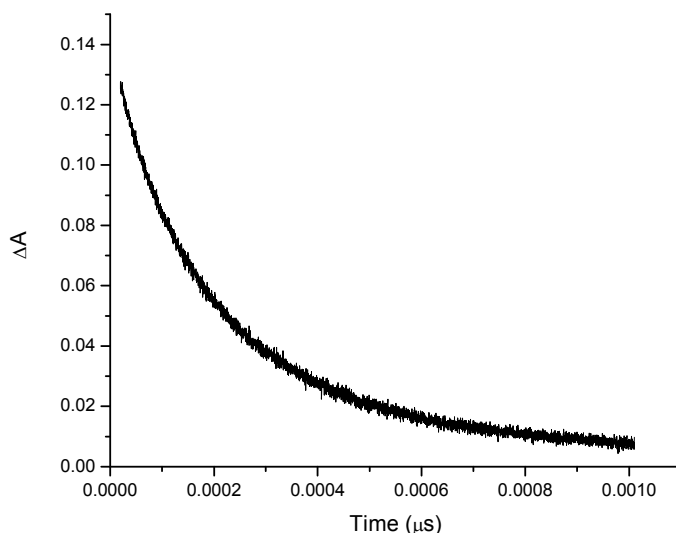


Figure 4.4: Transient differential spectrum of ZnAPc in DMSO. Excitation wavelength = 672 nm.

A representative decay profile is shown in Figure 4.5. The data in Figure 4.4 are obtained using absorbances from a series of traces similar to the one shown in Figure 4.5 at different wavelengths.



**Figure 4.5: Triplet decay curve of ZnAPc in DMSO at 490 nm. Excitation wavelength = 672 nm.**

Triplet quantum yields ( $\Phi_T$ ) are a measure of the fraction of absorbing molecules that undergo intersystem crossing (ISC) to populate the triplet state. The triplet quantum yield studies of the monofunctionalized Pcs in the presence of QDs (mixed or linked) were carried out in a DMSO:water or DMF:water 9:1 (v/v) mixtures are shown in Table 4.6. Values of  $\Phi_T = 0.48$  and  $0.39$  in DMSO:water and DMF:water, respectively are observed for ZnAPc, and  $\Phi_T = 0.65$  and  $0.37$  are observed for ZnAPPc in DMSO:water and DMF:water, respectively. For  $\text{ZnPc}^\alpha(\text{NH}_2)_4$  or  $\text{ZnPc}^\alpha(\text{PhNH}_2)_4$  which are

substituted at non-peripheral positions with amino or phenylamino groups, respectively, triplet-triplet absorption did not occur [67,68], due to the quenching of the first excited singlet state by the presence of amino group, inhibiting the formation of its triplet state by intersystem crossing. The quenching effect of the amino group is not expected to be affected much by the differences in solvents. However in case of the ZnPc derivatives, the triplet state parameters were observed due to the presence of only one amino (phenyl amino) group resulting in less quenching.

**Table 4.6: Photophysical parameters of ZnPc complexes in the presence of QDs in DMSO:water or DMF:water (9:1) ( $\Phi_T$  ZnPc in DMSO = 0.65,  $\Phi_T$  ZnPc in DMF = 0.56).**

Compound	DMSO:Water (9:1)		DMF:Water (9:1)	
	$\Phi_T$	$\tau_T$ ( $\mu$ s)	$\Phi_T$	$\tau_T$ ( $\mu$ s)
ZnAPc alone	0.48	208	0.39	3.1
ZnAPc mixed with QDs	0.32	221	0.34	5.2
ZnAPc linked to QDs	0.60	186	0.31	4.0
ZnAPPc alone	0.65	216	0.37	3.6
ZnAPPc mixed with QDs	0.64	206	0.25	2.7
ZnAPPc linked to QDs	0.69	205	0.21	5.3

It is expected that the  $\Phi_T$  of MPc complexes will increase in the presence of QDs due to the heavy atom effect of the cadmium and tellurium atoms making up the QD. However, for ZnAPc, there is an increase only on linking but a decrease on mixing in DMSO:water. For ZnAPPc, there is no change on mixing, but an increase on linking

with QDs in DMSO:water. In DMF:water there is a decrease for both linked and mixed ZnAPPc and ZnAPc complexes. The lifetimes for complexes in DMF:water are very short. Triplet lifetime values decreased where there is an increase in triplet yields as expected by the heavy atom effect. The triplet quantum yield and lifetime values obtained for the DMSO:water solvent system fall within the ranges given in Table 1.5.

## 5. GENERAL CONCLUSIONS

The low-symmetry monoamino zinc phthalocyanine and monoaminophenoxy zinc phthalocyanine derivatives have been successfully synthesized using the statistical condensation method. The unsymmetrically substituted 4-mono-aminophenoxy zinc phthalocyanine (ZnAPPc) and zinc amino phthalocyanine (ZnAPc) were successfully linked to the thiol capped quantum dots (QDs) and fully characterized. The linked ZnAPPc-QD complexes showed higher FRET efficiencies for the L-cys and TGA complexes making them ideal photosensitizers for photodynamic therapy.

Triplet quantum yields have been determined for ZnAPc and ZnAPPc in a DMSO:water mixture. The solvent mixture plays a major role, with the species in the DMSO:water mixture generally giving higher triplet quantum yields and longer triplet lifetimes. The newly synthesized low-symmetry derivative ZnAPc shows good photosensitizing properties which may also make them useful as photosensitizers.

## REFERENCES

- [1] J.H. Fendler in: *Nanoparticles In Solids and Solutions*, 3rd ed., Kluwer Academic Publishers, Netherlands, 1996.
- [2] T. Tsakalakos, I. Ovid'ko, A.K. Vasudevan in: *Nanostructures: Synthesis, Functional Properties and Applications*, Kluwer Academic Publishers, Netherlands, 2003.
- [3] M. Ozkan, *Drug Discovery Today* 9 (2004) 1065-1071.
- [4] X. Michalet, F.F. Pinaud, L.A. Bentolila, J.M. Tsay, S. Doose, J.J. Li, G. Sundaresan, A.M. Wu, S.S. Gambhir, S. Weiss, *Science* 307 (2005) 538-544.
- [5] H.M.E. Azzazy, M.M.H. Mansour, S.C. Kazmierczak, *Clin. Biochem.* 40 (2007) 917 - 927.
- [6] T. Jamieson, R. Bakhshi, D. Petrova, R. Pocock, M. Imani, A.M. Scifalian, *Biomaterials* 28 (2007) 4717-4732.
- [7] L. Hui in: *Synthesis and Characterization Of Aqueous Quantum Dots For Biomedical Applications*, 2008.
- [8] G. Schmid in: *Nanoparticles: From Theory To Application*, 2nd ed., Wiley-VCH, Germany, 2010.
- [9] S. Wang, R. Gao, F. Zhou, M. Selke, *J. Mater. Chem.* 14 (2004) 487-493.
- [10] F.M. Raymo, I. Yildiz, *Phys. Chem. Chem. Phys.* 9 (2007) 2036-2043.
- [11] T.J. Merkel, K.P. Herlihy, J. Nunes, R.M. Orgel, J.P. Rolland, J.M. DeSimone, *Langmuir* 26 (2010) 13086-13096.
- [12] C. Weisbuch, H. Benisty, R. Houdre, *J. Lumin.* 85 (2000) 271-293.
- [13] A. Eychmuller, A.L. Rogach, *Pure Appl. Chem.* 72 (2000) 179-188.
- [14] S.K. Shin, H.-J. Yoon, Y.J. Jung, J.W. Park, *Curr. Opin. Chem. Biol.* 10 (2006) 423-429.
- [15] J.-H. Wang, H.-Q. Wang, H.-L. Zhang, X.-Q. Li, X.-F. Hua, Y.-C. Cao, Z.-L. Huang, Y.-D. Zhao, *Anal. Bioanal. Chem.* 388 (2007) 969-974.

- [16] C. Seydel, *Science* 300 (2003) 80-81.
- [17] S. Moeno, M. Idowu, T. Nyokong, *Inorg. Chim. Acta* 361 (2008) 2950-2956.
- [18] P. Zhang, L. Li, C. Dong, H. Qian, J. Ren, *Anal. Chim. Acta* 546 (2005) 46-51.
- [19] Y. Rakovich, L. Walsh, L. Bradley, J.F. Donegan, D. Talapin, A. Rogach, A. Eychmüller, *Proc. SPIE* 4876 (2003) 432-437.
- [20] Y. Zhang, L. Mi, P.-N. Wang, J.-Y. Chen, *J. Lumin.* 128 (2008) 1948-1951.
- [21] A. Mandal, N. Tamai, *J. Phys. Chem. C* 112 (2008) 8244-8250.
- [22] C. Bullen, P. Mulvaney, *Langmuir* 22 (2006) 3007-3013.
- [23] N. Gaponik, D.V. Talapin, A.L. Rogach, K. Hoppe, E.V. Shevchenko, A. Kornowski, A. Eychmüller, H. Weller, *J. Phys. Chem. B* 106 (2002) 7177-7185.
- [24] B. Xing, W.-W. Li, K. Sun, *Mater. Lett.* 62 (2008) 3178 - 3180.
- [25] M. Idowu, J.-Y. Chen, T. Nyokong, *New J. Chem.* 32 (2008) 290-296.
- [26] H. Li, C. Han, *Chem. Mater.* 20 (2008) 6053-6059.
- [27] A.L. Rogach, T. Franzl, T.A. Klar, J. Feldmann, N. Gaponik, V. Lesnyak, A. Shavel, A. Eychmüller, Y.P. Rakovich, J.F. Donegan, *J. Phys. Chem. C* 111 (2007) 14628-14637.
- [28] L. Hua, H. Han, X. Zhang, *Talanta* 77 (2009) 1654-1659.
- [29] G. A. Martínez-Castañón, M. G. Sánchez-Loredo, J.R. Martínez-Mendoza, F. Ruiz, *J. Mater.* 1 (2005) 1-7.
- [30] W. Chidawanyika, C. Litwinski, E. Antunes, T. Nyokong, *J. Photochem. Photobiol. A* 212 (2010) 27-35.
- [31] H. Zhang, Z. Zhou, B. Yang, *J. Phys. Chem. B* 107 (2003) 8-13.
- [32] H. Peng, L. Zhang, C. Soeller, J. Travas-Sejdic, *J. Lumin.* 127 (2007) 721-726.
- [33] Y.-F. Liu, J.-S. Yu, *J. Colloid Interface Sci.* 333 (2009) 690-698.
- [34] Y. Zeng, C. Tang, H. Wang, J. Jiang, M. Tian, G. Shen, R. Yu, *Spectrochim. Acta A* 70 (2008) 966-972.

- [35] W.-H. Yang, W.-W. Li, H.-J. Dou, K. Sun, *Mater. Lett.* 62 (2008) 2564 - 2566.
- [36] A. Braun, J. Tcherniac, *Ber. Deutsch. Chem. Ges.* 40 (1907) 2709-2714.
- [37] P. Erk, H. Hengelsberg, in: K.M. Kadish, K.M. Smith, R. Guilard (Eds.), *The Porphyrin Handbook*, Academic Press, 2003, pp. 105-150.
- [38] R.P. Linstead, *J. Chem. Soc.* 42 (1934) 1016-1017.
- [39] J.M. Robertson, *J. Chem. Soc.* (1935) 615-621.
- [40] J.M. Robertson, *J. Chem. Soc.* 1 (1936) 1195-1209.
- [41] J.M. Robertson, L. Woodward, *J. Chem. Soc.* (1937) 219-230.
- [42] M.S. Rodriguez-Morgade, G. De La Torre, T. Torres, in: K.M. Kadish, K.M. Smith, R. Guilard (Eds.), *The Porphyrin Handbook*, Academic Press, 2003, pp. 125-160.
- [43] P.J. Gregory, *J. Porphyr. Phthalocya.* 3 (1999) 468-476.
- [44] D. Dini, M. Hanack, in: K.M. Kadish, K.M. Smith, R. Guilard (Eds.), *The Porphyrin Handbook*, Academic Press, 2003, pp. 1-36.
- [45] C.C. Leznoff in: A.B.P. Lever (Eds.), *Phthalocyanines, Properties and Applications*, New York, 1996.
- [46] E. Ben-Hur, W.-S. Chan, in: K.M. Kadish, K.M. Smith, R. Guilard (Eds.), *The Porphyrin Handbook*, Academic Press, 2003, pp. 1-36.
- [47] R.R. Allison, G.H. Downie, R. Cuenca, X.-H. Hu, C.H. Sibata, *Photodiagnosis Photodynamic Therapy* 1000 (2004) 27-42.
- [48] I. Rosenthal, C. Murali Krishna, P. Riesz, E. Ben-Hur, *Radiat. Res.* 107 (1986) 136-142.
- [49] R.K. Pandey, G. Zheng, in: K.M. Kadish, K.M. Smith, R. Guilard (Eds.), *The Porphyrin Handbook*, Academic Press, 2000, pp. 157-230.
- [50] M.C. DeRosa, R.J. Crutchley, *Coord. Chem. Rev.* 233-234 (2002) 351-371.
- [51] T. Torres, *J. Porphyr. Phthalocya.* 4 (2000) 325-330.
- [52] T. Nyokong, H. Isago, *J. Porphyr. Phthalocya.* 8 (2004) 1083-1090.

- [53] N. Nombona, E. Antunes, T. Nyokong, *Dyes Pigments* 86 (2010) 68-73.
- [54] W. Chidawanyika, T. Nyokong, *Carbon* 48 (2010) 2831-2838.
- [55] K. Ishii, N. Kobayashi, in: K.M. Kadish, K.M. Smith, R. Guilard (Eds.), *The Porphyrin Handbook*, Academic Press, 2003, pp. 1-42.
- [56] W. Chidawanyika, T. Nyokong, *J. Photochem. Photobiol. A* 206 (2009) 169-176.
- [57] A.W. Snow, in: K.M. Kadish, K.M. Smith, R. Guilard (Eds.), *The Porphyrin Handbook*, Academic Press, 2003, pp. 129-176.
- [58] N.B. Mckeown, in: K.M. Kadish, K.M. Smith, R. Guilard (Eds.), *The Porphyrin Handbook*, Academic Press, 2003, pp. 61-124.
- [59] M. Durmus, T. Nyokong, *Polyhedron* 26 (2007) 2767-2776.
- [60] N.B. McKeown, *Phthalocyanine Materials: Synthesis, Structure and Function, Chemistry*, Cambridge University Press, United Kingdom, 1998.
- [61] D.K. Chatterjee, L.S. Fong, Y. Zhang, *Adv. Drug Deliver. Rev.* 60 (2008) 1627-1637.
- [62] J. Britton, E. Antunes, T. Nyokong, *Inorg. Chem. Comm.* 12 (2009) 828-831.
- [63] S. Moeno, T. Nyokong, *J. Photochem. Photobiol. A* 201 (2009) 228-236.
- [64] S. Moeno, T. Nyokong, *Polyhedron* 27 (2008) 1953-1958.
- [65] M. Idowu, T. Nyokong, *Polyhedron* 28 (2009) 891-896.
- [66] A. Erdogmus, S. Moeno, C. Litwinski, T. Nyokong, *J. Photochem. Photobiol. A* 210 (2010) 200-208.
- [67] X.-F. Zhang, X. Li, L. Niu, L. Sun, L. Liu, *J. Fluoresc.* 19 (2009) 947-954.
- [68] X.-F. Zhang, Y. Di, F. Zhang, *J. Photochem. Photobiol. A* 203 (2009) 216-221.
- [68a] S. Dayal, J. Li, Y-S. Li, H. Wu, A.C.S. Samia, M.E. Kenney, C. Burda, *Photochem. Photobiol.* 84 (2008) 243-249.
- [68b] S. Dayal, Y. Lou, A.C.S. Samia, J.C. Berlin, M.E. Kenney, C. Burda, *J. Am. Chem. Soc.* 128 (2006) 13974-13975.
- [68c] S. Dayal, R. Krolicki, Y. Lou, X. Qui, J.C. Berlin, M.E. Kenney, C. Burda, *Appl. Phys. B-Lasers O* 84 (2006) 309-315

- [68d] A.C.S. Samia, X. Chen, C. Burda, *J. Am. Chem. Soc.* 125 (2003) 15736-15737.
- [68e] R.L. Morris, K. Azizuddin, M. Lam, J. Berlin, A.-L. Nieman, M.E. Kenney, A.C.S. Samia, C. Burda, N.L. Oleinick, *Cancer Res.* 63 (2003) 5194-5197.
- [69] A. Gilbert, J.E. Baggott in: *Essentials Of Molecular Photochemistry*, Blackwell Scientific, Oxford, 1991.
- [70] D.F. Shriver, P.W. Atkins in: *Inorganic Chemistry*, 3rd ed., Oxford University Press, New York, 1999.
- [71] J.G. Calvert, J.N. Pitts, *Photochem.* 285 (1967) 258.
- [72] S. Fery-Forgues, D. Lavabre, *J. Chem. Educ.* 76 (1999) 1260-1264.
- [73] A. Ogunsipe, J.-Y. Chen, T. Nyokong, *New J. Chem.* 28 (2004) 822-827.
- [74] R.F. Kubin, A.N. Fletcher, *J. Lumin.* 27 (1982) 455-462.
- [75] J.R. Lakowicz in: *Principles Of Fluorescence Spectroscopy*, Second, Kluwer Academic/Plenum, New York, 1999.
- [76] K. Boldt, O.T. Bruns, N. Gaponik, A. Eychmüller, *J. Phys. Chem. B* 110 (2006) 1959-1963.
- [77] J. Britton, E. Antunes, T. Nyokong, *J. Photochem. Photobiol. A* 210 (2010) 1-7.
- [78] M. Sanz, M.A. Correa-duarte, L.M. Liz-Marzan, A. Douhal, *J. Photochem. Photobiol. A* 196 (2008) 51-58.
- [79] H. Du, R.A. Fuh, J. Li, L.A. Cockan, J.S. Lindsey, *J. Photochem. Photobiol.* 68 (1998) 141-142.
- [80] S.J. Strickler, R.A. Berg, *J. Phys. Chem. B* 37 (1962) 814-822.
- [81] J. Turro in: *Modern Molecular Photochemistry*, The Benjamin/Cummings Publishing Co., Inc., New York, 1978.
- [82] J.S. Hsiao, B.P. Krueger, R.W. Wagner, T.E. Johnson, J.K. Delaney, D.C. Mauzerall, G.R. Fleming, J.S. Lindsey, D.F. Bocian, R.J. Donohoe, *J. Am. Chem. Soc.* 118 (2006) 11181-11193.
- [83] P. Jacques, A.M. Braun, *Helv. Chim. Acta* 64 (1981) 1800-1806.

- [84] J. Kossanyi, D. Chahraoui, *Int. J. Photoenergy* 2 (2000) 9-15.
- [85] T. Förster, *Discuss. Faraday Soc.* 27 (1959) 7-17.
- [86] S. Khene, A.N. Cammidge, M.J. Cook, T. Nyokong, *J. Porphyr. Phthalocya.* 11 (2007) 761-770.
- [87] T.H. Tran Thi, C. Desforge, C. Thiec, S. Gaspard, *J. Phys. Chem.* 93 (1989) 1226-1233.
- [88] J.H. Weber, D.H. Busch, *Inorg. Chem.* 4 (1965) 469-471.
- [89] W.W. Yu, L. Qu, W. Guo, X. Peng, *Chem. Mater.* 125 (2003) 2854-2860.
- [90] A. Mandal, N. Tamai, *J. Phys. Chem. C* 112 (2008) 8244-8250.
- [91] D. Wohrle, M. Eskes, K. Shigehara, A. Yamada, *Synthesis* (1993) 194-196.
- [92] M.J. Stillman, T. Nyokong, in: C.C. Leznoff (Ed.), *Phthalocyanines: Properties and Applications*, A.B.P. Lever, New York, 1989, p. 133.
- [93] X. Wang, L. Qu, J. Zhang, X. Peng, M. Xiao, *Nano Lett.* 3 (2003) 1103-1106.
- [94] J. Zhang, X. Wang, M. Xiao, *Optical Lett.* 27 (2002) 1253-1255.
- [95] E.Z. Chong, D.R. Matthews, H.D. Summers, K.L. Njoh, R.J. Errington, P.J. Smith, *J. Biomed. Biotech.* 54169 (2007) 1.
- [96] A. Javier, D. Magana, T. Jennings, G.F. Strouse, *Appl. Phys. Lett.* 83 (2003) 1423-1425.
- [97] M. Lunz, A. Louise Bradley, *J. Phys. Chem. C* 113 (2009) 3084-3088.